PAPER • OPEN ACCESS

The Divertor Tokamak Test facility research plan

OPEN ACCESS
IOP Publishing | International Atomic Energy Agency
Nuclear Fusion
Nucl. Fusion 66 (2026) 116017 (42pp)
https://doi.org/10.1088/1741-4326/ae7a8d

The Divertor Tokamak Test facility research plan

G. Giruzzi[1,*], P. Martin[2,3,4], C. Angioni[5], S. Brezinsek[6], F. Crisanti[7], C. Day[8], G. Dose[9], M.V. Falessi[10,11], P. Innocente[12], P. Mantica[13], E. Nardon[1], C. Sozzi[13], D. Terranova[3,12], E. Tsitrone[1], D. Van Eester[14], P. Vincenzi[3,12], G. Vlad[10], M. Wischmeier[5], P. Agostinetti[3], R. Albanese[15], G. Alberti[16], E. Alessi[13], R. Ambrosino[15], G. Artaserse[10], J.F. Artaud[1], L. Aucone[17], F. Auriemma[3], F. Bagnato[18], B. Baiocchi[13], L. Balbinot[18], T. Bolzonella[3], N. Bonanomi[13], L. Boncagni[10], D. Bonfiglio[3], R. Bonifetto[19], G. Brochard[20], H. Bufferand[1], A. Cardinali[10], N. Carlevaro[10], S. Carusotti[7], I. Casiraghi[13], A. Castaldo[10], C. Castaldo[10], M. Cavedon[17], S. Ceccuzzi[10,18], C. Centioli[10], M. Ciotti[10], G. Ciraolo[1], J.W. Coenen[6], Y. Corre[1], M. Dalla Palma[3,12], A. Dal Molin[13], C. De Piccoli[3], R. Dumont[1], G. Falchetto[1], A. Fassina[10], L. Figini[13], D. Fiorucci[10], M. Firdaouss[1], L. Frassinetti[21], V. Fusco[10], L. Gabellieri[18], A. Gallo[1], J. Garcia[1], J. Gaspar[22], F. Ghezzi[13], T. Giegerich[23], M. Gobbin[3,12], J. Hillairet[1], C. Hopf[5], Q.Y. Hu[17], M. Iafrati[10], P. Jacquet[24], E. Joffrin[1], D. King[24], Y. Kominis[25], P. Lauber[5], X. Litaudon[1], J. Lombardo[3], P. Maget[1], A. Mariani[13], D. Marocco[10], M. Missirlian[1], J. Morales[1], A. Murari[3], G. Nallo[19], R. Neu[5], M. Nocente[17], M. Notazio[7], S. Nowak[13], S. Peruzzo[3], L. Pigatto[3], C. Piron[10], L. Piron[2,3], F. Porcelli[19], G. Ramogida[10], D. Ricci[13], M. Richou[1], G. Rubino[26], R. Sabot[1], M. Salewski[27], G. Spizzo[3,12], F. Subba[19], C. Theiler[28], D. Testa[28], C. Tsironis[25], E. Vassallo[13], S. Varoutis[29], F. Veronese[3], N. Vianello[3], M. Wirtz[6], S. Wiesen[30], F. Zonca[10] and M. Zuin[3]

[1] CEA, IRFM, Saint Paul-lez-Durance F-13108, France
[2] Università degli Studi di Padova, Via 8 Febbraio 2, Padova 35122, Italy
[3] Consorzio RFX, Corso Stati Uniti 4, Padova 35127, Italy
[4] Centro Linceo Interdisciplinare B. Segre, Roma, Italy
[5] Max-Planck-Institut für Plasmaphysik, Garching D-85748, Germany
[6] Forschungszentrum Jülich GmbH, Institute of Fusion Energy & Nuclear Waste Management—Plasmaphysik, Jülich 52425, Germany
[7] University of Tuscia, DEIM, Via del Paradiso 47, Viterbo 01100, Italy
[8] Kyoto Fusioneering Europe GmbH, An der RaumFabrik 29, Karlsruhe 76227, Germany
[9] General Atomics, San Diego, CA 92121, United States of America
[10] ENEA C. R. Frascati, via E. Fermi 45, Frascati 00044, Italy
[11] Istituto Nazionale di Fisica Nucleare (INFN), Piazzale Aldo Moro 2, Roma 00185, Italy
[12] ISTP-CNR, Corso Stati Uniti 4, Padova 35127, Italy
[13] ISTP-CNR, Via R. Cozzi 53, Milano 20125, Italy
[14] Laboratory for Plasma Physics, LPP-ERM/KMS, Brussels, Belgium
[15] Consorzio CREATE, Via Claudio 21, Napoli 80125, Italy
[16] Politecnico di Milano, P.zza Leonardo da Vinci, 32, Milano 20133, Italy

[*] Author to whom any correspondence should be addressed.

[17] Università degli Studi di Milano-Bicocca, Piazza della Scienza 3, Milano 20126, Italy
[18] DTT S.c. a r.l., Via Enrico Fermi 45, Frascati 00044, Italy
[19] Politecnico di Torino, Corso Duca degli Abruzzi 24, Torino 10129, Italy
[20] Aix-Marseille Université CNRS PIIM UMR, Marseille 7345, France
[21] Division of Fusion Plasma Physics, KTH Royal Institute of Technology, Stockholm SE-100 44, Sweden
[22] Aix Marseille University, CNRS, IUSTI, Marseille F-13453, France
[23] Karlsruhe Institute of Technology, PO Box 3640, Karlsruhe D-76021, Germany
[24] UKAEA Culham Science Centre, Culham OX14 3DB, United Kingdom of Great Britain and Northern Ireland
[25] National Technical University of Athens, Association EURATOM-Hellenic Republic, Zografou, Athens 15773, Greece
[26] ISTP-CNR, Via Amendola 122/D, Bari 70126, Italy
[27] Department of Physics, Technical University of Denmark, Kgs. Lyngby, Denmark
[28] EPFL Swiss Plasma Center (SPC), Lausanne CH-1015, Switzerland
[29] Max-Planck-Institut für Plasmaphysik, Greifswald D-17491, Germany
[30] DIFFER—Dutch Institute for Fundamental Energy Research, De Zaale 20, Eindhoven 5612 AJ, Netherlands

E-mail: gerardo.giruzzi@gmail.com

Received 19 January 2026, revised 13 May 2026
Accepted for publication 9 June 2026
Published 21 July 2026

Abstract

The Divertor Tokamak Test facility (DTT) is a device presently under construction at the ENEA site in Frascati (Italy) in the framework of a joint public/private partnership. It has been designed as a superconducting tokamak with breakeven class performance, with the main objective of developing credible solutions for heat and particle exhaust, a key challenge in view of future fusion reactors. This needs to be addressed in a core-edge integrated approach, to assess the compatibility of exhaust solutions with reactor relevant core performance. In this paper, an overview is provided of the DTT research plan, recently developed by an international team. It covers the DTT programmatic objectives, research strategy and expected scientific contributions connected with the device characteristics, not only in the key area of heat exhaust and edge plasma physics, but also on other subjects of high fusion relevance, such as MHD stability in high performance scenarios, transport and turbulence, energetic particle physics, validation of advanced theoretical developments, as well as tests of technological solutions for reactor relevant components.

Keywords: DTT, tokamak, research plan, divertor tokamak test

(Some figures may appear in colour only in the online journal)

Contents

1. Introduction: DTT objectives and research strategy

A fusion reactor is characterized by a plasma core at high density and temperature and consequently very large power and particle fluxes to the plasma facing components (PFCs). The successful resolution of such integration issues is essential for the success of ITER, presently under construction, and any other future fusion power devices, given the foreseen large edge power and particle fluxes and the necessary very long duration of plasma discharges (from several minutes to continuous operation). The challenge of developing adequate power exhaust solutions for fusion reactors is not limited to the choice of appropriate plasma facing materials. The overall features of the divertor, first wall (FW) surrounding the plasma and other PFCs need accurate optimization by design and validation tests (magnetic configuration, shaping, cooling, etc). On the basis of these considerations, the need has been identified of a scaled tokamak experiment challenging the present PFC design and materials with plasma core conditions as close as possible to those of a reactor. The Divertor Tokamak Test facility (DTT) has been designed in order to meet this need, approaching, as much as possible in a scaled facility and without the use of tritium, bulk and edge plasma conditions relevant to a fusion reactor.

DTT is presently under construction at the ENEA site in Frascati (Italy). The construction is managed by a public-private consortium including all the public Italian institutions working in fusion and the largest Italian energy company (ENI). The design and construction activities are accompanied by intensive physics studies, carried out by various Italian institutes with international collaborations, including theory, modelling, diagnostics and control schemes developments. These studies are not limited to the DTT main mission of heat exhaust, but involve topics such as transport, MHD (magneto-hydro dynamics), energetic particle (EP) physics, heating and current drive, because the solution to the heat exhaust challenge requires an approach that ensures core-edge integration. The ensemble of these studies has led to the production of the DTT Research Plan [1], an extensive document developed by an international team, which describes the objectives and research strategy of the DTT experiment [1–3] and defines a set of programmatic headlines of its scientific programme. This document will be regularly updated and will catalyse and guide the research activities in preparation of the experimental phase. A synthesis of this document is presented in this overview paper.

The DTT Research Plan is based on the expected performance of a device that, by its characteristics, will be at the forefront of the international fusion programme in the decades 2030–2040, in preparation and in parallel with the exploitation of ITER. The main parameters of DTT are shown in table 1. The DTT main mission is that of exploring solutions for managing heat and particle exhaust in future fusion devices. This is a crucial and complex problem with various interconnected aspects: PFC materials, surface shapes, overall geometry and adapted plasma magnetic configurations. The DTT project has the ambitious objective of giving significant contributions to all these aspects of the problem. In particular, the issue of the optimum magnetic configuration for a tokamak reactor has been the subject of intensive research for years, leading to the proposal of several magnetic configurations that can be considered as alternative to the configuration chosen for ITER, as extensively discussed, for instance, in [4]. Entering a discussion of the relative merits of the various alternative configurations is beyond the scope of this article; in any case for the design of DTT the choice of maximum flexibility was made, in order to accommodate, as far as possible, not only the presently considered alternative configurations, but also possible new proposals coming as the output of future research. In this context, flexibility means not only the possibility of progressively installing various divertor generations, but also to conceive an initial divertor that could already accommodate and investigate different magnetic configurations. To this purpose, DTT is equipped with full tungsten actively cooled PFCs and the Wide Flat Divertor (WFD) has been presently selected as the initial option [5]. Figure 1 shows magnetic configurations accessible in DTT, computed by means of the CREATE-NL code [6]. A discussion of the properties of these configurations can be found in [4]. The DTT compact size and large auxiliary heating power allow achieving divertor heat loads relevant to ITER and reactor-grade devices. Note that what is depicted in figure 1 indicates a class of scenarios: for any of them, all the main divertor and plasma parameters can be varied and actively controlled, i.e. long or short duration, triangularity (up to -0.5 for upper negative triangularity (NT)), position of the second null, etc. In a priority order, Single Null (SN) scenario, X divertor (XD) scenario and NT scenario can be compared, even within the same discharge. After an initial phase with hydrogen, DTT will operate in deuterium and will explore an extensive parameter range with the aim of solving crucial issues for power exhaust. In particular, it will be investigated whether empirical scalings for the power energy decay length can be extrapolated to reactor-grade regimes or a more favourable behaviour could be expected. Further investigation will address detachment control, X-point radiation and ELM-free (i.e. without Edge Localized Modes (ELMs)) regimes (see section 3), as well as the compatibility of power exhaust solutions with an adequate energy confinement for reactor projections (see section 2).

The DTT heating and current drive capability, at the end of its progressive implementation, will be provided by three different systems (see section 4):

- ECRH (electron cyclotron resonance heating): based on 4 clusters of 8 gyrotrons at 170 GHz/1 MW (to resonate at the fundamental electron cyclotron (EC) frequency for toroidal magnetic field $B_T \sim 6$ T or at the second harmonic

Table 1. DTT main design parameters.

Major radius R (m)	2.19
Minor radius a (m)	0.70
Volume (m^3)	35
Gas	Deuterium
Plasma current (MA)	5.5
Vacuum $B_{toroidal}$ at $R = 2.19$ m	5.85
Electron density $\overline{n_e}$ (10^{20} m^3)	1.5
Auxiliary power P_{tot} (MW)	45
P_{ECRH} (MW)	29
P_{ICRH} (MW)	6
P_{NBI} (MW)	10
Discharge duration (s)	$\sim$60

for $B_T \sim 3$ T), with an installed power up to 32 MW (delivered power $\sim$29 MW).
- ICRH (ion cyclotron resonance heating): two modules composed by antennas fed in parallel by two tetrodes at $60 - 90$ MHz with 1 MW/tetrode, with an installed power up to 9.5 MW (delivered power $\sim$6 MW).
- NBI (Neutral Beam Injection): one neutral beam injector based on the negative ion source technology, with an injection energy of 510 keV and 10 MW of power entering the plasma.

During full power operation at nominal current and field, average electron temperatures in excess of 5 keV will be attained, with a resistive time in the range 10–15 s. Therefore, in order to obtain a stationary current profile, a discharge duration $\sim$60 s is required, with a flat-top of at least 30 s and of course longer at lower current. This pulse duration will also allow constant recycling flux at the divertor targets, necessary to study material migration and deposited layers. Thus DTT has been designed as a moderately long pulse (although not steady-state) device, thanks to the availability of a solenoidal flux in excess of 16 Vs and moderate (considering the typical plasma densities of operation) non-inductive current drive capability, provided by EC waves and NBI. In a full power scenario at nominal current and field, a non-inductive current fraction (including the bootstrap contribution) $\sim$25%–30% is predicted, and 50%–60% in a hybrid scenario at reduced current.

Machine protection, plasma control and scientific exploitation will be guaranteed by the phased development of an exhaustive system of about 80 diagnostics, as described in section 4.3.

As for DTT plasma characteristics and dimensionless parameters, the following are as close as possible to those typical of ITER and reactor-grade tokamaks:

- metallic (tungsten) plasma facing materials;
- the wall load parameter $P_{sep}/R \sim 15$ MW/m, where P_{sep}/R is the ratio of power flowing out the separatrix to major radius, and B_T $P_{sep}/R = 90$ T MW/m;
- scenarios with substantial impurity seeding for divertor protection;
- simultaneous high edge density and low pedestal collisionality, with shallow neutral penetration, allowing the assessment of the compatibility of ELM-free power exhaust solutions with high energy confinement;
- scrape-off layer width;
- confinement properties;
- dominant electron heating with low torque input;
- energetic ions dimensionless orbit widths and speed to Alfvén speed ratio

Figure 2 compares a subset of dimensionless parameters of DTT with those of ITER (2019) and of a European first-of-a-kind reactor concept (named EU-DEMO in [7].) baseline scenarios. For DTT we show both the reference baseline scenario at half of the Greenwald density n_{GW} and one at lower density (0.32 n_{GW}).

The DTT scientific exploitation, after the end of the construction phase, will follow the expected evolution of the machine along three distinct phases, as shown by the sketch of figure 3. The first DTT plasma is intended to be a scientifically exploitable plasma, using deuterium after an initial phase in hydrogen, with reduced but still valuable parameters: magnetic field on axis $B_T = 3$ T (later 6 T), plasma current $I_p = 2$ MA and auxiliary heating power $P_{aux} = 8$ MW of ECRH, also allowing operation in H-mode.

The DTT **first phase** will be dedicated to validating operation at all the initially available technical parameters (reduced plasma current and injected power, starting with also reduced toroidal field). Since the very beginning, the divertor will consist of actively cooled W monoblocks, capable to sustain up to 20 MW m^{-2} of heat flux and compatible with all the magnetic configurations of figure 1. During this phase, the input power will progressively increase up to a coupled power of 14.5 MW of ECRH and 3 MW of ICRH. Disruption and runaway electrons (REs) studies will start already in this phase and will be carried on in all phases. Mitigation experiments with SPI (Shattered Pellet Injection) in support of ITER will be carried out as early as possible, depending on the availability of the SPI system.

In the **second phase**, DTT will achieve higher performances, increasing the heating power by the injection of 10 MW of NBI into the plasma. This will allow testing the actively cooled tungsten divertor under a large power flux (in particular conditions even up to 20 MW m^{-2}). The controlled injection of bulk and edge radiating impurities, together with the possibility to vary the average density by a factor close to two, will allow studying the role of plasma radiation in the various scenarios (priority will be given to SN, SN-NT and XD—acronyms being defined in the legend of figure 1). The use of divertor test modules (at very high pressure—15 MPa—and cooling temperature—250 °C—to allow reactor relevant cooling conditions) will allow testing different PFC materials. All these experiments should allow the validation of a divertor concept to be proposed for a reactor-grade tokamak, even if not yet fully optimized.

In the **third phase**, the injected power will be increased to the nominal 45 MW, by adding 14.5 MW of ECRH and 3 MW of ICRH. During this phase, DTT will concentrate on its main

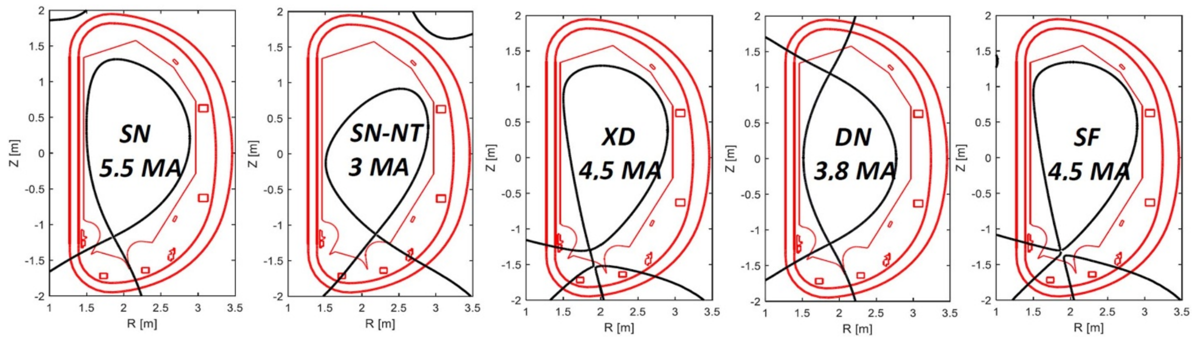

Figure 1. DTT magnetic configurations, obtainable at different plasma currents: from left to right: Single Null, Single Null—Negative Triangularity, X-Divertor, Double Null, SnowFlake.

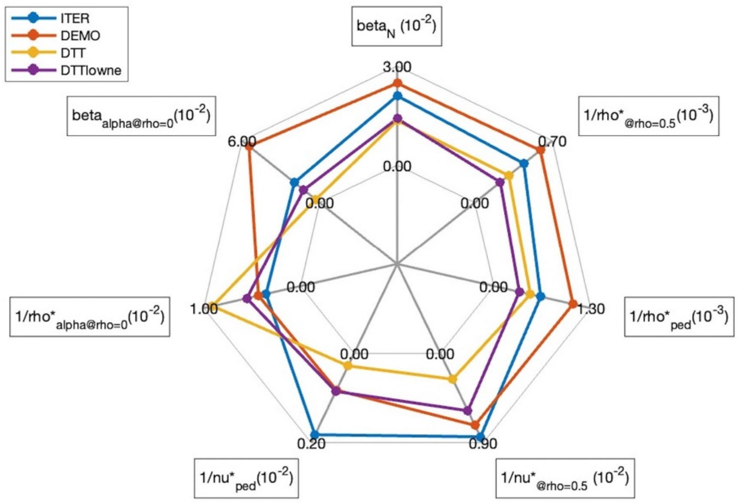

Figure 2. Spider plot of dimensionless parameters connected with high-performance plasmas for DTT (nominal and low-density scenarios), ITER and the reactor concept described in [7] (labelled as DEMO). From top, clockwise: normalized beta, inverse normalized gyroradius at mid-radius, the same at the top of pedestal, inverse collisionality at mid-radius, the same at the top of pedestal, inverse normalized gyroradius of energetic particles (for ITER and DEMO alpha particles, for DTT NBI + ICRH driven fast ions) at the plasma centre, energetic particles beta at the plasma centre. We used the following definitions: collisionality $\upsilon_{\mathbf{e}}* = 69.21\,(\mathrm{qRn_eZ_{eff}ln\Lambda_e})/\left(\mathrm{T_e}^2\epsilon^{3/2}\right)$ with $\ln\Lambda_e = 15.2 - \frac{1}{2}\ln n_e\left(\mathrm{E20\ m^{-3}}\right) + \ln \mathrm{T_e}\,(\mathrm{keV})$, inverse aspect ratio $\epsilon = r/R$, with local values of minor radius coordinate r [m], safety factor q, effective charge number Z_{eff}, electron density n_e [10^{19} m^{-3}], electron temperature T_e [eV]; normalized gyroradius $\rho* = 4.57\ 10^{-3}\sqrt{T_iA}/(aB_T)$ with the ion temperature T_i in keV, A = ion mass number (=2.5 for DT), B_T in T, minor radius a in m; $\beta = 2\mu_0\,p/{B_T}^2$ with p the pressure in Pascal; $\beta_N = \beta$ a B_T/I_p with the plasma current I_p in MA.

target: the proposal of a complete solution (magnetic topology, divertor shape and material) for the divertor and possibly FW of a reactor-grade tokamak, based on the experimental validation carried out on DTT. In this phase, DTT will be exploited in conditions (core, edge, EPs) that will be highly relevant also for burning plasma physics, despite the absence of tritium.

The plan of the paper is the following. In section 2, the reference DTT scenarios are described, together with the integrated transport modelling used to develop them and transport physics research objectives. In section 3, the research programme related to the main objective of the experiment is discussed: divertor and scrape-off (SOL) physics, plasma-wall interaction and connected technological developments. Section 4 is devoted to heating, fuelling and diagnostic systems, from the point of view of their use and impact on the research programme. Section 5 presents the physics studies that will complement and support the main research programme, i.e. MHD instabilities, disruption and runaways, EPs and theoretical developments. In section. 6, concluding remarks are presented, together with the top-level headlines of the DTT research programme.

2. DTT Scenarios and integrated transport modelling

The development and assessment of DTT baseline and advanced scenarios for various divertor configurations and the heating system implementations of the three DTT programme

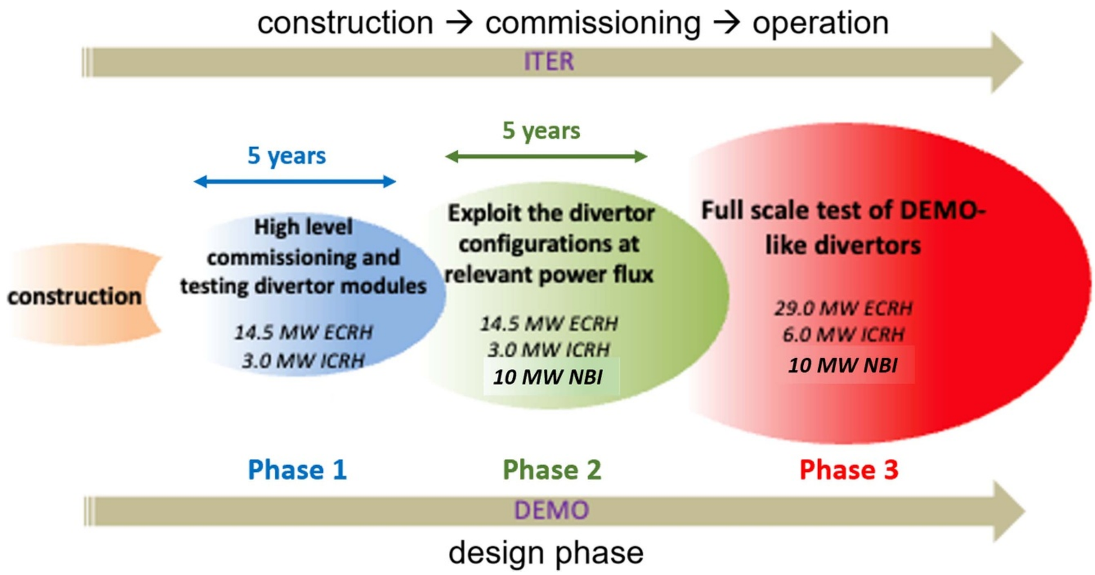

Figure 3. Planned DTT timeline, with respect to the ITER construction, commissioning and first operation phase and first-of-a-kind reactor (labelled as DEMO) programme evolution.

Table 2. Summary of DTT heating phases and planned scenarios.

Scenario	I_p (MA)	B_T (T)	Divertor	Power installed (MW) EC	IC	NBI
			Phase 1 ∼ 5 years			
A	**2**	**3**	SN/XD	**8**	**0**	**0**
A NT	1.5	3	NT	8	0	0
B	**2**	**3**	SN/XD	**16**	**4.75**	**0**
B NT	1.5	3	NT	16	4.75	0
C	**4**	**6**	SN/XD	**16**	**4.75**	**0**
C NT	3	6	NT	16	4.75	0
			Phase 2 ∼ 5 years			
D	**5.5**	**6**	SN	**16**	**4.75**	**10**
D XD	4.5	6	XD	16	4.75	10
D NT	4	6	NT	16	4.75	10
D at low B_T	2.75	3	SN	16	4.75	10
			Phase 3 > 10 years			
E	**5.5**	**6**	SN	**32**	**9.5**	**10**
E XD	4.5	6	XD	32	9.5	10
E NT	4	6	NT	32	9.5	10
E at low B_T	2.75	3	SN	32	9.5	10

phases has been carried out with extensive use of magnetic equilibria and integrated transport modelling. In this section, the reference scenarios that are at present considered for operation in the three phases are introduced (section 2.1); highlights of the integrated modelling results for some of the scenarios are presented in section 2.2; the DTT research programme in the area of transport and confinement is discussed in section 2.3. More detailed discussion of scenarios and transport modelling can be found in Chaps. 2 and 4 of the DTT Research Plan document [1].

2.1. DTT reference scenarios

As the heating systems will be implemented in steps, the DTT scenarios will evolve along different heating phases. Table 2 summarizes the DTT foreseen scenarios in these phases, setting the terminology for naming the scenarios used throughout the Research Plan and this paper. DTT will mainly operate in positive triangularity (PT) with B_T clockwise and I_p counter-clockwise (from above), but the NT configuration foresees reversing the B_T without reversing I_p, to achieve unfavourable

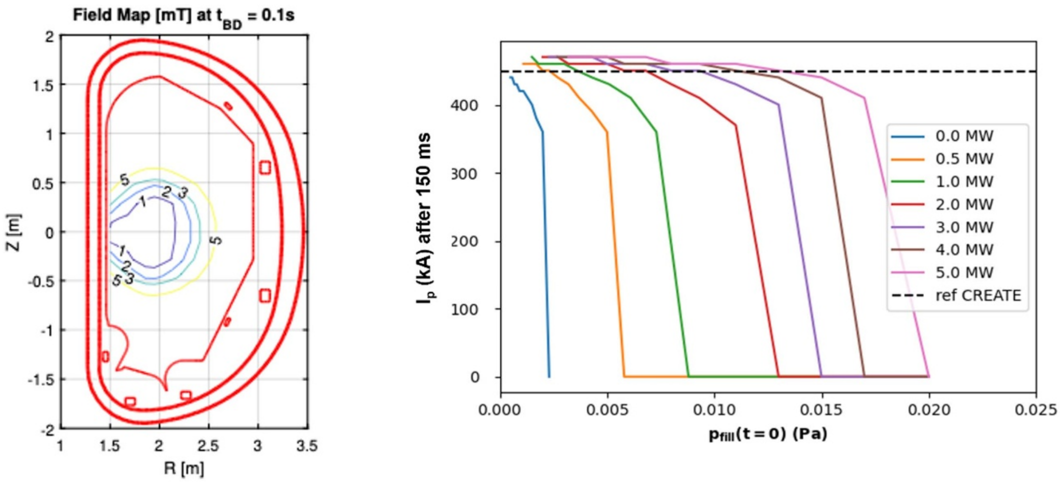

Figure 4. (Left) Reference breakdown conditions calculated by CREATE-BD. Iso-field lines obtained when the requested toroidal electric field is 0.8 V m^{-1} for Ohmic scenarios. (Right) Plasma current as calculated by BKD0-GRAY after 0.15 s of simulation for different prefilling pressure at different ECH powers (6 T). The reference plasma current (dashed black line) is calculated by CREATE-BD, assuming the plasma as a massive conductor with poloidal cross section that fills the breakdown region.

∇B drift in order to avoid H-mode without having counter-current NBI.

As shown in figure 1, the flexibility of the DTT machine allows producing a variety of alternative magnetic configurations [8], which increase divertor radiation without excessive core performance degradation, in order to study different solutions to the power exhaust problem. So far only the following divertor configurations have been fully studied and assessed: (1) SN with PT; (2) X-Divertor (XD), a configuration also with SN and PT; (3) NT. These configurations can be realized with a maximum flat-top plasma current of 5.5 MA, 4.5 MA and 4 MA respectively. Plasma elongation at separatrix is $k = 1.78$, 1.85, 1.75 respectively, and average triangularity at separatrix is $\delta = 0.45$, 0.37, -0.15.

The electromagnetic equilibria have been designed using the CREATE-NL code [6], assuming initially bell-shaped pressure and current profiles, and eventually recomputed using profiles calculated by physics-based transport models. These calculations allow estimating the flux consumption in the different phases of the discharge and the associated discharge duration. The present design of the Central Solenoid (CS) provides an ideal solenoidal flux of 16.6 Vs and a pre-magnetization flux of 16.2 Vs; a breakdown flux consumption of the order of 0.8 Vs for the creation of the first plasma at 0.1 MA is assumed. For the E scenario at 5.5 MA, with internal inductance $l_i = 0.8$, the resistive flux consumption during the plasma current ramp-up was evaluated through simulations based on first-principle transport models. The resulting evolution corresponds to an effective Ejima coefficient [9] $C_{\mathrm{Ejima}} \approx 0.45$, consistent with experimental observations in devices such as JET. A start of flat-top flux of 1.1 Vs (i.e. a flux consumption until EOF of 14.5 Vs) was achieved. A plasma current ramp-up rate of 400 kA s^{-1} has been assumed to make the evaluated resistive losses compatible with the experimental data extracted by existing devices, such as JET. Note that the DTT CS/PF coil system has been engineered to sustain significantly higher ramp rates (up to ~650 kA s^{-1}) in terms of current, voltage, and AC loss constraints. During the flat top, a $V_{\mathrm{loop}} = 0.18$ V is assumed to consider the resistive losses with a bootstrap fraction $I_{\mathrm{bs}}/I_{\mathrm{p}} = 0.22$. The duration of the flat-top is determined by the end of flat-top equilibrium having the reference flat-top plasma shape and minimum boundary flux, which is $\Psi_{\mathrm{EOF}} = -3.55$ Vs. This means that the flux consumption allowed until EOF is 19.75 Vs. This allows a flat-top duration of about 30 s. A margin is also taken into account to perform the HL transition. The flux consumption during the ramp-down is estimated considering the opposite effect of the resistive flux losses and the inductive flux gain. Assuming a plasma current ramp-down rate of -250 kA s^{-1}, the flux loss during ramp-down is approximately 4.5 Vs. It is worth mentioning that, since a new version of the DTT CS is currently under evaluation, a slight modification of the flux consumption during the whole scenario could be obtained.

On DTT, a robust and reliable breakdown relies on the use of EC power. To prepare for different scenarios, a series of simulations were conducted employing the codes BKD0 [10] and CREATE-BD [11] (figure 4, left), alongside the GRAY code [12] for assessing EC absorption. In DTT, the operational range includes a purely ohmic start-up with a toroidal electric field of 0.8 V m^{-1} and a stray field of 3 mT in a large region. Additionally, an EC sustained breakdown at 6 T, corresponding to the fundamental resonance frequency of 170 GHz used in the DTT ECH system, was explored. As depicted in figure 4 (right), the comparison involves assessing the plasma current achieved after 150 ms of simulation for various prefill pressures without impurities. The results indicate that in the ohmic scenario, the prefill pressure threshold for sustaining a breakdown is relatively low, about 2 mPa. By introducing EC power—up to 5 MW of the initially available 8 MW for the DTT initial plasma—the pressure limit increases by a factor of 10, thereby significantly expanding the operational range for current start-up. Such a pressure window should be able to

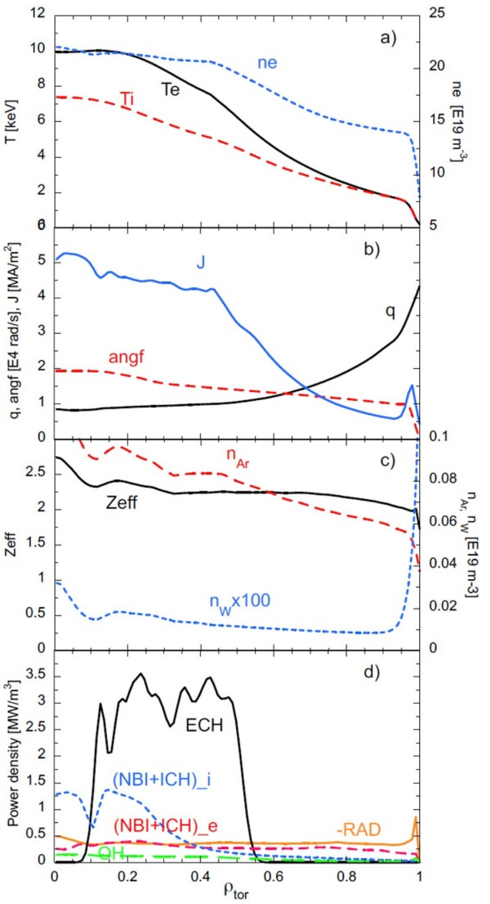

Figure 5. Radial profiles calculated with JINTRAC for the E SN scenario flat-top phase of: (*a*) electron and ion temperatures, electron density; (*b*) toroidal rotation and safety factor; (*c*) Z_{eff}, seeding impurity and tungsten densities; (*d*) ohmic, ECH, NBI + ICH collisional power density to ions and electrons.

guarantee a successful breakdown also considering the presence of impurities.

DTT is equipped with systems that can affect the plasma rotation velocity and can therefore be exploited, to a certain extent, as rotation control tools, beneficial for controlling mode locking and plasma transport properties. First, DTT will feature a set of non-axisymmetric (NAS) coils, mainly for error-field and ELM control, which generate a three-dimensional magnetic field, with influence on plasma rotation. In addition, from Phase 2 DTT will be equipped with a tangential neutral beam injector (see section 4.1.3), thereby providing external momentum input. Integrated numerical simulations include rotation due to NBI, as shown in figure 5, with negligible effect on heat transport. Simulations focused on the effects of magnetic coils will be necessary to quantify the impact of these systems on plasma rotation in DTT and on the resulting MHD stability.

2.2. Highlights of integrated modelling results

Integrated modelling simulations for DTT have been carried out both for flat-top profiles and for the whole discharge time history. The JINTRAC [13] code has mainly been used for flat-top simulations whilst the ASTRA [14, 15] transport code has been used for the time-dependent simulations. Full discharge simulations with the 0.5-D integrated modelling METIS code [16] have also been performed. The TGLF-SAT2 [17] quasilinear model for turbulent transport (including only perpendicular B fluctuations) and the NCLASS [18] model for neoclassical calculations of the main species were used. For neoclassical impurity transport the FACIT [19] module has been used in ASTRA and the calculated impurity profiles transferred to JINTRAC. Two impurities were modelled: a seeding impurity (Ar, Ne or N) and tungsten (W). The H-mode pedestal in JINTRAC was taken from EUROPED predictions [20] and kept fixed, setting the boundary at the top of the pedestal, whilst the IMEP [21] workflow was used in ASTRA to achieve self-consistent pedestal values in the time-dependent simulations. The ECRH, ICRH and NBI power depositions were calculated in JINTRAC with the GRAY [12], PION [22] and PENCIL [23] codes, respectively. In ASTRA, RABBIT [24] was used for NBI, whilst the ICRH profiles were taken from JINTRAC and the ECH power, which is the only heating system used in ramp-up and ramp-down, was modelled using Gaussian profiles for sake of simplicity.

Figure 5 shows an example of the main plasma profiles at flat-top for the scenario E baseline SN calculated with JINTRAC as detailed above, using a simplified continuous sawtooth model that increases diffusivities and resistivity inside the $q = 1$ surface, to reproduce an average effect of sawteeth. A rather broad ECH power deposition was chosen to avoid excessive difference between the electron temperature T_{e} and ion temperature T_{i}, leading to density pump-out effects in strongly dominant TEM regimes [25]. The seeded impurity was dosed to achieve effective charge $Z_{\mathrm{eff}} \sim 2.2$ and radiative power $P_{\mathrm{rad}} \sim 30\%$ of input power, with $n_{\mathrm{W}}/n_{\mathrm{e}} \sim 2 \times 10^{-5}$ in the core. Central values of $T_{\mathrm{e}0} \approx 10$ keV, $T_{\mathrm{i}0} \approx 7.5$ keV, and electron density $n_{\mathrm{e}0} \approx 2.2 \times 10^{20} \mathrm{m}^3$ are reached, as well as $\beta_{\mathrm{N}} \sim 1.26$ and energy confinement time $t_{\mathrm{E}} \sim 0.24$ s (calculated using total power without accounting for P_{rad}). More details on the flat-top simulations with JINTRAC of different DTT scenarios are reported in [1, 26, 27]. Extensive studies of scenario E baseline NT at 6 T/4 MA can be found in [28, 29]. The study led to the conclusion that, although the lack of pedestal is not completely recovered by improved core transport in NT, still good performance with central values of pressure reduced by ~10% with respect to PT H-modes could be achieved, in absence of ELMs.

The time dependent simulations made using ASTRA cover the whole confined plasma radius, up to the separatrix. The evolution of the whole plasma discharge, from the early ohmic limiter phase up to the H-mode flat-top phase, is simulated. All the different phases (L-mode, LH transition and H-mode) are treated in a single simulation, with the plasma parameters at the LH transition determining the H-mode pedestals. T_{e}, T_{i}, n_{e}, the impurity densities, and the plasma current density j_{p} are predicted in these simulations. Details of the simulation methodology can be found in [1] (appendix C). Results of simulations obtained in this way can be found in [30]. Here results for the full-field, full current, full-power

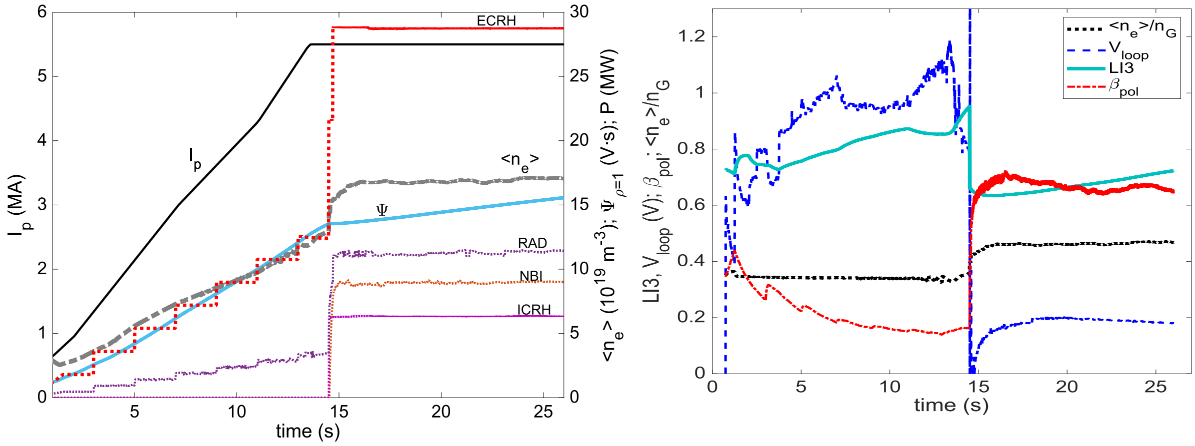

Figure 6. **(*a*):** Time evolution for scenario E of the plasma current (I_p), auxiliary heating powers (ECRH, NBI, ICRH), power radiated within the separatrix (RAD), poloidal magnetic flux at the separatrix (Ψ) and line-averaged electron density ($\bar{n}_e$). The jump in $\bar{n}_e$, following the strong increase in ECRH heating at $t = 14.6$ s, marks the transition into H-mode. **(*b*):** Time evolution for scenario E of the plasma inductance (LI3), loop voltage (V_{loop}), poloidal beta (β_{pol}) and the Greenwald density ratio ($\bar{n}_e\ /n_G$). The jump in all of these parameters, at $t = 14.6$ s, is due to the transition into H-mode. (a) and (b) Reproduced from [30].

case (scenario E) are reproduced from [30] as an illustrative example.

The ECRH heating is deposited both on-axis ($\rho_{tor} = 0.2$) and off-axis ($\rho_{tor} = 0.6$) during the current ramp-up phase in order to maintain the internal inductance below the machine limits. One pair of gyrotrons (each gyrotron delivers 0.9 MW of heating power) is turned on from the beginning of the simulation, during the limiter phase. Starting at $t = 3$ s, when the limiter phase ends and the plasma enters the divertor configuration, one pair of gyrotrons is switched on every two seconds (see figure 5(*a*)). At $t = 13.5$ s, after the end of the current ramp-up phase, the ECRH power is moved fully on-axis. At $t = 14.5$ s, the remaining gyrotrons, the ICRH and the NBI power are switched on, reaching full heating power and triggering the LH transition. The time waveforms of the heating powers and of the radiated power are shown in figure 6(*a*). The ratio between $\bar{n}_e$ and the Greenwald density during the ramp-up is kept at $\bar{n}_e/n_{GW} \approx 0.35$. The impurities used in modelling this scenario are the seeding gas (Ne in the L-mode phase and Ar in the H-mode phase) and W. Ne and Ar will be puffed in order to regulate the radiated power, while W will mainly come from the DTT tungsten divertor and main chamber and its concentration will be less controllable. In the simulations, a fixed ratio was kept between the lighter impurity and the W concentration at the separatrix $n_W/n_{Ne,Ar} = 0.03$. The imposed radiated power is 25% of the total auxiliary heating power. The time-evolution of some plasma parameters of interest is shown in figure 6(*b*). The evolution of $\bar{n}_e$ follows the current ramp, as desired, while the evolution of the temperatures follows the ramp in heating power. $\bar{n}$ shows a clear jump at the LH transition around $t = 14.5$ s. In this case, $\bar{n}_e/n_{GW}$ goes from approximately 0.35 during the L-mode phase, to approximately 0.47 during the H-mode phase. Values of the internal inductance and of the poloidal beta are found to be within the level of acceptance for plasma control. The poloidal magnetic flux at the separatrix, Ψ_b, reaches a value of 14.6 Vs at the LH transition. The loop voltage is around $V_{loop} = 0.2\ V$ during the H-mode phase. Considering these two numbers and the fact that DTT will have a total magnetic flux of 19.7 V·s available before the ramp-down phase, the flat-top phase of the DTT scenario E is expected to last between 20 and 30 s. The core value of T_e reaches $T_e = 12$ keV, while T_i arrives at 9 keV, with n_e as high as $22 \cdot 10^{19}\ m^{-3}$. Given the choice of a Greenwald fraction of about 0.5 for the reference full power scenario, we find $T_e > T_i$ over almost the whole plasma radius.

An important aspect of the DTT research is provided by the possibility of exploring the domain of existence and the performance of stationary regimes that feature sufficiently small or no ELMs. These regimes would be desirable in a reactor plasma, in which large type I ELMs cannot be tolerated. This is of particular relevance considering the capability of DTT of concomitantly matching the collisionalities at both the separatrix and at the pedestal top that are expected in a future reactor, a critical element towards a complete and reliable core-edge integration. As discussed in [1] (section 2.7), DTT will be able to access small ELMs regimes such as:

- the enhanced D-alpha (EDA) H-mode [31], characterized by high fuelling, high density and high triangularity, with a quasi-coherent mode at the plasma edge;
- the quasi-continuous exhaust (QCE) regime [32, 33], characterized by high fuelling, high density, high triangularity and sufficiently high safety factors, with type-II ELMs;
- the compact radiative divertor (CRD) [34], characterized by very strong impurity seeding and the presence of an X-point radiator (XPR);
- the I-mode regime [35], obtained with the ion grad-B drift directed away from the X-point, characterized by the presence of a pedestal in the temperature profiles and the absence of a strong pedestal in the density profile;
- the Wide Pedestal Quiescent H-mode (WPQH) [36];

- NT scenarios [29], accessible with different negative values of top triangularity and featuring an improved edge with respect to a standard L-mode, which allows recovering high core pressure in the absence of an H-mode pedestal.

Advanced scenarios with large fractions of bootstrap current and significant fraction of non-inductive current drive are also possible, but at half nominal magnetic field (2.9 T) and plasma currents between 1 MA and 2 MA (see Sec.2.8.2 of [1]).

As a variant to the standard baseline scenario, which is characterized by a large radius of the $q = 1$ and large sawteeth, a Hybrid scenario has also been studied at $I_p = 3.8$ MA, $n_e = 0.45\ n_{GW}$, characterized by early X-point formation and a fast (600 kA s^{-1}) ramp-up assisted by ECRH and ECCD, achieving at flat-top a wide low shear region and $q_0 \sim 1$, marginally sustained for more than 12 s [37].

2.3. *Transport and confinement research objectives*

The main characteristics of the DTT device from a tokamak confinement standpoint are provided by the high magnetic field and high total auxiliary heating power with respect to the plasma size. With a minor and major radius of 0.7 and 2.2 m respectively, and a plasma volume up to about 35 cubic meters, DTT plasmas can reach currents in excess of 5 MA thanks to the very high magnetic field, up to ~6 T. These properties imply that DTT plasmas can be considered to cover a complementary domain of parameters with respect to tokamaks which, for a given similar plasma size, are more limited in maximum current due to a lower value of the magnetic field. In this respect, an extremely interesting feature of DTT is the possibility of operating the highly powered ECRH system (up to 32 MW) both at full field in 1st harmonic ordinary propagation (O1) mode and at half field in the 2nd harmonic extraordinary propagation (X2) mode. Operation at half field (~3 T) and half current allows DTT to also produce plasma discharges that become directly comparable to those obtained in low field tokamaks, which have a lower capability of reaching high current through high magnetic field, but providing the possibility of achieving operation at high plasma beta. Operation at high beta, in contrast, will be limited at full magnetic field.

The main properties, capabilities and limitations of DTT with respect to transport and confinement research objectives (see section 4.2 of [1]) can be summarized as follows:

- High field, high current, high heating power, dominant electron heating, flexibility in heating at both full field / full current and half field / half current
- ECRH density cut-off at Greenwald density limit, edge opacity to neutral penetration
- High density and low collisionality
- Full W walls like ITER and foreseen in fusion reactors
- Small L-mode operational window at half field, broader L-mode operational window at full field
- Capability of operating with favourable and unfavourable grad B configurations for H-mode access
- Limitations: limited auxiliary ion heating, limited length of flat-top at maximum current and density (close to the Greenwald limit), modest current drive capabilities at full field and full current

The DTT expected achievable domains of parameters connecting engineering parameters with volume-averaged dimensionless plasma parameters are shown in figures 7 and 8. These plots are obtained by making use of available scaling laws. In particular, L- and H-mode operational windows are determined according to the Martin's scaling law [38] for the LH transition, at both half and full magnetic field, with a reduction of ~25% due to the metallic wall. The plasma confinement is described with the IPB98 scaling laws for L-mode confinement [39] and with the ITPA20 ITER like [40] for H-mode confinement.

Figure 7 shows an example with 40 MW of auxiliary heating at 5.8 T; dimensionless parameters are plotted as a function of the plasma current for different values of the electron density (dashed horizontal line is the ITER baseline reference, solid line is a DEMO-like reference). This plot exemplifies the capability of DTT plasmas to cover reactor relevant volume-averaged (almost pedestal top) collisionalities at the same densities foreseen for reactor operation, of about 10^{20} m^{-3}. At the same time, it can be observed that even with 40 MW of auxiliary heating, DTT has limited capabilities of reaching reactor relevant values of β_N.

The limitations in reaching high values of β_N at full magnetic field can be overcome by allowed operation at half magnetic field, where the ECRH can be operated in X2 mode. This is demonstrated in figure 8, where plasmas at 2.9 T and 2.7 MA have been considered with increasing heating power, again at different line-averaged electron densities. Here, at low power, the L-mode operational window can be identified.

Figure 8 demonstrates the capability of DTT operation at half magnetic field of combining reactor relevant β_N above 2 with reactor relevant volume-averaged collisionalities of $\nu_{e^*} < 10^{-2}$ at reactor densities around 10^{20} m^{-3}, with applied heating powers around 30 MW. This feature is at present unique in combination with full W walls, although in the future other full W devices will be in operation.

As a consequence of the DTT characteristics and dimensionless parameters that can be achieved at both full and half field, the following main missions in the area of transport and confinement research have been identified:

- Explore compatibility of power exhaust strategies with the existence of high confinement regimes (particular relevance to be given to stationary ELM-free and small ELM regimes with high confinement).
- Achieve ELM-free scenarios (I-mode, EDA H-mode, seeded no ELM regimes (XPR—CRD), QH, small ELMs (QCE = type II ELMs).
- Explore and possibly demonstrate the capability to reach detachment in each of these regimes.
- Explore impact of ELM control techniques.

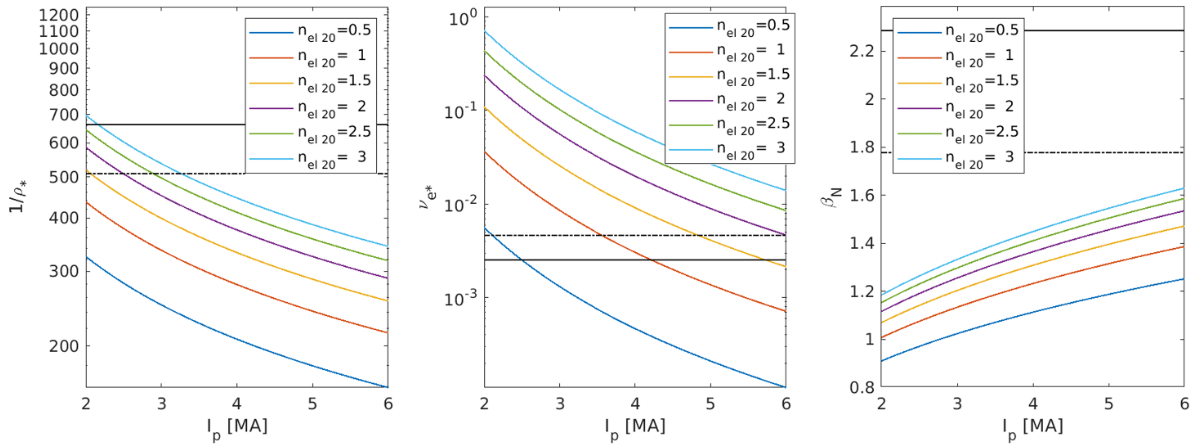

Figure 7. Dimensionless plasma parameters (from left to right: volume-averaged values of $1/\rho_*$, ν_{e*} and β_{N}) as a function of the plasma current in MA, for different values of the line-averaged density at 5.8 T, with 40 MW of auxiliary heating. We recall that at 5 MA, a line-averaged density of 1.5 10^{20} m^{-3} corresponds to a Greenwald fraction of 0.42. Horizontal lines give DEMO-like (solid) and ITER (dashed) reference values. From the application of the scaling laws, the thermal stored energy is computed and then used to compute the dimensionless parameters. This is also used for the calculation of β_{N}. The expression of ν_{e*} used in these plots is $\nu_{e*} = 5\ 10^{-5} \ln\Lambda\, Z_{\mathrm{eff}}\, R\, q\, n_{\mathrm{e}} /(T_{\mathrm{e}}^2\,(r/R)^{1.5})$, with lengths in meters, density in 10^{19} m^{-3} and temperature in keV.

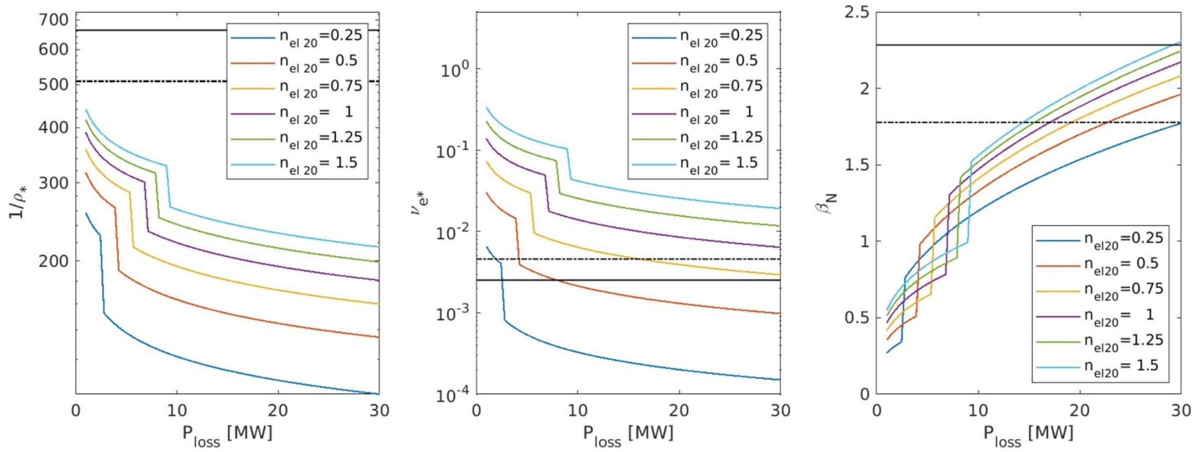

Figure 8. Dimensionless plasma parameters (from left to right volume averaged values of $1/\rho_*$, ν_{e*} and β_{N}) as a function of the heating power in MW, for different values of the line averaged density at 2.9 T and 2.7 MA. We recall that at 2.7 MA, a line-averaged density of 10^{20} m^{-3} corresponds to a Greenwald fraction of 0.57. Horizontal lines give DEMO (solid) and ITER (dashed) reference values.

- Document role of radiation from required impurity seeding on confinement, accessibility of confinement regimes and performance.
- Demonstrate control of profiles of impurity densities and radiated power density, impact of reactor-like pedestal on peripheral impurity screening and on seeding scenarios.
- Characterize the access to high confinement regimes (in particular H-mode) with dominant electron heating, high radiation fractions and limited edge neutral penetration, particularly important in combination with W wall and high B_{T}.
- Document the confinement (core and pedestal) properties over the large variations of parameters allowed by the DTT design (field, current, power and density).
- Perform comparisons of confinement and transport properties at low and high field (and correspondingly low and high current) in the same device.
- Improve existing scaling laws for both confinement and LH transition power, particularly concerning the dependences on plasma current, magnetic field and density, as well as on ρ^* and collisionality.
- Explore plasma rotation (intrinsic and with external torque) at low collisionality and low ρ_*.

These missions have to be accomplished taking into account the evolution of the machine characteristics in the various phases, as listed in table 2. In this respect, a tentative research programme on transport and confinement physics can be summarized timewise as follows:

- **Commissioning** (including actively cooled W PFCs)
  Initial operation with reduced field and current and reduced power.

- **Phase 1, heating phase A** (8 MW ECRH, 3 T, 2 MA)
  With a maximum power of 8 MW, access to H-mode is in principle possible, but available power window above the LH threshold is relatively limited (expected operation is below 1.5 P_{LH}). Initial operation in hydrogen will allow first isotope experiments. Isotope studies, based on deuterium - hydrogen comparisons, will also be possible in later phases of the DTT operation, following the development of the research interests.
- **Phase 1, heating phase B** (16 MW ECRH, 4.75 MW ICRH, 3 T, 2 MA)
  A large number of transport experiments can be performed, particularly in connection with LH transition and turbulent transport. These experimental results can be also planned for future direct comparisons with corresponding experiments in later phases at maximum field and current. The exploration of I-mode in reversed B_T configuration is also possible with sufficient excess in heating power.
  Moreover, at 2.5–2.7 MA/3 T there is already the possibility of exploring the ITER Baseline Scenario (less than 20 MW required, with a combination of ECRH and ICRH).
  High beta operation is potentially possible, but still limited in this phase by the maximum available power. In contrast, accessibility to small ELMs and ELM-free stationary regimes can start to be investigated.
- **Phase 1, heating phase C** (16 MW ECRH, 4.75 MW ICRH, 6 T, 4 MA)
  While this phase is of relatively limited interest from the standpoint of scenario development, given the combination of high magnetic field and current and low power, from the standpoint of transport studies this phase is of high potential interest. With an LH power threshold of 16.5 MW at half of the Greenwald limit at 4 MA, the available power for robust H-mode operation at maximum allowed current and magnetic field of this phase is limited. In contrast, a large operational window becomes available for L-mode transport studies, LH transition studies and LI transition studies (in unfavourable grad B configuration), comparing plasmas at different magnetic fields and currents. This is also of high interest for the characterization of global confinement properties.
- **Phase 2, heating phase D** (16 MW ECRH, 4.75 MW ICRH, 10 MW NBI, 6 T, 5.5 MA)
  The availability of the NBI heating power opens the possibility of robust operation in H-mode reaching a maximum current of 5.5 MA. Beam power and energy can be modulated depending on plasma parameters and scenario. Confinement and transport studies can compare different currents and fields also in H-mode operation. Accessibility to small ELM and stationary ELM-free regimes at high magnetic field and current can be explored. I-mode operational window at 6 T can also be determined (upper boundary in power likely still limited by available power).
  Hybrid/advanced tokamak (e.g. at 2–2.5 MA/3 T) scenarios also become possible (likely requiring up to 10 MW NBI to reach sufficiently high beta operation) with W walls. Capabilities of heating and current drive can be investigated and exploited, diagnostics and control capabilities can be assessed. These capabilities provide an additional DTT mission in developing reactor relevant scenarios with reactor-like wall and compatibility with exhaust at reactor relevant beta. Note that at full field DTT scenarios will not have reactor relevant beta values, but can marginally reach those of the ITER baseline. In contrast, at maximum current and field, DTT can reach reactor relevant values of ρ^* and collisionality.
- **Long term: Phase 3, heating phase E** (32 MW ECRH, 9.5 MW ICRH, 10 MW NBI, 6 T, 5.5 MA)
  All experiments and foreseen scenarios become possible at the maximum nominal heating power levels, allowing full exploitation, also with different divertors.

3. Divertor and SOL physics, plasma-wall interactions (PWI)

The main objective of DTT is to explore reactor-relevant plasma exhaust solutions, while keeping an integrated approach to core-edge scenarios. DTT is meant to accompany ITER exploitation and set the basis for a first-of-a-kind reactor design in this crucial area. As far as plasma exhaust is concerned, the divertor is a key component, which will have to face unprecedented heat, particle and neutron loads compared to present-day devices and relevant for future ones (see, e.g. [41], for ITER and [42] for a European demonstration reactor design). DTT has been specifically designed to provide new insights in this area, in particular:

- Testing whether the advanced divertor solutions (e.g., high radiative SN scenarios, alternative divertor configurations (ADC) or liquid metals) can be technically integrated and are able to withstand the strong thermal loads foreseen in a reactor [43];
- Improving the experimental knowledge in the area of plasma exhaust and PWI for parameter ranges that cannot be addressed by present devices.

The most relevant figures of merit for power exhaust are P_{SOL}/R and $P_{SOL}B_T/R$ (with P_{SOL} the total power entering the scrape-off layer), related to the heat flux able to reach the divertor target. As far as these quantities are concerned, DTT, in its final stage of operation at full power, lies significantly above present-day machines and reaches reactor relevant parameters in terms of power exhaust: in heating phase E, DTT will have $P_{SOL}/R = 15$ MW m^{-1} and $P_{SOL}B_T/R = 85$ MW.T m^{-1}.

In this Section, the DTT PFCs are briefly described and the main heat and particle exhaust research subjects that will be addressed are presented (section 3.1). Far SOL physics and FW loads are discussed in section 3.2. PWI studies specific to the W components (wall conditioning, erosion, fuel retention etc) are discussed in section 3.3. Technology developments on PFC materials and components for FW and divertor are presented in section 3.4.

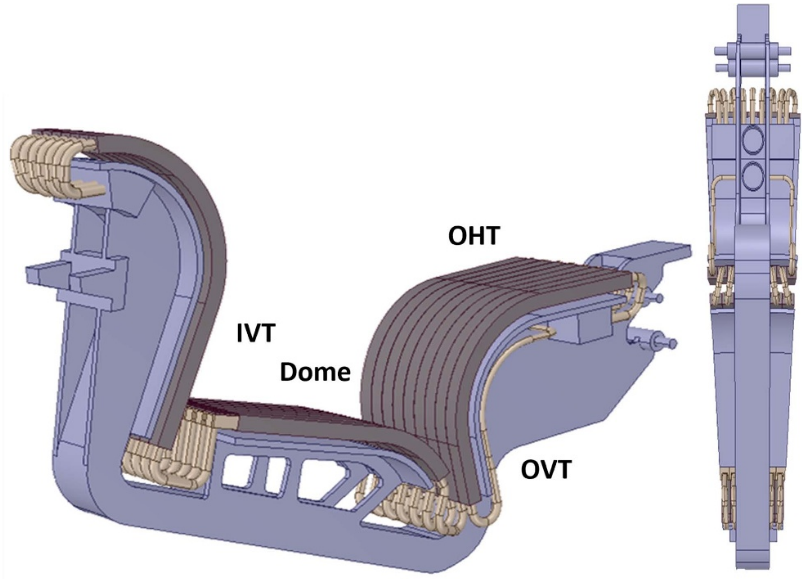

Figure 9. Side view and bottom view of the divertor module with 9 monoblocks row on the OVT and 7 monoblocks row on the dome and IVT. Image courtesy of S. Roccella and the DTT IVC-team.

3.1. DTT PFCs for heat and particle exhaust research

The first implementation of the DTT divertor has been designed in a flexible way, so that a wide range of ADC, such as the X divertor (XD), the Super X divertor (SXD), the SnowFlake (SF), the Double Null (DN), and the NT configurations can be accommodated for comparison with the SN reference divertor configuration. The presently selected shape is the so-called WFD, composed by three sections [44]: the inner vertical target (IVT), the flat central part (Dome) and the outer vertical target/horizontal target (OVT/OHT), as shown by figure 9. The central Dome acts as a standard dome in terms of neutrals sub-divertor closure for SN configuration with strike points on IVT/OVT and as a CHT for XD, NT and SF configurations. The divertor accepts all previously described configurations and also their long leg variants, moving the inner strike point upward on the IVT. It is composed by 54 divertor modules (one of which is shown in figure 9), three for each 20° sector; out of these, four modules will be designed and equipped for specific research objectives (test modules). In the standard modules, the configuration is based on the ITER-grade bulk W monoblock concept. They will be cooled by water in the 30 °C–130°C range (which allows replicating ITER conditions). The technology has been qualified up to 20 MW m^{-2}. As in ITER, the divertor monoblocks are shaped toroidally in order to protect leading edges.

The first wall (FW) [45] consists of three main components: the inboard (IFW), the outboard (OFW) and the top (TFW). All FW modules are actively cooled by water at 60 °C. The OFW and TFW will be realized by plasma spray tungsten coating on Inconel panels and can stationarily dissipate up to 0.5 MW m^{-2}. In the IFW, 50% of the wall is realized by 18 W monoblocks limiters using the same technology of the divertor, allowing a maximum stationary conductive heat flux (toroidally averaged) of 7.5 MW m^{-2}. This higher limit can be useful during the initial limiter phase of discharges and for limiter experiments.

The PFCs (FW and divertor) can be cleaned and conditioned by heating up to 200 °C (up to 165 °C for ducts and bellows), glow discharge cleaning (GDC) and boronization after maintenance activities (B_T off). GDC and boronization can be done also on weekends switching off the toroidal field but with heating at lower temperature (FW up to 130 °C, ducts and bellows up to 100 °C). Ion cyclotron wall cleaning (ICWC) will be available between pulse operations when B_T is on.

DTT will serve to address several aspects of fundamental SOL physics for elaborating heat flux mitigation techniques and particle exhaust at reactor relevant parameters, such as e.g. SOL collisionality, neutrals opacity, plasma density, SOL connection length. The advantages of DTT in this research field can be summarized as follows.

- While the dimensions of the divertor will be certainly smaller than those of ITER or a reactor, the device has the potential of having neutral mean free path to divertor size ratios that are highly relevant for these larger devices.
- The expected high recycling fluxes and the consequentially high divertor neutral pressure, combined with the large volume of the divertor, will facilitate the validation of the role of neutralneutral collisions with respect to the evaluation of the overall tokamak pumping efficiency.
- The high neutral pressure, combined with high recycling fluxes and plasma densities, provide a test-bed to scrutinize the role of atomic as well as molecular volumetric processes with respect to power, but especially to momentum removal and thereby addressing a highly disputed subject on the role of molecular physics.
- With its size and the high toroidal field, as well as sufficiently long pulse durations, implying a constant recycling

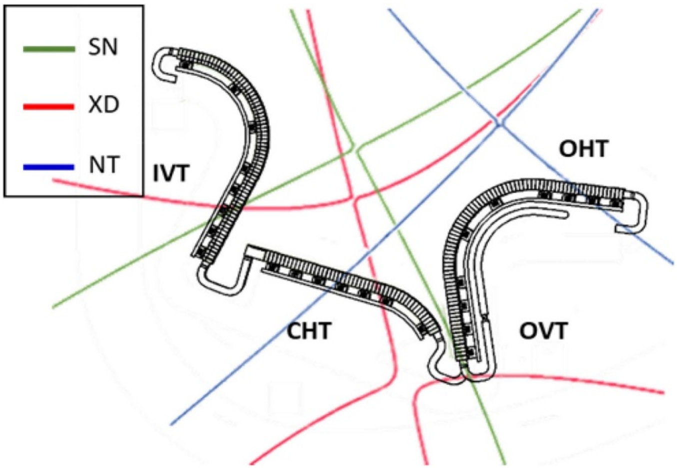

Figure 10. Separatrices and strike points for the DTT divertor and three different magnetic configurations: SN, XD, NT. IVT: inner vertical target; OVT: outer vertical target; OHT: outer horizontal target; CHT: central horizontal target. Image courtesy of S. Roccella and the DTT IVC-team.

flux at the targets, DTT will allow investigating the predicted role of B_T in facilitating the access to detachment.
- It is expected that the machine size and high B_T will favourably impact the compressibility of the impurity and thus its enrichment in the divertor.

Such findings should then be compared to experimental data from JT-60SA, JET, WEST, ASDEX Upgrade, TCV and MAST-U. With respect to SOL perpendicular particle and heat transport, DTT will be able to address the key point of the role of the ion vs. the electron heat channel and thus the regimes in which the empirical Eich scaling [46] dominates over the numerical predictions from the turbulence code XCG1 for the SOL power width λ_q [47].

The experimental programme will start with SN operation, as this is the current reference for ITER and the most accessible in terms of control after commissioning of the device. Further on, ADC will be used for parameter studies to access the various physics dependences related to perpendicular transport. In its course of operation, DTT shall attain the following milestones, in order to achieve the aforementioned goals:

- investigate heat flux mitigation techniques by strike point sweeping for machine protection, in line with establishing detachment control as the performance of the device is increased in terms of current, field and heating power;
- assess the accessibility to detachment by variations of fuelling and impurity seeding for various magnetic configurations, as these become available for operations;
- investigate various degrees of detachment from partial to full detachment and their impact on the choice of impurity levels and mixes on plasma performance;
- investigate the performance of various fuelling methods (supersonic molecular beam injection, pellets, regular gas valves) and the impact of their poloidal location;
- investigate the parallel heat flux to the divertor targets as a function of the magnetic configuration and topology;
- develop and establish reliable real time control methods for power and particle exhaust;
- access and retain detachment across the various phases of the discharge independently of the magnetic configuration, to assess the dynamic resilience towards a loss of power exhaust control;
- the high-priority study of small and no-ELM regimes compatible with exhaust solutions, as these are currently believed to be the most reactor relevant regimes. Such operational scenarios include the EDA H-mode, the QCE as well as the X-point radiating regime.

Furthermore, the use of Resonant Magnetic Perturbation (RMP) coils (3D effects) is foreseen in connection with the expected small λ_q to address ITER related issues of detachment under non toroidally symmetric conditions. A similar research programme can then be addressed with ADC, which can be implemented by moving the strike points, as illustrated in figure 10 for the most promising configurations, i.e. XD and NT.

Intensive plasma edge and SOL modelling with state-of-the-art codes has been carried out to guide the definition of the divertor design [48] and is now continuing [49] with the objectives of preparing experiments and identifying the most interesting scenarios, as well as the most suitable diagnostics that will be necessary for an efficient scientific programme. Particular attention was given to impurity seeding in various magnetic configurations, using the SOLEDGE2D-EIRENE combination of codes [50, 51]. Simulations show that seeding is necessary for detachment as foreseen for ITER. For DTT, Argon provides better performance both in terms of Z_{eff} and impurity concentration C_{imp}. The SN scenario allows detachment at full current with $Z_{eff} = 2.8$ and an impurity concentration $C_{imp} = 1\%$. DTT will be equipped with a divertor gas injection system, as traditionally used in tokamaks. Good pumping capacity in SN for both D and seeding gases is found in these simulations, while low seeding pumping is recorded for other divertor configurations.

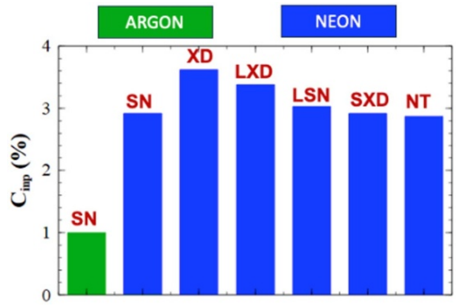

Figure 11. Simulated impurity concentration for various divertor configurations (see [48]) and argon and neon seeding.

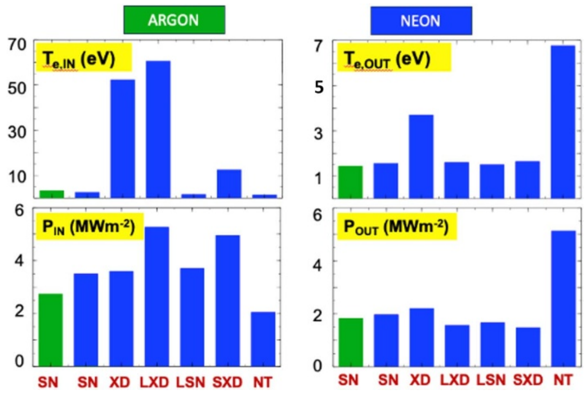

Figure 12. Simulated electron temperatures and power on the divertor at the inner and outer targets, for the same configurations as figure 11.

Figure 11 shows the simulated impurity concentration for various divertor configurations, including long-leg variants of SN (LSN) and XD (LXD) and another variant of XD (SXD) called super-XD (see figure 2 of [48]). Figure 12 shows the electron temperatures and the power on the divertor at the inner and outer targets. When detachment is achieved, the total power to the targets is < 6 MW m^{-2}, which is well below the maximum allowed for tungsten monoblocks (20 MW m^{-2}). Detachment is difficult at the IVT for XD and LXD configurations, as well as at the OHT for NT. Note that for the XD and LXD configurations the grazing angle is lower than for the SN (1° vs 1.9°). For this reason the parallel power flux is significantly higher, the inner strike point remains attached and the temperature is therefore much higher than for the SN case, which is fully detached. On the outer target the grazing angle is also lower (0.3–0.4°), however the strike point is still detached and the temperature remains low. Also note that the modelling was done without considering the effect of the drifts. It can be expected that with the drifts the density will increase on the internal target, thus reducing the plasma temperature perhaps to the detachment level.

The impact of ELMs on divertor erosion and the tungsten source from the divertor region in scenarios A and E was estimated using the ERO2.0 code [52]. The main assumptions follow those in [53]. During the intra-ELM phase, D ions with an incident energy equal to the expected pedestal-top temperature (1 keV) and with the magnetic field impact angle are assumed to impinge either only on the vertical target near the outer strike point or, as an extremely conservative case, on the entire outer target. The eroded W particles are then traced across intra- and inter-ELM phases. The poloidal cross-section distribution of the W density, normalized to the electron density (n_W/n_e), for the two investigated scenarios with the conservative ELM assumption is shown in figure 13. It is found that n_W/n_e is expected to remain below the 10^{-5} limit in the core region for both scenarios. Scenario A exhibits reduced screening capabilities on the horizontal outer target compared to scenario E.

As a risk mitigation strategy, DTT shall investigate alternative actuators and qualify their requirements for detachment control and during ramp-up. Candidate technologies are SMBI and micro shattered pellet injection, a novel first-of-a-kind approach. XPR configurations [54] have also been simulated (see figure 14) with the SOLEDGE2D-EIRENE code, showing that they can be attained with impurity concentrations ∼2% [49].

3.2. Far SOL physics and first wall loads

While the divertor is the most heavily loaded component in terms of plasma exhaust, the FW is also a key player for PWI, in particular during plasma ramp-up and ramp-down phases. As it represents a large surface with a poorer impurity screening efficiency compared to the divertor, it can also be a significant source for impurity core contamination during the flat-top part of the discharge, depending on the local plasma conditions. Those plasma conditions (in particular incident wall fluxes and energy) are not well defined at present, as the far SOL physics is complex and needs further investigation. The first wall also has to withstand transient loads due to off-normal events, such as disruptions or Vertical Displacement Events (VDE). Finally, during NBI operation at low plasma density and high injection energy/power, shine-through losses can affect a localized region of the FW opposite the injection port. Ongoing studies aim to optimize FW components located in this area facing the beam trajectory.

Optimizing the plasma ramp-up and ramp-down will be done in close connection with scenario development, taking into account the following constraints:

- minimizing flux consumption in the ramp-up phase to ensure a sufficient duration for the flat-top;
- avoiding MHD, in particular linked to the complex interplay with W transport and subsequent impact on plasma core profiles;
- avoiding plasma control issues (restricted l_i and β range).

As was shown in full W devices, restricting the limiter phase to a duration as short as possible and applying ECRH early in the discharge is key to ensure that the right target in terms of plasma conditions can be reached for the subsequent phase of the discharge. The following points are of particular interest from the point of view of plasma exhaust and PWI:

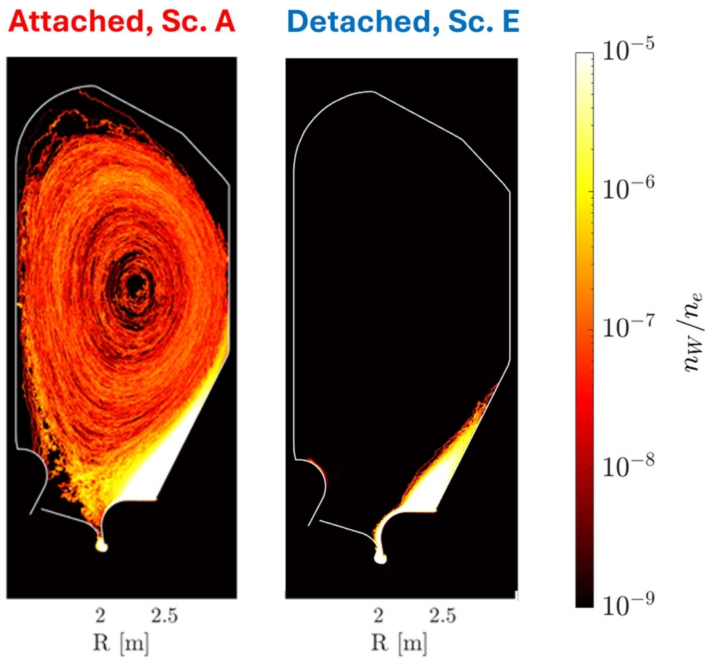

Figure 13. W concentration for scenarios A and E, computed by means of the ERO2.0 code.

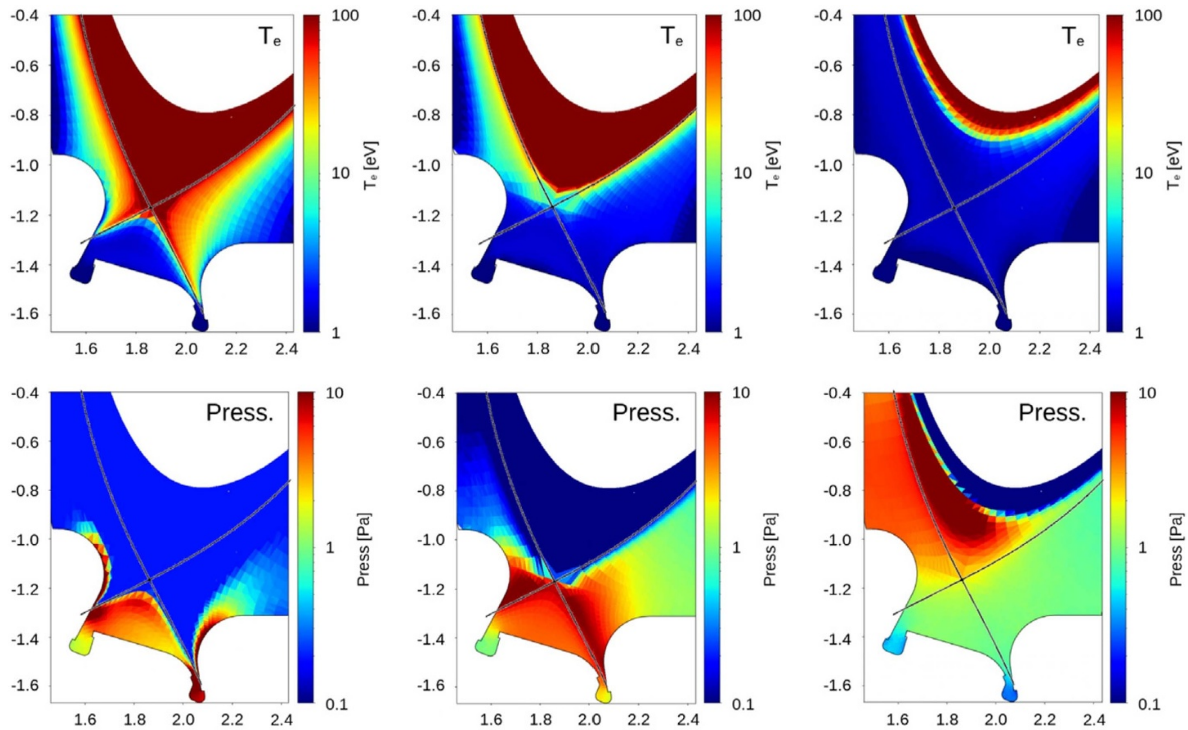

Figure 14. SOLEDGE2D-EIRENE simulations (from [49]). 2D plots of electron temperature (top) and total neutral pressure (bottom) in the divertor area. From left to right: initial standard detached case, XPR case and a case evolving to radiative collapse. Reprinted from [49], Copyright (2025), with permission from Elsevier.

- minimize W influx from the first wall to the plasma core during ramp-up/ramp-down and characterize first wall erosion and material migration during this phase;
- ensure acceptable heat loads on the first wall during ramp-up/ramp-down;
- assess the impact of boronization on the W influx from the first wall.

Next step fusion devices are expected to operate at high separatrix density/divertor neutral pressure in order to ensure plasma partial (or even full) detachment and stay within tolerable heat loads on the divertor. DTT will also have to stay in this regime (high density/partial divertor detachment) when operating at high power and will therefore contribute to progress in the understanding of far SOL transport in relevant conditions. The main items to be investigated include:

- characterization of the wall loads (from plasma, chargeexchange neutrals, radiation) and associated W erosion/migration during all phases of the discharge for the reference SN configuration (including the impact of ELMs) and overall in-vessel power and energy balance;
- characterization of the far SOL plasma and turbulent SOL transport at high separatrix density/divertor pressure for various scenarios (reference type I ELMy H mode, mitigated and ELM-free regimes), varying in particular the turbulent parameter α_t (defined in [55].), the fueling method (gas vs pellets);
- impact of the divertor configurations (reference SN configuration versus alternative configurations) on far SOL plasma and wall loads, as well as associated W erosion/migration;
- characterization of wall loads due to off-normal events (unmitigated/mitigated disruptions, vertical displacement events (VDEs), REs impact, etc).

3.3. PWI in a full tungsten environment

Tungsten is presently considered as the most promising plasma facing material for fusion reactors and has been chosen for the PFC of ITER, which will be a full-W machine.

DTT offers an outstanding opportunity to study PWI in a full W environment under relevant high power operation and investigate the behaviour of various divertor configurations in this regard. In addition, DTT will contribute to the validation of PWI codes for extrapolation to next step devices (e.g. for local and global W migration or fuel retention). Finally, DTT will be equipped with test divertor modules (TDM), allowing dedicated PWI studies as well as test of advanced materials and cooling schemes for the PFC.

More specifically, the following items will be investigated during the full DTT lifetime:

- *Wall conditioning.*

DTT is equipped with a variety of wall conditioning techniques of relevance for ITER: baking, GDC, standard boronization, ICWC, with also the possible use of EC Wall Conditioning (ECWC). Adding an impurity powder dropper could also be considered. The main research subject in this area will be the impact of boronization on plasma recycling (main fuel) and intrinsic impurities (tungsten and oxygen level in particular) during a campaign and defining the optimized boronization parameters/frequency.

- *W erosion and subsequent material migration.*

In order to understand and control W contamination, a significant part of the DTT research programme will be devoted to the quantitative evaluation of W gross erosion sources from main chamber and divertor and to W screening in the SOL, as a function of plasma regimes (from attached to detached divertor conditions, in L and H modes, with and without impurity seeding, ELMing or ELM free plasmas) and divertor configurations. The long pulse capability of DTT will also allow detailed studies of material migration and the structure of deposited layers (thickness, layer stability during operation/vents, composition, fuel trapping). All these studies call for the extensive development of a specific advanced diagnostic system (see section 4.3).

- *Fuel retention and recovery; dust production and removal.*

In full W devices using boronization as conditioning technique, as potentially contemplated for ITER, fuel retention is expected to be dominated by co-deposition with boron. DTT will complement the scarce database from present-day full W devices on this topic. Both particle balance, allowing assessment of fuel retention on a shot-to-shot basis, and post mortem analysis, providing campaign integrated results, will be performed. This will imply assessment of fuel retention, comparison of fuel recovery efficiency for the various techniques contemplated for ITER (baking/GDC/ICWC), assessment of dust production and characterization of the collected dust.

- *W morphology changes under plasma loading.*

W morphology modifications under plasma loading could lead to enhanced W erosion or degraded heat exhaust capability. DTT will provide an integrated test of components under relevant combined heat/particle plasma loads. The main research items in this area are related to assessment of W material properties changes under D plasma loading (blistering) and He operation (nanostructures, W fuzz) and under high power loading (W recrystallization, cracking, local melting).

- *PWI impact on machine protection.*

As DTT will be operated with actively cooled components, a reliable wall monitoring system is key to protect the integrity of PFC and avoid long shutdown periods in case of water leaks. Wall reflections and erosion/redeposition on the PFC, leading to strong local W emissivity changes makes infrared (IR) data interpretation challenging both for physics and for machine protection. Therefore significant experimental time will be allocated for testing machine protection schemes in the early phase of operation of DTT, as well as to set up a procedure to monitor W emissivity changes during operation.

3.4. Technology developments on PFC materials and components for first wall and divertor

The state-of-the-art PFC developed for ITER are currently the most challenging, since ITER decided to operate as full-W facility, but cannot be directly extrapolated to a power plant reactor. New plasma-facing materials and design concepts for components compatible to high neutron and particle fluxes are necessary in order to improve the performance and operation stability, as well as increase lifetime in view of future fusion reactors with high duty cycle and high fluence, equivalent to approximately five full-power burning years before components replacement is required. Such new technologies need to be qualified under representative fusion-relevant conditions provided by DTT, such as long pulse, high field, high power density and high plasma density. In particular, DTT complements the portfolio of metallic tokamaks in the international fusion programme and provides unique opportunities for the comparison of different concepts, materials and components in one reactor-relevant device next to the operation of ITER.

Key issues of plasma-facing materials to be addressed are:

- re-crystallisation of tungsten as refractory material with significant reduction in toughness
- narrow operation temperature range for copper alloys as heat sinks (about 250–350 °C for CuCrZr)
- high local stresses due to discrete material interfaces
- absence of self-healing properties

After testing and qualifying pure W-armoured PFC in WEST and the expected first ITER divertor operation, DTT shall be used at a later stage to test innovative concepts and accompany ITER research. DTT has the unique capability of providing a large area (hundreds of cm^2 in the divertor, and thousands of cm^2 in the main FW) specifically dedicated to material studies at reactor-relevant fluxes of heat and particles as well as at relevant impact energies and plasma conditions. Candidate advanced W-based armour and heat sink materials, and associated processes to be tested comprise the following list of currently most promising investigated materials for both the divertor and the FW:

- fibre-reinforced tungsten composites (Wf/W, Wf/Cu)
- tungsten alloys based on nanostructuring
- functionally graded materials (W/Fe, W/Cu) with optimised spatial fraction in order to minimise the local stresses under the plasma exposure
- self-passivating tungsten alloys (W-Cr-Ti, W-Cr-Y)
- porous tungsten (or other refractory material) as self-healing materials (W foam filled with lithium)
- thick tungsten coatings (plasma-sprayed W),
- 3D printed tungsten (latticed W)
- liquid metals (Sn) to prepare a liquid metal divertor solution.

The further development of these materials, or even new concepts emerging by the time of DTT availability, will have to be combined with thermo-mechanical simulations of plasma exposure (thermal transient and mechanical models also using optimization algorithms), cyclic heat flux testing of samples and strong interaction with material manufacturers to determine the characteristic material properties.

DTT will be equipped with long-term samples, to be integrated in the FW, as well as a sample manipulator for short-term exposure. Specially designed divertor and first wall test modules will be made available for dedicated campaign phases, offering the possibility to compare plasma-facing materials solutions under reactor-relevant controlled tokamak conditions next to each other. These experiments will bridge to the research in other laboratory experiments focusing on individual aspects of the qualification, such as high plasma fluence impact (linear plasma facilities), high repetitive heat flux impact (electron beam and ion beam facilities) or neutron-damage aspects (facilities in hot cells). They will close the gaps to the reactor conditions, which only in an integrated manner can be obtained in a magnetically confined reactor itself. An additional technology gap concerns electrical properties of insulating materials under reactor-like environment conditions. A particular aspect for such testing is the *in-situ* characterization of materials for insulation of plasma-facing components (as necessary for GDC electrodes and in-vessel sensors).

A combination of *in-situ* measurements, such as spectroscopy, IR thermography, laser-induced breakdown spectroscopy (LIBS), laser induced desorption spectroscopy (LIDS), and post-mortem analysis, such as Thermal Desorption Spectrometry (TDS), Nuclear Reaction Analysis (NRA), Secondary Ion Mass Spectrometry (SIMS), LIDS, LIBS metallography, as well as microscopy, such as Electron Backscattered Diffraction (EBSD) and energy dispersive spectroscopy (EDS), is necessary to characterize the materials and their evolution over the DTT operational phases.

Once the technology for building actively cooled components is developed with particular materials, an integrated component test has to be carried out. A key role for the confirmation of material choices on the level of a component will be played by the so-called Divertor Test Modules (DTMs). DTMs are cassettes, which are located at privileged locations, directly in front of the ports dedicated to the divertor remote handling at DTT. Therefore, the extraction and substitution of such modules will require the least amount of downtime of the device. Moreover, the divertor water system of DTT is designed to accommodate a dedicated, separated cooling apparatus for the DTMs, which can operate at the coolant conditions of pressurized water reactors (up to 250 °C, up to 15 MPa). The four DTMs are the main tool for integrated divertor materials and components testing in DTT.

Such testing can go from ´only material´ qualifications used for the PFCs, over embedded instrumentation (e.g. integrated in the manufacturing process by 3D printing), up to testing breaking technologies, such as liquid metals for PFC including different designs, but keeping the toroidal symmetry of the device intact.

The integral component testing in a DTM allows also studying joining techniques (e.g. stable joints between

/W/Cu/Steel) and manufacturing technologies. A promising novel approach is advanced manufacturing (additive manufacturing, laser sintering/melting, infiltration) which allows complex geometries and transitional structures with control of material microstructure. 3D printing is a potential method for low-cost production of shaped and optimized W components. DTT can act as an integrated test facility at the main chamber and divertor components for this technology, which has high potential to reduce the post-processing and shaping of monoblocks in order to avoid leading edges.

Another key objective of DTT is the testing of pre-damaged components, which is currently outside of the scope of present-day devices operating at high magnetic field. This will allow directly reaching defined and high damage and ageing levels, and to understand limits of acceptability by the impact different damage types have on the associated loss of performance (degradation of the armour material and energy extraction capability of the component). Analysing the evolution of such defects and their impact is crucial for the engineering design of the components for future devices towards improved lifetime. Many types of damage have to be applied to the components:

- artificial cracks (pre-cracked or damaged by melting events simulated by e-beam/laser/plasma loads),
- interfacial defects,
- irradiation damage simulated by using synchrotron-irradiation (30 MeV) and its combination with other pre-damaging,
- W ion self-damage or proton damage,
- He-induced damage and embrittlement,
- recrystallization (pre-recrystallized tiles and in-situ recrystallization),
- melting/solidification,
- misalignment,
- damage induced by thermal shocks and ELM-like loading (repetitive thermal cycles).

A complementary aspect to the characterization of pre-damaged components is their performance after repair (molten and solidified, laser repair, in-operando erosion/coating), in order to demonstrate the whole lifecycle of such a component. In this context, additional to ex-situ repair, DTT offers the opportunity to develop and test an *in-situ* repair system.

A second DTT divertor is also planned to be installed. The first divertor design in DTT is optimized for a SN configuration, but it is also compatible with a number of different magnetic equilibria (XD, DN, NT) at reduced maximal plasma current. However, DTT shall ultimately be used to operate the best performing optimized divertor solution. A roadmap for decision shall be included to give timely input. This needs to be correlated with the DTT divertor physics programme. According to the ITER Research Plan, a second divertor for ITER is foreseen after few years into the Fusion Power Operation (FPO) phase (DT operation). DTT can then be a test-bed for the technology of the second ITER divertor and its behaviour in a tokamak environment (PWI, toroidal shaping, assembly, thermal fatigue, etc).

The DTT PFCs come with a complex active cooling structure. It is a unique opportunity to develop detailed thermal and thermohydraulic models of the DTT plasma-facing systems. Both the (nominal) plasma operation and selected accidental transients (disruption with RE generation, …) will be investigated. For validation of the models, the numerical results of the predictions (temperature distribution, local melting of the plasma facing materials) will be compared to the measurements during DTT operation to validate (and if necessary improve/calibrate) the models. The validated thermal models will then be available for upscaling to power plant level, and deriving the correct cooling strategy.

In the present European first-of-a-kind reactor design, blanket modules are covered with actively cooled PFCs made with EUROFER97 as heat sink material and thin W as plasma-facing material. Such a design has been tested by manufacturing at medium scale only. DTT has the capability to install full-scale blanket modules (which have a toroidal extension of $\sim$1.5 m) if put along the poloidal direction. Therefore, DTT can be used as test-bed for the comprehensive validation of PFCs having such a dimension. It is therefore planned to utilize one single FW module as a test bed for a reactor relevant first wall mock-up. For this purpose, a dedicated cooling circuit shall be allocated to such a module, such as water-cooled lithium lead (WCLL) or Helium cooled pebble bed (HCPB). Due to the design choices that still have to be made, as well as the need of DTT to be at its full-power capabilities to provide the proper loading, such experimental campaign has to be planned in the later stages of Phase 3.

4. Heating, fuelling and diagnostics

For the DTT missions, a powerful and diversified heating and fuelling system is required, in order to inject 20 MW in the first phase and 45 MW at its full development, while keeping a plasma central density in the range of 2.5×10^{20} m^{-3}. The main characteristics, lines of development and items of the experimental work to be implemented in order to bring such systems to full performance, subject to the functional requirements, are summarized in this section.

4.1. Heating systems and associated research

Here the three DTT heating systems are briefly described and their relevance in the context of ITER and future fusion reactors is discussed. Connected subjects, such as commissioning procedures, related diagnostics and modelling are also addressed.

4.1.1. ECRH system. ECRH will be the primary heating system in DTT. Electromagnetic waves in the ECR range are very effectively coupled to the plasma up to the density cut-off of about 3.5 10^{20} m^{-3} in O1 propagation (fundamental Ordinary

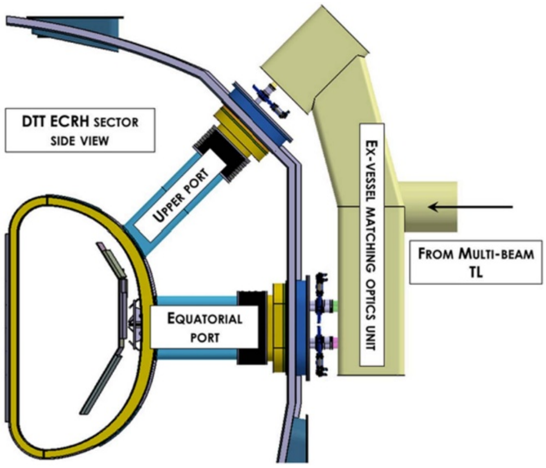

Figure 15. Side-view of a DTT sector housing the ECRH antennas.

mode) at 5.85 T and up to 1.7 10^{20} m^{-3} in X2 mode (second harmonic eXtraordinary mode) at half field operation of 2.9 T.

DTT will be equipped with the most powerful ECRH system before that of ITER, incorporating several cutting-edge technical innovations. Basic components of the systems are 32 gyrotron sources at 170 GHz of 1 MW each, arranged in clusters of 8 units fed by 4 main high voltage power supplies. The ECRH power can be modulated up to 5 kHz frequency. The 8 microwave beams of each cluster are transmitted by a first-of-a-kind multi-beam, evacuated quasi-optical transmission line to one of the four sectors dedicated to the ECRH launching systems. Each ECRH sector is equipped with 6 independent, plasma-facing launching mirrors located in the equatorial port and 2 in the corresponding upper port (figure 15). Each launching mirror is steerable in both poloidal and toroidal directions (figure 16) providing access and optimal absorption to the whole plasma core for power deposition and current drive [56]. The upper launcher has favourable access to the 2/1 and 3/2 rational surfaces and is mainly dedicated to the control of the MHD activity while the equatorial launcher is dedicated to heating and current drive for scenario access and the other tasks. The achievable steering range and the corresponding current drive efficiency are summarized in figure 17.

The flexibility of ECRH allows a wide range of applications in DTT, assisting the implementation of plasma scenarios along the whole discharge duration from start-up to termination and also for machine walls conditioning Electron Cyclotron Wall Cleaning (ECWC). The whole process of bringing to maturity the use of ECRH for the various, to some extent competing tasks is valuable for the preparation of the ECRH operation in ITER given the similarities of the two systems. DTT, as ITER and fusion reactors, will be predominantly an electron-heated device. A specific contribution that DTT can develop is the study of the indirect ion heating through the interaction with the electron channel at reactor relevant density. This is a key point in particular in the transients entering and leaving the phase of the discharge in which a significant amount of fusion power is expected in ITER and fusion reactors. The role of ECRH in a number of operational conditions and physics tasks can be summarized as follows.

- *Electron Cyclotron Wall Cleaning (ECWC)*

Short EC pulses (typically a few hundreds of ms per pulse) in He or D_2 plasma. O1 polarization (with toroidal injection angle ∼20°) or X2 (with perpendicular injection).

- *EC assisted breakdown*

Both the O1 and X2 absorption schemes for EC assisted breakdown can be adopted for the plasma start-up in DTT. In the first case, toroidally oblique launch favours the conversion of the unabsorbed O1 wave to X1 by an oblique reflection on the metallic surface of the inner wall. The diagnostics set for EC wall cleaning and assisted breakdown include a Fast camera, Thomson scattering, Interferometry, SPRED (survey, poor resolution, extended domain spectrometer in the vacuum ultraviolet range), Passive CXRS (chargeexchange Recombination Spectroscopy, in the visible range), RGA (Residual Gas Analyzer), EC stray radiation detector, pressure gauges, mass spectrometry, spectroscopy, Langmuir probes and magnetic probes.

- *EC assisted ramp-up*

Simulations have shown that balancing the ECRH on-axis and off-axis components of the deposition profile in the phase in which the current is ramped up (while the plasma density is rising) reduces the plasma internal inductance favourably, limiting the flux consumption. This optimization is also applicable for the plasma termination, counteracting the peaking of the current density profile [30].

- *EC heating and current drive in flat-top*

The allowed range of angles of the launchers permits to reach the whole plasma volume, from central to peripheral core plasma (ρ ∼ 0.7–0.8), with complete absorption. This will ensure bulk heating and core current drive (CD) for profile tailoring, and NTM mitigation in correspondence of the main rational surfaces. The maximum value of driven co-current is about 25 kA MW at ($\rho_{tor} \sim 0.1$) [57].

- *Sawteeth control*

Scenario E has a safety factor profile with a wide plasma region affected by sawtooth activity. Despite the wide flexibility of the ECRH system, reducing the size of the region affected by the sawteeth is only marginally possible in this scenario.

- *EC beam control at high density*

The density perturbations related to pellet fuelling have been considered to estimate the potential impact on the EC propagation and consequently the need of beam realignment to

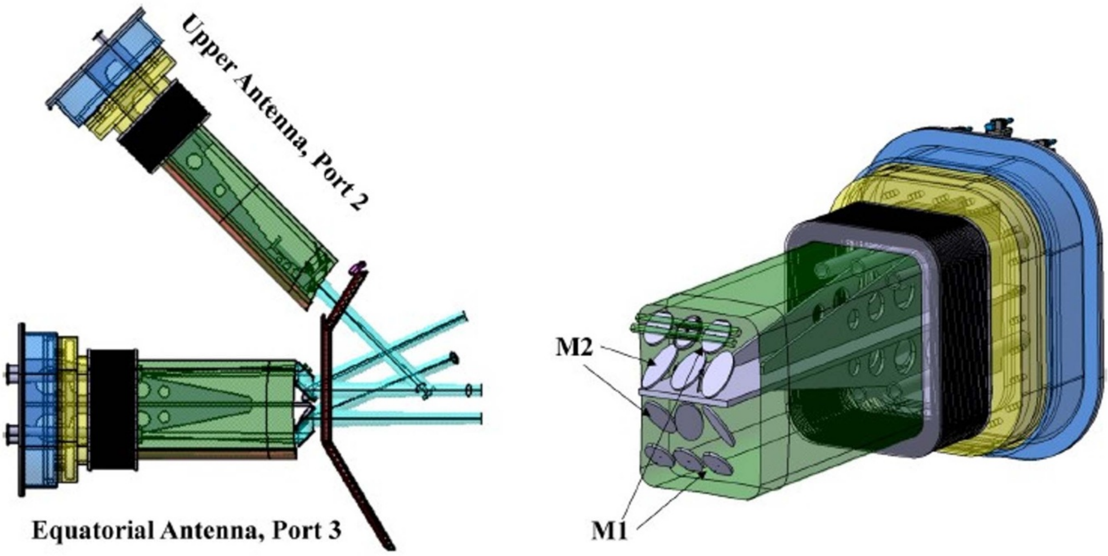

Figure 16. DTT ECRH system. Left: upper and equatorial antennas of a sector (left). Right: front of the equatorial antenna with mirrors M1 and M2.

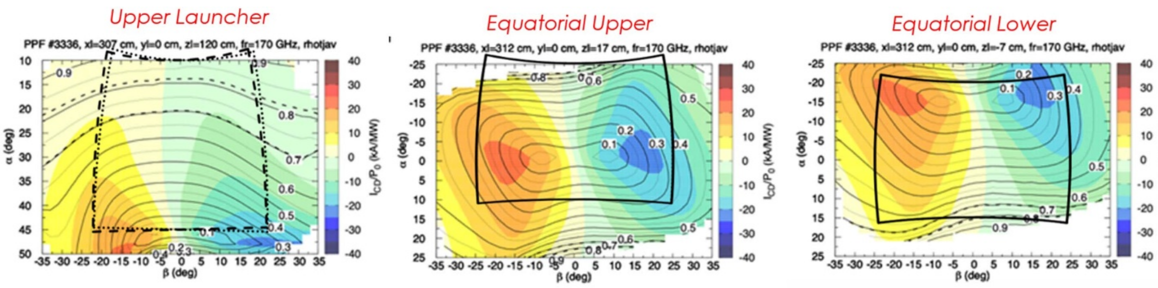

Figure 17. Current drive [kA/MW] efficiency for the DTT reference scenario E. Black curves represent the ρ_{tor} normalized radius, dashed lines the 2,1 and 3,2 magnetic surfaces. The mechanically accessible steering range of the ECRH beams is enclosed in the approximately rectangular area. α, β are respectively the poloidal and toroidal injection angles.

compensate for refraction around the 2/1 magnetic surface ($\rho \sim 0.8$). For the pellet size and frequency required for plasma fuelling (<1 mm, 16 Hz), no significant adjustments are required. Manageable adjustments of the EC beam aiming ($\sim 2°$) are required for larger pellet size [58].

- *Neoclassical Tearing Modes control*

Generalized Rutherford Equation (GRE) analysis shows that the uncontrolled 2,1 mode can grow up to $\sim$0.15 m, likely leading to disruption. Preliminary evaluations show that the mode growth can be controlled and even suppressed with 4–7 MW of ECCD, depending on the control approach (modulated or cw) and on the promptness of the actuator application.

- *Impurity control*

The beneficial role of core electron heating, particularly ECRH, in reducing the central accumulation of heavy impurities (W) has been experimentally demonstrated and is widely used as a tool to complement the control of the plasma scenario. An initial assessment of this effect in the DTT scenarios can be found in [26].

Simulation codes for beam propagation, power absorption and non-inductive current drive are well developed and validated tools, applicable in many plasma conditions relevant for most of the above-described tasks [10–15]. The exploitation of the ECRH capabilities implies the development of control schemes involving several diagnostics, including at least: equatorial ECE (fast radiometer and a wide-band spectrometer), fast density measurement for the control of the kinetic profiles, EC stray detectors for the optimization of the injection settings, magnetic probes for MHD control, and bolometers in the visible range for impurity control.

4.1.2. ICRH system. Ion cyclotron waves will be the main source of ion heating in DTT, an essential tool for wall cleaning in the presence of magnetic field and a key player for the production of energetic ion tails, giving access to regimes of interest for burning plasma physics. Up to 9.5 MW of RF power is intended to be installed in the reference heating mix of DTT. The foreseen frequency range extends from 60 to 90 MHz.

The DTT ICRH system [57] will be composed of 1 (min) to 3 (max) modules, the final choice to be taken during the initial

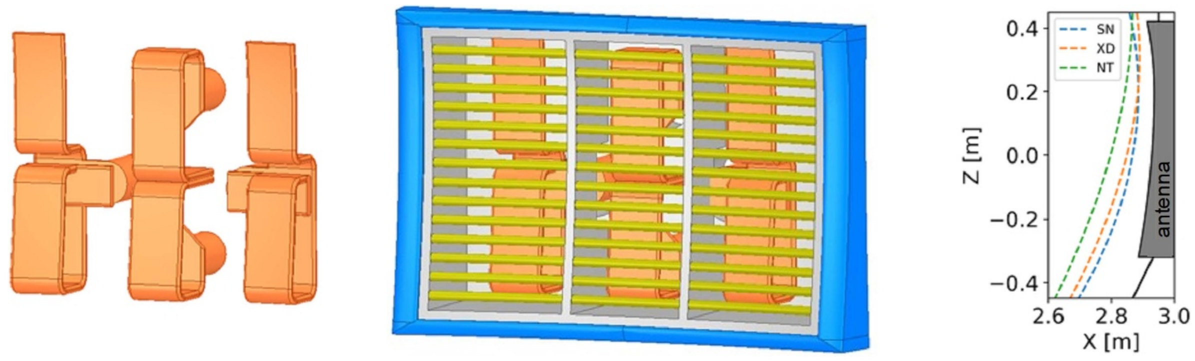

Figure 18. Present DTT ICRH antenna design: 3-strap structure (left), 3D view of the antenna in its antenna box with Faraday screen (middle) and qualitative side view of the front end of the antenna box with last closed flux surface for various foreseen plasma shapes (right).

experimental phase. Each module consists of four solid-state transmitters [58], two 4-feed, 3-strap antennas and an ELM-resilient matching scheme relying on external 3 dB hybrid couplers. Each module is expected to couple 3 MW to the DTT reference plasma scenario for 50 s every hour. During wall conditioning operations, a larger duty cycle of 1 h every two hours with a maximum coupled power of 200 kW was instead assumed [59].

The optimal design for the DTT ICRH launcher was found to be a 3-strap antenna with lateral folded straps and an end-fed centre-grounded central strap [60]. Figure 18 provides a sketch of the launcher. Optimized coupling is ensured through a (largely external) matching circuit with 3 dB hybrid couplers and impedance transformers, allowing to catch changes in the plasma load so that the power reflected to the generator remains modest at all times [61]. The antenna box as well as the straps are poloidally curved but not specifically tailored to any particular configuration. The mean antenna-plasma distance can be adjusted to enhance coupling both by moving the launcher radially and by modifying the plasma shape. Active cooling is mandatory to withstand the heat loads during entire full-performance plasma pulses.

Due to its flexibility, ICRH will be able to contribute to the DTT programme in a wide variety of ways. It can provide wall conditioning in between pulses and can be of help at the plasma start-up as well as plasma 'landing' (real-time controlled exit of H-mode of high-performance discharges). Exploiting antenna phasing not only allows coupling power but also transferring—modest—momentum into the plasma, which locally can impact the current density (current drive), MHD stability (pacing) or confinement (turbulence). Fundamental cyclotron heating remains powerful at low temperatures while harmonic heating is best suited for the high-temperature flat top phase; both can be optimized depending on specific needs [62]. For gaining insight into the role that fast ions populations play in influencing and steering MHD and turbulence, minority and trace-ion 3-ion heating schemes [63] offer options. Harmonic heating of majority ions or fast ion beams can also be exploited in the foreseen range of frequencies and fields.

Figure 19 illustrates key scenarios at full B_T-field. The left subplot provides the directly absorbed power fraction as computed by the 2D wave solver TORIC [64] for the standard minority heating scheme, either involving a H or a 3He minority at concentrations around 4%. The right subplot provides the single pass absorption for the 3-ion scheme using a 0.1% 3He trace as the third ion type immersed in an H + D mix, as obtained from a 1D wave equation solver TOMCAT [65]. Aside from its main role as a plasma heating technique, ICRH is instrumental in getting insight into the interplay between fast ion populations and plasma instabilities. As it requires a resonance condition to be satisfied, ion heating by RF waves is necessarily well localized, an effect that is routinely exploited experimentally. In particular to avoid the undesired excitation of NTMs by the violent crashes following fast particle stabilization of sawteeth: these crashes can be forced prematurely by pacing the RF power.

Given DTT's focus on exploring various plasma configurations to study divertor loads, ensuring optimal coupling will require closely monitoring the edge density (adopting e.g. a Li beam or reflectometry) and having means to actively or indirectly adjust it. Protection cameras should monitor hot spots and arc detection for safe operations. Ways to explore how impurity generation, due to the RF sheath effects, can be kept minimal will inherently be a sub-aspect of the DTT experimental programme; providing detailed insight requires the proper diagnostic tools (e.g. spectroscopy). The fact that RF waves boost the perpendicular energy of specifically targeted ion sub-populations requires dedicated fast particle diagnostics, but equally offers opportunities for learning how to control fast-particle-induced phenomena.

4.1.3. NBI system. NBI will be available starting from Phase 2 of DTT, to contribute to plasma heating, drive toroidal current, inject torque and generate a high-energy ion tail, which is of great interest for EP and burning plasma physics studies.

DTT will be equipped with a state-of-the-art NBI system, based on negative-ion acceleration up to 510 keV particle energy. This high injection energy is required for proper beam absorption at high plasma density, e.g. as foreseen in DTT reference scenario E SN and to study super-Alfvénic EPs (see

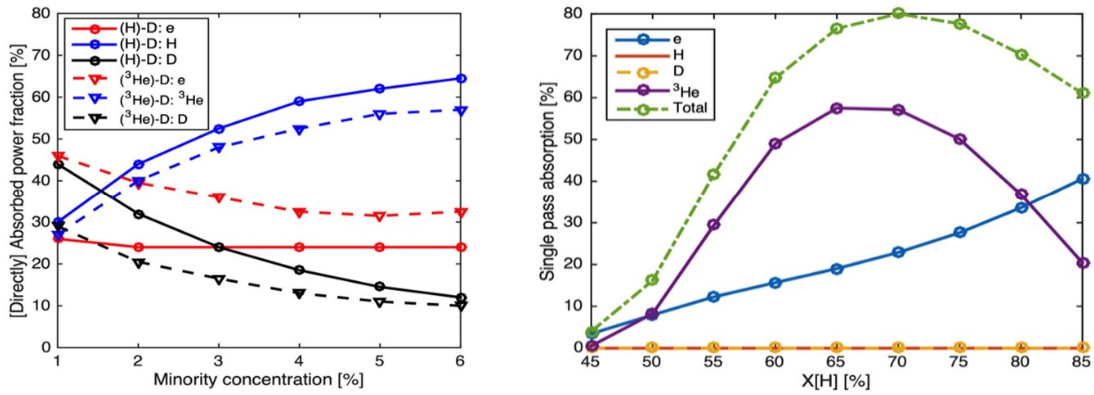

Figure 19. Example of the directly absorbed power fraction as a function of the H or 3He minority concentration in a D plasma for the standard minority heating scheme with minority concentrations of a few percent (left) and single transit absorption for the 3-ion scheme involving 0.1% of 3He as the trace ion in a H + D plasma (right).

section 5.3). The system [66, 67], sketched in figure 20, is designed to deliver ∼10 MW at full energy to the plasma, with horizontal, tangential injection (average tangency radius $R_{\mathrm{tang}} \sim 1.95$ m) in the same direction as the plasma current I_{p} to minimize trapped particle population and first-orbit losses. Absorbed power, shine-through, driven current and torque provided by the NBI system have been evaluated, as discussed in [68]. The presence of stray magnetic fields in the injector area will result in beam duct losses with a consequent slight reduction of the injected power to the plasma, and in the movement of NBI shine-through footprint on the DTT FW [68]. The beam can accelerate H or D ions and originates from a single injector featuring a single negative-ion source. To have an efficient coupling to the variety of plasmas that will be tested in DTT, especially in terms of density and shapes, DTT NBI will be capable of varying its injection energy in the range 10%–100% of the nominal value, with the associated injected power varying approximately linearly with energy in the range $E_{\mathrm{NBI}} \approx 250$–510 keV.

Although DTT does not envisage DT operations (except possibly Tritium trace experiments), high energy NBI will contribute to ITER-relevant EPs physics in fusion operation phases, which are expected to take place after the first DTT NBI operations. Synergy for NBI commissioning of high-energy, negative-ion based NBI system and first beam operations is also foreseen between ITER and DTT, exploiting the experience of JT-60SA, which will soon test 500 keV NBI. ITER-DTT synergy is particularly relevant due to several similar design solutions.

NBI-heated scenarios with dominant electron heating and low plasma rotation are relevant for studies of ITER and reactor heating conditions. The DTT range of magnetic field and plasma current, and the high-energy NBI enable the exploration of EP physics similar to those expected for ITER alphas, as discussed in section 5.3. Significant contributions to ITER are expected also for ionization cross-section validation at high energy, both in D and H. DTT is also an ideal framework to use, test and validate EP modelling tools. The installation in DTT of several EP-related diagnostics will also serve to the development of measurement techniques relevant for MeV-class ions in future reactors.

NBI will be able to contribute to most DTT scenarios, characterized by different magnetic configurations and plasma conditions, thanks to $E_{\mathrm{NBI}}/P_{\mathrm{NBI}}$ modulation capabilities. Depending on injection parameters, heating schemes, and plasma conditions, the electron/ion heating ratio and current-drive can be adjusted, and different EP distributions can be obtained. NBI in the reference *E* scenario is characterized, according to ASCOT Monte Carlo code [69], by a negligible shine-through fraction [67, 68], with relevant beam ionization in the outer part of the plasma. At nominal injection energy in SN plasmas, shine-through losses exceed 1% when plasma density is decreased below $1{\cdot}10^{20}$ m^{-3}. A first investigation in case of 1% of NBI shine-through (at nominal NBI injection power and energy) resulted in a peak heat flux of ∼0.5 MW m^{-2} on the FW.

For reference scenario E SN plasma, the population of beam EPs is formed mainly by confined passing particles (∼84%), with a small fraction of trapped orbits (∼15%). Stagnation EP orbits are found close to the magnetic axis (<∼1%). By decreasing the beam injection energy or increasing plasma density (and hence moving ionization position towards the edge), the fraction of passing EP orbits decreases and EP orbit losses, though rare, increase [68]. Even considering the presence of magnetic field ripple, orbit losses remain negligible for this scenario [70, 71]. The electron/ion heating ratio is approximately 60:40% for scenario E, with a current drive in the order of 0.2 MA (∼20 kA MW^{-1}, i.e. ∼$0.1{\cdot}10^{20}$ A Wm^{-2}). Lowering the injection energy to 250 keV, the driven current strongly decreases to ∼0.05 MA (also due to injection power reduction) and the power ratio to plasma ions increases up to almost 55%. Figure 22 (*a*) and (*b*) show typical power and driven current density profiles expected in the DTT SN-type plasma E, for two NBI configurations at different injection energy and power. The relevant ion heating ratio is due to the relatively high electron plasma temperature, which determines a significant contribution of EP-plasma ion collisions during the slowing down. This is seen in figure 22 (*c*), which represents the NBI EP distribution function for scenario E: the

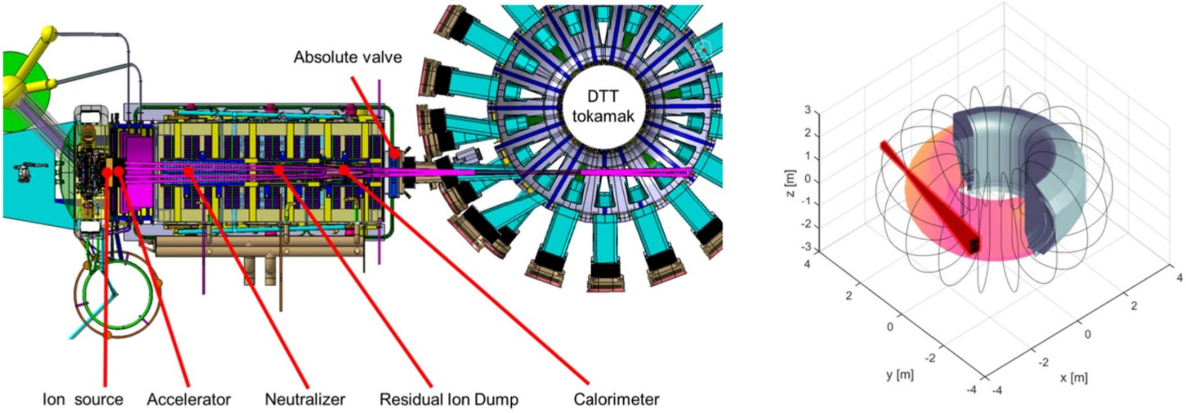

Figure 20. DTT neutral beam injection sketch.

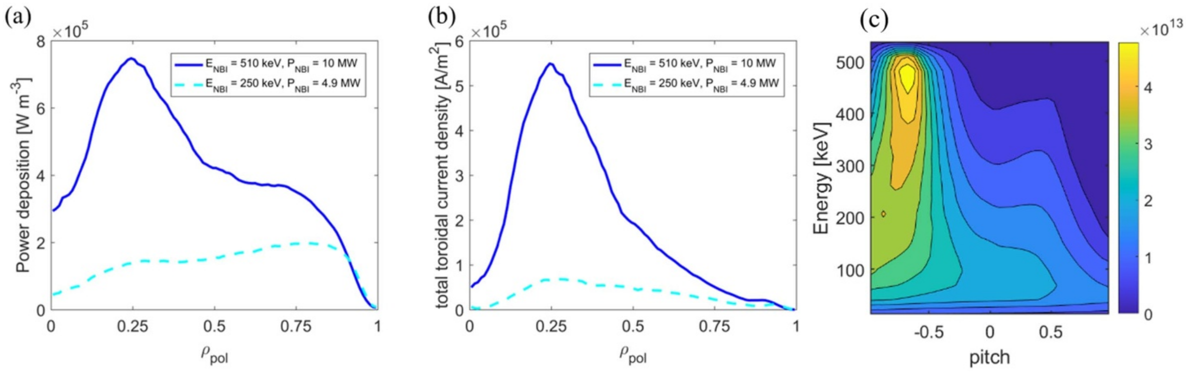

Figure 21. NBI deposited power (*a*) and driven current density (*b*) profiles in scenario E for two different NBI configurations. Panel (c) shows the volume-integrated, steady-state, EP distribution function at nominal injection parameters.

newly born fast ions, characterized by an almost tangential pitch close to -1, are rapidly subject to pitch-angle scattering at lower energies due to ion collisions. The possibility of variations in DTT of $E_{\mathrm{NBI}}/P_{\mathrm{NBI}}$, plasma density (and temperature due to different heating schemes) and synergy with ICRH open the possibility of studying a variety of NBI EP population distributions (see section 5.3).

To scientifically exploit NBI from the operational/physics point of view, several diagnostics are being designed, as mentioned in more detail in section 4.3. First of all, diagnostics are essential to monitor beam shine-through losses. IR cameras will be employed, and the use of thermocouples installed on PFCs is currently under evaluation. Other diagnostics then include FIDA (Fast-Ion D Alpha) for fast ion energy and density characterization, FILD (Fast Ion Loss Detector) and I-NPA (Imaging Neutral Particle Analyser) diagnostics for the characterization of fast ion losses, as well as a Time-of-Flight (TOF) spectrometer for fast ion (and neutron) energy spectrum measurements.

4.2. Fuelling systems and technology developments on matter injection

The particle injection systems in DTT serve various purposes: achieving the desired density and assisting in tailoring its profile, ELM pacing, injection of noble gas impurities for creating a radiative mantle protecting the divertor and massive gas injection (MGI) for disruption mitigation.

The main gas injection system is positioned in the midplane. The gas injection required for both main ion and impurity injection, excluding the MGI case for disruption mitigation, is about 200 Pa m^3 s^{-1} [72]. Mass spectrometer stations are used to monitor the residual gas and to detect vacuum leaks. The number of pumps needed for evacuating the DTT vacuum chamber depends on its total area, including ports and ICRH antennas. By allowing for the specific INCONEL 625 vacuum vessel (VV) and FW outgassing rate of 6.7×10^{-9} Pa m^3 s^{-1} m^{-2} at 100 °C, after all cleaning procedures, the effective pumping speed needed for pumping the torus down to a pressure $P = 1.33 \times 10^{-7}$ Pa is about 10 m^3 s^{-1}.

The pellet injection system is critical for the DTT experiment and therefore specific modelling was carried out in order to identify the design characteristics of the system and its flexibility (not only mass, speed and injection rate but also injection position and direction). Opting for independent pellet injectors for gas fuelling and ELM-pacing allows in principle a better coverage of the requirements for each task. Fuelling pellets need deep plasma penetration and mass deposition, while ELM pacing pellets require shallow penetration and smaller mass. In this respect, first analyses indicate that adequate fuelling (see figure 22) is only guaranteed for high field

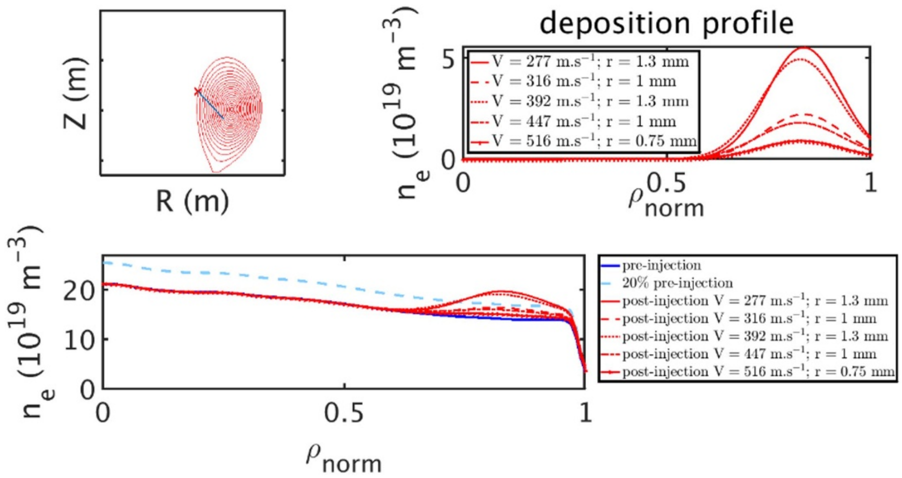

Figure 22. (*a*) Injection geometry, (*b*) deposition profile and (*c*) pre- and post-injection densities for a pellet injection.

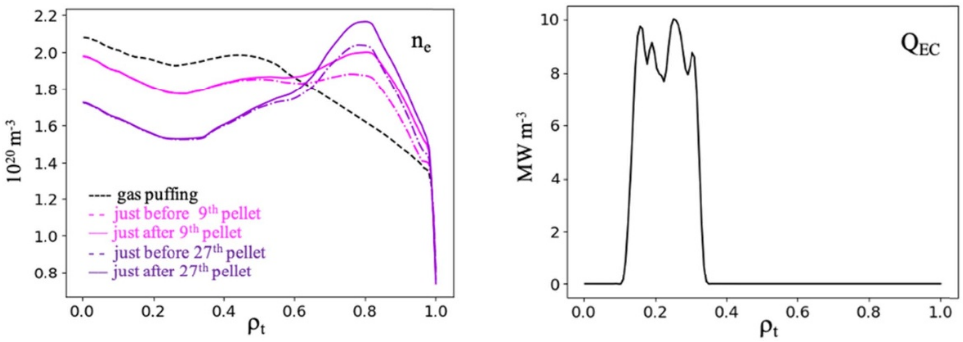

Figure 23. Left: electron density profiles as calculated by the simulations of the DTT full power scenario E with transport model QuaLiKiz, solving the transport equations up to the separatrix with pellet injection as fuelling method and with Ne as seeding gas. The temporal slices of the density profile just before (dashed line) and just after (solid line) the 9th (magenta) and the 27th (violet) pellet are represented. The density profile obtained by the corresponding gas puffing simulation is shown with the black dashed line. Right: EC power deposition profile, as used in the reference DTT full power scenario E. Reproduced from [25].

side (HFS) injection, exploiting the ∇B-drift motion for a technically acceptable injection speed. On the other hand, ELM pacing pellets can be injected both from the HFS and LFS (Low Field Side) of the machine, given the very small penetration required, but injection frequencies are critical in order to limit the energy due to stimulated ELMs. Note that injection frequencies are also important for the fuelling pellets in order to sustain the desired operation density profile.

A theory-based integrated modelling effort of the plasma response to deuterium fuelling in the flat-top phase (in H-mode) of the full power scenario E was performed using the 1.5D transport code JETTO with the quasilinear anomalous transport model QuaLiKiz for the core region [25]. It was found that the amount of neutral flux at the separatrix needed in order to sustain the desired pedestal density level with gas puffing is so large that the feasibility limits of the foreseen pumping system are exceeded, regardless of the type of impurity introduced, thus making the use of pellets mandatory. This result was confirmed by further integrated simulations performed with the transport code ASTRA with the quasilinear anomalous transport model TGLF [30], which indicated that gas puffing is suitable for the whole ramp-up phase (in L-mode) of the full power scenario, while pellet injection is required for the flat top phase (in H-mode). The simulations performed with pellet fuelling predict that the pedestal density is well sustained with realistic parameters for the DTT injector. The sustainment of the core density depends strongly on the EC power deposition width: a very peaked EC power deposition profile does not allow high density plasmas, which are required for the full power scenario (see figure 23), while broadening the EC power deposition profile permits to achieve the expected density (see figure 24). Negligible modifications of the EC deposition are found during a single pellet cycle and after several pellet cycles, indicating full compatibility between the EC system and the pellet injection system for the full power scenario.

Given the fact that HFS injection is mandatory for fuelling, the present design of the pellet injector assumes an injection line entering from port 3 and going around the vacuum vessel and then down the central column. This poses limits on the maximum sustainable injection speed to be around 500 m s^{-1} (or less, given the curvature of the line) and therefore either

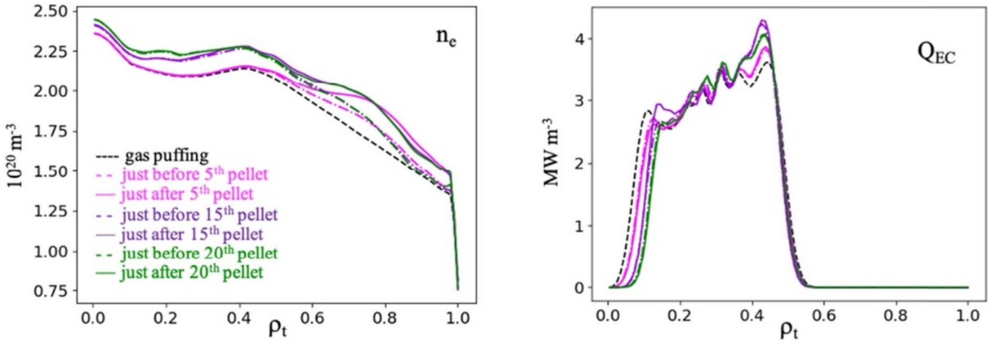

Figure 24. As in figure 23 for a broad EC deposition profile. Left: electron density profiles The temporal slices of the density profile just before (dashed line) and just after (solid line) the 5th (magenta), the 15th (violet) and the 20th (green) pellet are represented. The density profile obtained by the relative gas puffing simulation is shown with the black dashed line. Right: EC power deposition profile. Reproduced from [25].

a centrifuge or a pneumatic injector are technically viable options. A more detailed assessment of the required injection frequencies may still discriminate between the two solutions. SMBI systems are also being considered for fuelling, although operation at high density does not show significant improvement with respect to standard puffing systems, differently from low-density operation where they provide a valuable option.

Diagnostics requirements for fuelling systems can be split into two main aspects: pellet diagnostics and neutral gas diagnostics. As for pellet diagnostics, apart from the standard systems used to measure pellet mass (microwave cavity), velocity and fragmentation (optical barrier detectors), it will be fundamental to have fast cameras in order to detect the ablation cloud evolution and possibly Position Sensitive Detectors (PSD) to reconstruct the 3D pellet trajectory as well as the time evolution of the ablation cloud. As for neutral gas measurements, it will be important to measure neutrals pressure as an indication of gas recycling and PWI, by means of pressure gauges. These measurements will be also important to assess the performance of the divertor system and in this respect a Neutral Gas Analyzer (NGA) system will be installed to measure the evacuated gas under the divertor.

4.3. Diagnostic systems

The phasing of DTT diagnostic deployment closely follows the machine operational phases described in the Research Plan, as well as the requirements for machine protection and plasma control. While this classification is well consolidated for the initial high-level commissioning phase, it remains subject to further optimization for the progressive implementation of diagnostics in the subsequent operational phases [1]. Phase 1 comprises DTT First Plasma and early experimental operations, where a reduced amount of external heating power will be installed. As such, the diagnostic equipment planned for this phase is conventionally divided into two groups: a commissioning set, to support the high-level commissioning and early experimental phase, and a Phase 1 set, which will address the requirements of the Research Plan for the latter part of DTT Phase 1. DTT diagnostic capacity will then progressively evolve with the increase of external heating power to meet the research objectives planned for the subsequent experimental phases (Phase 2 and 3).

DTT is planned to start operations with a full set of systems for machine protection and plasma control, with all the in-vessel components already installed for the First Plasma. As the access to the VV will be severely limited after the assembly, all in-vessel diagnostic components must be installed during the assembly phase, even if they will not be employed during the commissioning. This approach is generally adopted to grant a smooth installation of the full diagnostic set, while properly addressing the integration constraints and requirements of the subsequent experimental phases. DTT metal walls and PFCs will be already actively water-cooled during the early operational phases [2, 45, 73]. These characteristics add to the already demanding constraints posed by the machine design and its relatively compact size, which require the diagnostics to be compatible with Remote Handling activities for maintenance, and narrow and crowded space for their installation. Additionally, all these systems must be able to withstand high thermal loads during plasma operations (maximum wall heat flux $\sim$0.5 MW m^{-2} [74]) and baking (maximum $T_{\text{baking}} = 200$ °C), as well as strong EC stray radiation ($\sim$0.5 MW m^{-2} from preliminary estimations) and high level of neutron fluxes expected during the high-power experimental phase [75]. To provide proper protection for diagnostics during plasma operations, grant homogeneous heating during baking, and ease the remote extraction for maintenance operations, some of the DTT ports (upper diagonal, equatorial and above divertor) are designed to host port plugs structures (figure 25) [76]. This section gives an overview of the current definition of DTT diagnostic equipment, which has evolved since previous publications [77], reflecting an extensive optimization process carried out in parallel with the consolidation of the DTT Research Plan and the progress in the design and integration of diagnostic systems.

4.3.1. High-level commissioning diagnostics (early Phase 1).

Table 3 lists the diagnostics planned to be installed during the Commissioning phase and ready for First Plasma. To fulfil its

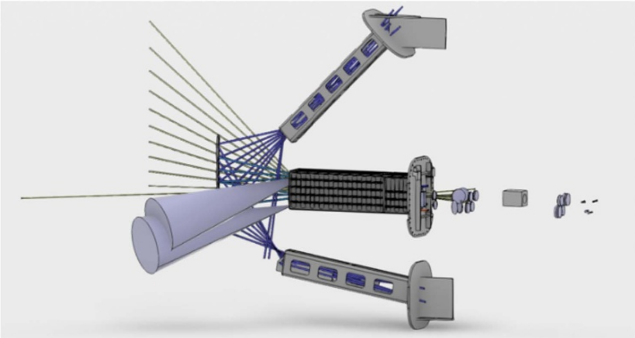

Figure 25. Render image of DTT Port Plug structures. The lines of sight of the vertical interferometer, also covering the divertor region, are visible (blue lines), along with the viewing cones of the visible spectroscopy system and the Z_{eff} Bremsstrahlung system (green lines).

mission of exploring advanced magnetic configurations, DTT requires a sophisticated and robust set of magnetic diagnostics to accurately control plasma current, plasma shape and vertical stabilization.

Furthermore, the DTT magnetic set is optimized to ensure machine protection and reliable plasma equilibrium from the beginning of plasma operation. The measurement of several quantities, ranging from basic plasma parameters (plasma current, loop voltage, plasma position, etc) to more advanced quantities (plasma perturbations, plasma shape, eddy and halo currents), is ensured by the magnetic diagnostic system. The DTT magnetic sensors equipment consists of about 1000 sensors installed internally and externally to the VV chamber, consisting of Bi-axial pick-up coils [78], high frequency printed sensors, saddle loops, flux loops, diamagnetic loops, Hall probes, fibre optic current sensors (FOCS), shunts and internal Partial Rogowski coils.

Through model-based iterative optimization, the system is designed to keep errors in plasma current reconstruction below 1% and errors in the current centroid position below 1 cm. Additionally, Bi-axial pick-up coils will be installed on the divertor cassette to provide data for the shape control to perform an accurate estimation of the position of the X and Strike point for advanced divertor configuration.

The Commissioning equipment includes several visible optical and spectroscopy systems (e.g. Visible D-α, Z_{eff}, Infra-Red, Visible Wide Angle and Fast Visible Cameras) for plasma breakdown detection and analysis. The IR camera system, carefully designed to meet the requirements for machine protection and measuring performance, plays a critical role during this early phase, as it will be used to monitor the surface temperature of plasma-facing components, allowing for the detection of abnormal heat loads and the validation of thermal limits under low-power conditions. SXR and VUV spectrometers [79] will be employed for radiation and impurity monitoring.

Thomson scattering (LIDAR configuration [80]) and ECE systems (Heterodyne radiometer and Michelson Interferometer) will be employed to probe plasma electron temperature, providing multiple benchmark measurements also for diagnostic commissioning, with the ECE system playing a particularly significant role due to its high temporal resolution and its strong impact on real-time plasma monitoring and operational control. Plasma electron density will be provided by a Tangential Interferometer and a Vertical Interferometer (with a reduced set of lines of sight during this phase). The former will be employed for the primary density feedback control, whereas the latter will serve as a secondary support and back-up measurement during this early operational phase. An SXR system, with a reduced number of lines of sight, is planned to provide further information on the position of the $q = 1$ surface, complementing fast ECE measurements, which allow a more direct localization through the observation of the sawtooth inversion radius. Additionally, bolometric cameras will be employed to measure the radiated power, with a reduced set of lines of sight to cover essential plasma regions. Both systems will evolve to provide a full tomographic reconstruction during Phase-1.

Although the neutron production will be limited during the commissioning phase Neutron Yield Monitors (NYM) are planned to be placed around the tokamak between the equatorial ports of sectors #1 and #2, #4 and #5, #10 and #11, and #15 and # 16 [81]. A subset of the neutron monitors with the highest detection efficiency will be installed and experimentally calibrated during commissioning (in-vessel calibration). This will ensure the availability of time-resolved neutron measurements and safety/interlock protocols since the early phase. It will also allow the full set of neutron monitors—including lower-efficiency detectors that require cross-calibration—to be fully operational and reliable once significant neutron production begins.

Similarly, the installation of the Neutron Activation System (NAS) is planned since the commissioning to monitor neutron production even in low-yield regimes and to validate/benchmark the MCNP (Monte Carlo N-Particle) models used, together with in-vessel measurements, for the calibration of the NYM [81, 82]. The system provides a robust, accurate and wide-range measurement of the time integrated neutron yield due to its proximity to the plasma and the possibility to optimize its efficiency by changing the mass of the activation foils.

Since significant amounts of REs are expected during commissioning and early Phase 1, one hard x-ray (HXR) monitor is foreseen at each of the four NYM locations for machine protection purposes. These detectors will measure the presence of REs through the bremsstrahlung radiation produced as the electrons interact with the tokamak structures, providing sensitivity to identify toroidal asymmetries in the emission, thanks to a relatively uniform toroidal coverage. Additionally, a RE imaging spectroscopy (REIS) system will be installed to detect in-flight supra-thermal electrons [83], providing a key diagnostic capability during the commissioning phase for the early characterization of RE dynamics and their spatial distribution, supporting machine protection.

4.3.2. Experimental Phase 1 diagnostics. Experimental Phase 1 diagnostic design and development follow the

Table 3. DTT high-level commissioning and early Phase 1 diagnostic equipment.

	Diagnostic system
Magnetics	Flux loops Saddle loops Biaxial & Monoaxial Pick-up coils Rogowski coils and Current Shunts Hybrid Hall probes High Frequency Pick-up coils
Scattering & Spectroscopy	Total Radiated Power Bolometric Cameras (partial configuration) Visible Spectrometer Survey & Z_{eff} Bremsstrahlung Visible D-alpha array SXR Sensors (partial configuration) VUV & SXR spectrometers Lidar Thomson Scattering
Interferometry & Microwave	Tangential Interferometer ECE Heterodyne Interferometer ECE Michelson Interferometer Vertical Interferometer (Partial configuration)
Plasma-Wall Interaction	InfraRed and Visible Wide-Angle cameras Event detection FAST Visible camera Langmuir probes & Fast Thermocouples Neutral Gas Analyzer & Optical Gas spectroscopy EC Stray Detection Bolometers & Sniffer Probes
Neutron, Gamma and Fast particles	Hard X-Gamma Ray & Neutron Yield Monitors Runaway Electron Imaging Spectroscopy Neutron Activation System

requirements specified in the Research Plan, mainly expanding the Optical diagnostic set capabilities (Edge and Divertor Thomson Scattering [84], CXRS, Interferometry and Microwave systems [85]), especially in the divertor region. A dedicated diagnostic set is deployed to investigate plasma-wall interaction, edge turbulence and divertor power exhaust, combining imaging and probe-based measurements (GPI, IR cameras, Langmuir probes), as shown in table 4.

The installation of a Diagnostic Neutral Beam Injector (DNBI) will be accompanied by a robust set of beam-based diagnostics to explore impurity and turbulent transport. A Charge CXRS system will provide DTT with radially and temporally resolved impurity ion temperature, density and velocity profiles, from which the $E \times B$ and radial electric field can also be determined. A Motional Stark Effect (MSE) diagnostic that measures the polarization of Balmer-α spectral lines emitted by the DNBI and, from that, the magnetic pitch angle, will be employed primarily to support equilibrium reconstructions codes. Interestingly, this system can also provide measurements of the local electric field fluctuations caused by microturbulence. Therefore, combined with magnetic and Faraday rotation diagnostics (Interferometer/Polarimeter), the MSE can be used to separate the contribution of the electromagnetic turbulence from the electrostatic. Besides, a BES (Beam Emission Spectroscopy [86]) system, along with the Turbulence Reflectometer, will provide additional measurements of density fluctuations and 2D imaging of turbulence and correlation lengths.

A Gas Puffing Imaging (GPI) [87] will be installed to perform turbulence imaging in the edge region and, along with a reciprocating Langmuir probe that provides measurements of floating potential and density fluctuations, will expand DTT turbulence probing capabilities in the SOL. Advanced studies of divertor configurations will be achievable thanks to a high-performance bolometric tomography system [88, 89], which, in its full configuration, will provide detailed maps of radiated power, supporting the development and optimization of divertor detachment scenarios, heat flux control, and advanced magnetic configurations. At the same time, additional IR cameras will be installed to measure the heat flux in the divertor, expanding DTT capabilities to investigate its power exhaust programme in that region. Besides, the planned embedded sensor configuration is designed to support the exploration of plasma–surface interactions and heat fluxes in the divertor. The visible spectrometer, essential during the commissioning phase, will be upgraded during this phase with an improved line-of-sight design, providing adequate coverage of divertor targets. This system is complemented by a Multi-Spectral Visible Imaging System and a VUV imaging divertor spectrometer, which expand the capabilities for spatially and spectrally resolved measurements of impurity radiation and plasma parameters, supporting the exploration of detachment and radiative cooling techniques.

The soft x-ray tomography will be upgraded during this phase, reaching its full configuration. Together with a high-resolution x-ray crystal spectrometer, which provides

Table 4. DTT experimental Phase 1 additional diagnostic equipment.

	Diagnostic system
Plasma-Wall Interaction	Divertor Infra-Red Cameras Gas Puffing Imaging Reciprocating Langmuir Probe Redeposition microbalance probes Sample Introduction System Laser Induced Breakdown Spectroscopy—Divertor Laser Induced Desorption Spectroscopy—Wall & Divertor
Scattering & Spectroscopy	Bolometric Tomography (full configuration/toroidal non-uniformity detection) SXR Tomography (full configuration) Visible Multi-Spectral Imaging System VUV Spectrometer Imaging Divertor X-ray Crystal Spectrometer Laser Blow Off Diagnostic Neutral Beam Injector Charge Exchange Recombination Spectroscopy Motional Stark Effect Beam Emission Spectroscopy Thomson Scattering External Edge & Divertor
Interferometry & Microwave	Vertical Interferometer/Polarimeter (full configuration) Divertor Interferometer Turbulence & Density Profile Reconstruction Reflectometry

additional ion temperature and plasma flow measurements to benchmark CXRS data, they will offer further insights into emissivity structures and impurity content.

Finally, impurity transport and material migration studies will be possible thanks to the installation of several laser-based systems (Laser Blow-Off, LIBS, and Laser-Induced Desorption Spectroscopy), along with Redeposition Microbalance probes and a Sample Introduction System. Overall, the Phase 1 diagnostic upgrade establishes a comprehensive and well-integrated framework for the investigation of transport, edge turbulence, and divertor physics, while laying the foundation for more advanced electromagnetic and fast particle studies in subsequent operational phases.

4.3.3. Phase 2 and Phase 3 diagnostics. Phase 2 and Phase 3 diagnostics (table 5) will be installed to probe advanced reactor-relevant scenarios that will become progressively available during the high-power DTT phase, i.e. after the installation of the NBI system (for Phase 2), and the full upgrade of ECRH and ICRH (29 MW and 6 MW, respectively) systems for Phase 3, providing DTT with a robust diagnostic set to investigate turbulence, electromagnetic activity, fast particle physics, and global plasma activity in an integrated environment.

The installation of a high-power NBI will open to the exploration of Fast Ions physics [67] with a FIDA (Fast Ion $D\alpha$) spectrometer that measures local fast-ion density, and a FILD (Fast Ion Loss Detector) system that detects fast ions escaping the plasma. Additionally, DTT Imaging NPA will provide detailed 2D energy and pitch-angle distributions of confined fast ions, complementing FIDA and FILD systems. A Neutron Gamma-ray (GR) Camera and TOF spectrometer [90] will complement neutron emission diagnostics, providing spatial and energy-resolved measurements to monitor fast-ion behaviour and heating efficiency in advanced configurations.

In this experimental phase, the DTT turbulence diagnostic equipment will be completed, further enhancing and extending the device probing capabilities. A Phase Contrast Imaging (PCI) will be installed to measure spatially and temporally resolved density fluctuation [91], granting access to a broad range of turbulence scales. This will give, among others, information on the interplay between TEM and ITG modes. The combination of these systems with the radially resolved ion flow measurements provided by CXRS, and thus the ExB shear and radial electric field, will significantly enhance DTT capabilities to investigate turbulence-driven transport across a wide range of plasma regions. At the same time, a dedicated set of diagnostics more specifically sensitive to electromagnetic turbulence will be installed, including Correlation and Imaging ECE systems (CECE and ECEI), that will be used to probe electron temperature fluctuations and reconstruct two-dimensional turbulence dynamics [92], providing access to electron-scale signatures of electromagnetic activity. These measurements complement the robust network of Bi- and Mono-axial pick-up coils, that directly measure magnetic fluctuations and are specifically optimized to capture the magnetic component of turbulence and MHD-related activity.

Electromagnetic activity and MHD stability will be further investigated through Toroidal Alfvén Eigenmode diagnostic heads and tangential soft x-ray imaging (GEM-based systems), complemented by high-resolution HXR spectroscopy to identify fast-ion driven instabilities and their impact on global plasma performance. At the same time, edge plasma and power

Table 5. DTT Phase 2/3 additional diagnostic equipment.

	Diagnostic system
Magnetics	Toroidal Alfvén Eigenmodes diagnostic heads
Scattering & Spectroscopy	Thermal He Beam Polarimetric Thomson Scattering Tangential GEM SXR Imaging
Interferometry & Microwave	Phase Contrast Imaging Correlation & Imaging ECE Plasma Position Reflectometry
Neutron, Gamma and Fast particles	Neutron Gamma-Ray Camera Time-Of-Flight Neutron Spectrometer HXR Spectrometers FIDA (Fast Ion D-α) FILD (Fast Ion Loss Detector) Neutral Particle Analyzer Cherenkov probe

exhaust physics will be further supported by a Thermal Helium Beam system, providing localized measurements of edge plasma parameters and contributing to the characterization of boundary transport regimes under high heat flux conditions.

A Cherenkov probe is planned to be installed during this phase to expand DTT runaway detection system set, providing measurements of in-flight supra-thermal electrons at lower energy compared to the REIS. An additional set of IR cameras will be installed during this phase, completing the machine protection diagnostic set while significantly enhancing the capability to investigate power exhaust physics. In particular, these systems will support the study of heat flux distribution, detachment scenarios, and advanced divertor configurations.

Finally, DTT will serve as an optimal testbed for testing and developing innovative diagnostic techniques. A Polarimetric Thomson Scattering (PTS) system [93] is planned to be installed and commissioned during this phase to probe T_e in high-temperature plasmas, where spectral Thomson and ECE systems often showed discrepancies [94], with the goal of providing an independent technique to benchmark T_e measurements above 10 keV. Besides, a Plasma Position Reflectometry (PPR) is being developed within EUROfusion collaboration projects. This system complements magnetic diagnostics as a monitor for plasma position and shape, providing real-time measurements of electron density profiles for plasma position control with a diagnostic intrinsically insensitive to neutron fluxes [95, 96]. This system is also able to locate Alfvén resonances and, as such, could provide critical information for the optimization of the Ion Cyclotron Heating. Consequently, an earlier installation, albeit limited, is currently being considered. It is worth mentioning that innovative systems such as the PTS and the PPR are expected to play a crucial role for next generation machines [97].

DTT diagnostics are being developed by ENEA under a collaboration agreement with the DTT Consortium, within the framework of DTT construction activities, and in synergy with EUROfusion activities, as well as with Italian research institutions and industry. With some of the systems already in the engineering phase (diagnostic set for magnetic measurements), and many others in advanced design, DTT is actively advancing towards the assembly and preparing for the machine commissioning and future experimental challenges.

5. MHD, Energetic Particles physics and theory developments

The ambitious scientific program of DTT, while primarily focused on heat exhaust research, can only be successfully achieved through the implementation of fully integrated core-edge scenarios that are robust against MHD instabilities and disruptions. This approach will leverage the properties of EP to attain performance levels relevant to burning plasma. Furthermore, achieving the research objectives of the DTT project will require a strong and innovative theoretical and modelling framework that guides and supports the experiments, playing a crucial role in their interpretation. This section outlines the planned research topics in the areas of MHD instabilities and their control, disruptions and runaways, EPs, and theoretical developments.

5.1. MHD instabilities and their control

The expected MHD instabilities in the DTT scenarios comprise internal kink modes (sawteeth), NTMs, ELMs, as well as infernal modes. MHD instabilities associated to a high β_N such as NTMs will be especially encountered in scenarios at reduced I_p and B_T (A, B and low-field variants of scenarios D and E). DTT will be equipped with two key actuators for MHD control: a powerful ECRH system (see section 4.1) and a set of in-vessel NAS coils shown in figure 26.

5.1.1. Ideal and resistive modes. Ideal and (classical) low-n resistive MHD stability studies have been performed [98] for the E (full power, SN) and A (SN) scenarios, in the PT configuration, using the CHEASE equilibrium solver [99] combined

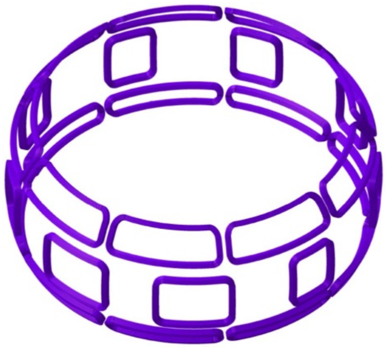

Figure 26. Simplified view of the Non-AxiSymmetric (NAS) coils.

with the MARS code [100], which solves the full MHD linear, resistive equations. When sawteeth are not included in the modelling effort, the $q = 1$ radius predicted by JINTRAC is quite large and the q profile is flat in the core with a low value. For example, ρ_{tor} $(q = 1) \approx 0.55$ (where ρ_{tor} is the square root of the normalized toroidal flux) and $q_0 \approx 0.5$ in the E scenario. This q profile results in a large, predominantly $m/n = 1/1$, internal kink mode being unstable. At higher n values, infernal modes are found in the E scenario, which may limit the achievable plasma performance. These are low-n to medium-n instabilities excited by the large pressure gradient combined with the low shear in the core. In the A scenario, infernal modes are stable due to the lower pressure gradient. For the E scenario, a sensitivity study with respect to q_0 and β was performed [98]. Unstable external kink modes were found, but only at values of q_0 or β far above what is expected from the integrated modelling, indicating that this scenario is not expected to suffer from Resistive Wall Modes (RWMs) (note that in their present design, the NAS coils would be too slow for RWM control). A sawtooth model was included in a set of JINTRAC simulations [26]. With a Kadomtsev complete reconnection model, a long sawtooth period (0.72 s) and large crashes ($\Delta T_e \approx 5.1$ keV) were found for the E scenario. However, JINTRAC simulations including an incomplete reconnection model [101] suggest that this will result in somewhat smaller sawtooth period and crash size. Predicting the sawtooth period is important because it has been found empirically to be related to the β_N value above which sawteeth trigger NTMs. For this reason, it is important to consider sawtooth control methods, such as sawtooth pacing. This could be done with ICRH (like, e.g. in JET), ECCD (like, e.g. in TCV) or even possibly with NBI.

In order to assess the stability and impact of NTMs in DTT scenarios and to evaluate the EC power required for their stabilization or suppression, the NTM module integrated in the European Transport Solver (ETS) [102] has been used. The NTM module solves the generalized Rutherford and torque balance equations to evaluate the NTM evolution in terms of its amplitude, frequency and phase. NTMs can be controlled/-suppressed by raising the current inside the island via ECCD. In DTT, upper EC launchers delivering up to 7.2 MW at 170 GHz with good current drive efficiency at the $q = 3/2$ and $q = 2$ magnetic flux surfaces will be available for NTM control [103]. These launchers will be steerable in real time and, thus, in principle, able to track the NTM position. As shown in figure 27, JINTRAC simulations for the E scenario find that a full suppression of the 2/1 NTM can be obtained by early ECCD intervention or using modulated ECCD in phase with the island O-point. Such early intervention is however extremely demanding for the control system, which should be sensitive to islands as small as 2–3 cm and able to provide phase detection for proper power modulation (feasible up to 5 kHz).

5.1.2. Pedestal and ELMs. The pedestal height and width used as boundary conditions in the integrated modelling of DTT scenarios discussed in section 2 have been obtained [104] using the Europed code [20]. Sensitivity studies have been performed, in particular with respect to the density at the separatrix, and a moderate effect on pedestal properties and global profiles was found [104]. It is to be noted that, given the high density at the separatrix, the E scenario might be in a Type II or small ELM regime.

ELM control with RMPs will be used in DTT, with strong relevance to ITER and future reactors. The RMPs will be produced by a set of three rows of nine NAS coils (a configuration close to the ITER one), shown in figure 26. The MARS-F code has been used to compute, in toroidal geometry and including flow, the resistive plasma response to different external fields with toroidal mode numbers $n = 1$, 2 or 3 [105]. The resonant components of external fields are found to be significantly screened in DTT reference full power scenarios, as shown in figure 28, with $n = 2$ and 3 being the most useful to trigger edge response. Conversely, $n = 1$ perturbations have stronger coupling with the plasma core and are likely less useful for ELM control. Depending on the number of active coils and scenario, coil currents between 20 and 40 kAt are predicted to be effective for ELM mitigation [105]. As discussed in [105], the DTT NAS system will allow slowly rotating RMPs, with a frequency up to 7 Hz, which will be particularly useful to avoid locked modes or control their location. The development of ELM control with RMPs during the operation of DTT will be part of the general development of H-mode scenarios discussed in section 2. ELM pacing by pellet injection may also be an option in DTT (see section 4.2). Besides active ELM control, an important research topic in DTT will be the development and study of small ELMs and ELM-free regimes, as discussed in section 2.

5.1.3. Error fields. Error fields (EFs), i.e. spurious magnetic field perturbations, shall be minimized in the phase of coil design and installation, as well as during plasma operation due to their detrimental effect on plasma performance. The NAS coils will be used for this purpose, thus acting both as ELM control coils and EF correction coils. Depending on the scenario, these tasks could be performed simultaneously by all NAS coils or with different dedicated subsets of NAS coils. EFs expected from manufacturing and assembly errors of DTT superconducting coils have been calculated using a stochastic procedure based on a linearized model and it has

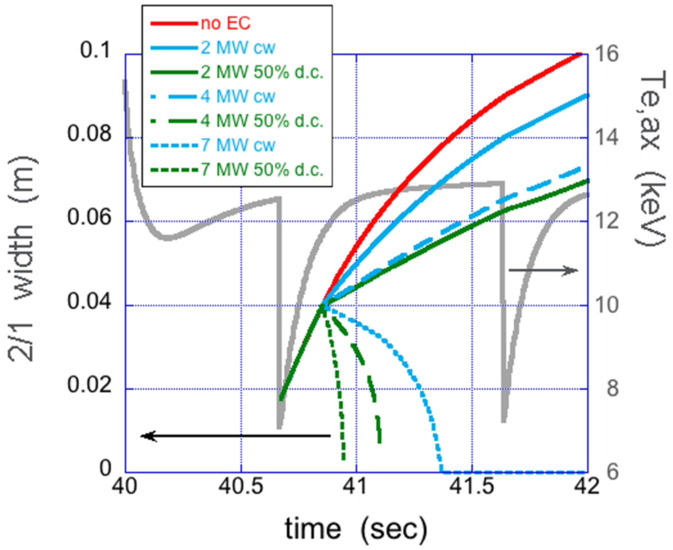

Figure 27. Prediction with JINTRAC + NTM module of the 2/1 island width evolution for different EC power levels (either steady [blue] or modulated [green] in phase with the O-point) in the E (full power) scenario. In grey line, the central electron temperature shows sawtooth activity with a period of around 1 s.

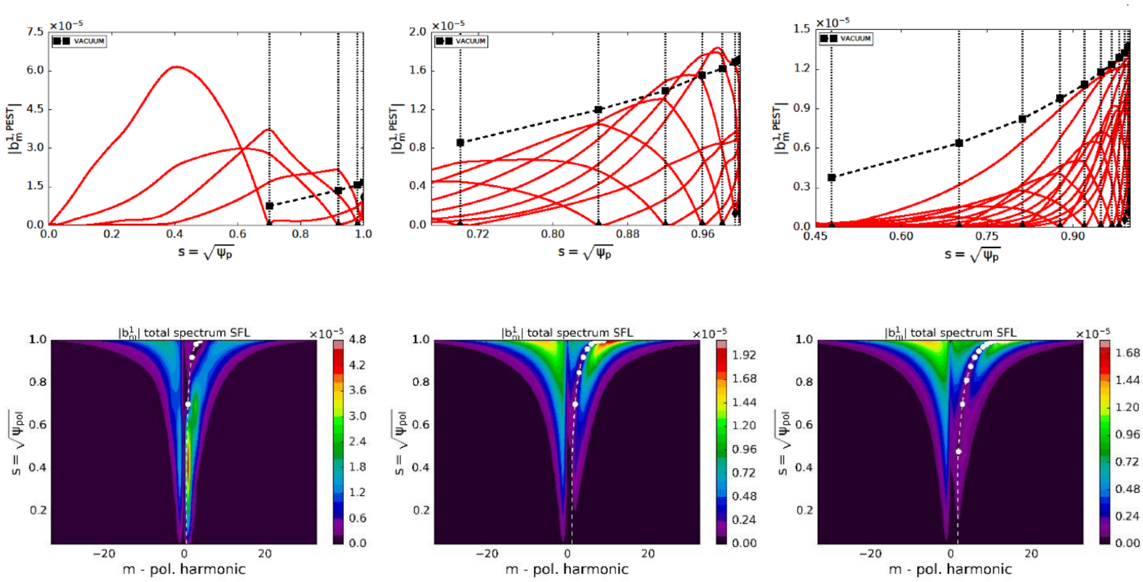

Figure 28. (Top) Radial profiles of plasma response harmonics for the first (i.e. radial) contravariant component of the perturbed field, compared to the vacuum field value at rational surfaces marked by black squares. (Bottom) From left to right, poloidal spectra of $n = 1$, 2, 3 unit-current perturbations from mid-plane coils.

been estimated that NAS coils currents of 50 kAt will be sufficient to correct the so-called 'three-mode error index' under 50 ppm with a 95% probability [106].

The presence of EFs will be assessed performing dedicated vacuum discharges and identification studies with plasma during the early operation of DTT. The main method that will be used is the novel non-disruptive compass scan method [107].

5.2. Disruptions and runaways

DTT will be a relatively large machine with large B_T and I_p in which disruptions will be an important issue. The DTT mechanical structures were designed to withstand ∼1000 full performance disruptions, assuming that half of them could be VDEs in the worst conditions [27]. The VDE control strategy for DTT is based on a plasma vertical stabilization controller [77] that stabilizes the vertically elongated and unstable plasma column by means of the in-vessel coils; this controller has in input the vertical velocity of the plasma centroid and the current flowing the in-vessel coils, and generates as output the voltage references for these coils. If needed, in order to avoid current saturation in the in-vessel coils, the superconductive poloidal field coils can also used as actuators for vertical stabilization. The global disruptivity (including minor and mitigated disruptions) expected in DTT, based on experience from present machines such as JET and ASDEX Upgrade, has been estimated as 30%, with unmitigated disruptions at full performance representing 20% of all disruptions, i.e. ~1000 events over the life of DTT. Thus, disruption mitigation is in principle not strictly needed in DTT as far as the mechanical integrity of the machine is concerned.

The thermal quench (TQ) and current quench (CQ) characteristic times have been estimated according to scalings defined in [108]. This led to a minimum linear CQ duration of 4 ms. Much longer CQ durations (40 ms) have also been considered based on observations of unmitigated disruptions in tokamaks with metallic walls. These could imply larger ElectroMagnetic (EM) and thermal loads due to larger and longer lasting halo currents.

During the operation of DTT, disruptions will be monitored, in particular in terms of their TQ and CQ timescales, as well as induced and halo currents (measured by Rogowski coils and shunts) and mechanical loads (measured by strain gauges, possibly including optical ones).

Disruption prevention and avoidance is a key topic for ITER and future tokamak reactors, in which disruptions will have to be exceptional events or even completely absent. Thanks to its resilience to disruptions, DTT may act as a testbed for disruption prevention and avoidance algorithms and strategies, in particular those under development for ITER. 'Disruption prevention' means controlling the plasma in such a way that no critical limits are overcome. This will be addressed with the help of closed loop plasma scenario simulations, including a modelling of the Plasma Control System (PCS). In DTT, the development of disruption prevention schemes may concern in particular the ramp-up phase and involve tailoring the current density profile by additional heating, as well as the ramp-down phase, possibly attempting to delay the HL back transition as tested at JET [109]. 'Disruption avoidance' means exception handling (EH); i.e. being able to react adequately in case a critical limit is overcome (in spite of disruption prevention attempts) or an unforeseen event destabilizes the plasma. The DTT PCS will include EH, following the guidelines used for ITER, but with reduced complexity. Furthermore, DTT will present similarities with ITER in terms of its actuators (in particular ECH and the NAS coils) and of the metallic wall, providing a good testbed for ITER disruption avoidance strategies. For example, DTT will be able to test strategies to react to an excess of impurities or to a breach of H- or L-mode density limits [110], and to test the joint use of ECH and NAS coils in case of mode locking. In addition, the above-mentioned closed loop plasma scenario simulations may be used to develop fast plasma shutdown strategies.

Like ITER, DTT will be equipped with a Disruption Mitigation System (DMS) based on the Shattered Pellet Injection (SPI) technique. Also in this area, DTT may act as a companion to ITER on which the tools pre-selected for ITER could be deployed and tested. The DMS will be triggered when an unavoidable disruption is predicted. This will require implementing a disruption prediction algorithm. The DTT SPI system will comprise two (optionally four) multi-barrel injectors in two toroidally opposite upper oblique ports. From the maximum total plasma thermal energy of around 14 MJ (including fast ions), it has been estimated that 10^{23} atoms per pellet are appropriate, corresponding to cylindrical pellets of diameter ≈12 mm and length ≈18 mm. The injection velocity is foreseen to be greater than 300 m s^{-1}, leading to a flight time well below 10 ms. The option of an additional MGI system is considered for operation before the commissioning of the SPI system.

Several tokamaks have performed SPI experiments in recent years, but none has used SPI as a routine DMS, in contrast to what is planned for DTT and ITER. The use of the DMS in DTT aims at minimizing risks related to mechanical fatigue as well as a possible degradation of the PFCs. Concerning the general physics of disruptions, with its high I_p and B_T relatively to its size (which, among other effects, results in a high Greenwald density limit), DTT will produce valuable data to test disruption models in an unusual range of parameters. DTT will also allow investigating the physics of disruptions in NT configurations, which may be of interest in relation with possible NT reactor design studies. Finally, in a late phase of operation DTT may allow assessing how liquid metal divertors cope with TQ heat loads. Such divertors might indeed prove much more resilient than solid divertors, which would relax the requirement of mitigating TQ heat loads.

REs are probably the most concerning disruption-related issue for ITER and future tokamak reactors. Once these machines are activated, unavoidable RE 'nuclear' seeds combined with an avalanche amplification by many orders of magnitude may produce multi-MA RE beams even in mitigated disruptions, which represent a large risk of causing important damage [111]. It is not clear whether natural disruptions will produce RE beams in DTT. The use of a full W wall may lead to rather slow CQs, which tends not to promote RE generation, as observed at JET [112]. On the other hand, DTT will operate at higher I_p and B_T than JET, which promotes RE generation. JOREK [113] simulations suggest that, while RE production should be small in the A scenario thanks to the relatively low I_p (2 MA) [114], the E scenario will be much more RE-prone due to an avalanche gain of $\sim 10^5$ associated to the large I_p (5.5 MA). If RE beams turn out to occur in natural disruptions, it is likely that they may be avoided in SPI- or MGI-mitigated DTT disruptions. Recent experiments in several devices (e.g. ASDEX Upgrade, COMPASS, DIII-D) have shown that the application of NAS fields may reduce the RE current, which can be of interest to ITER as a complement to SPI and can be tested on DTT. On the other hand, if natural disruptions do not produce RE beams in DTT, a recipe to produce such beams should be developed as a pre-requisite to experiments on RE mitigation. This recipe would typically involve the massive injection of impurities (e.g. Ne or Ar) in the form of either gas or shattered pellets.

Since the generation of multi-MA RE beams seems very difficult to avoid in ITER and future tokamak reactors (during the nuclear phase of operations, at least), mitigation of and/or resilience to RE beam impacts is a crucial topic for these machines. Concerning ITER, it is hoped that H_2 SPI into RE beams will lead to a benign termination, as observed in present devices [115]. DTT will offer the possibility to further test this key strategy, which would be of high interest to ITER, in particular during Phase 1 of the DTT operation and at high I_p. Concerning the European first-of-a-kind reactor design, the current strategy for resilience to RE beam impacts is based on sacrificial limiters. Design studies regarding possible sacrificial limiters in DTT are ongoing.

Two diagnostic systems are planned to measure bremsstrahlung radiation from REs in the HXR/GR energy range, meant to be available respectively for Phase 1 and Phase 2. The Phase 1 system is a set of four HXR/GR detectors using BC-509 liquid scintillator at different toroidal positions in the torus hall. These will be complemented, at each position, with one neutron monitor using NE213 liquid scintillator and one GR monitor using a sodium iodide NaI (Tl) inorganic scintillator.

5.3. Energetic Particles physics studies

A significant focus of the DTT research mission is studying 'core-edge integration' with different plasma shapes at ITER and reactor relevant parameters. In these conditions, DTT is expected to generate energetic ions through various methods, such as NBI (Negative NBI) and ICRH. These energetic ions are anticipated to interact with Alfvén waves, including Toroidal Alfvén Eigenmodes (TAEs) and Reversed Shear Alfvén Eigenmodes (RSAEs) [116, 117], among others.

Because of the weak similarity scaling approach considered in designing the device [118] (see section 5.4), the supra-thermal ions in DTT are characterized by typical dimensionless orbit widths that are expected to be similar to those of burning fusion plasmas and are generally smaller than in present-day devices (the dimensionless orbit width of the supra-thermal ions is defined as the characteristic Larmor radius or magnetic drift orbit size normalized to the machine size). Furthermore, the ratio of supra-thermal ion speed to the Alfvén speed in DTT is comparable to what is expected in ITER, ensuring that the strength of EP drive of Alfvénic fluctuations via wave-EP resonant interactions is qualitatively and quantitatively the same. Furthermore, the spatio-temporal cross-scale coupling between core turbulence and Alfvénic fluctuations is preserved thanks to the choice of the thermal plasma dimensionless orbits and the plasma β. Owing to these similarities in dimensionless parameters and plasma properties, the integrated physics behaviours of DTT plasmas are expected to be similar to those anticipated in ITER and will be reactor relevant. As a consequence, the Alfvénic fluctuation spectrum in DTT, resonantly excited by EPs, is expected to be characterized by toroidal mode numbers (n) of the order of 10, which is similar to what is expected in reactor-grade plasmas [119].

In burning plasmas, EPs play a peculiar role as mediators of cross-scale couplings [120, 121]. The DTT high performance plasmas can be divided in an inner core region, characterized by weak magnetic shear and low-frequency Alfvénic activity, and an outer core region, with typically finite magnetic shear and dominated by radially extended TAEs, as discussed in [117]. As predicted by theory and numerically verified, the interlink of these two regions is crucially affected by the q-profile. The q-profile not only controls the linear stability and structure of the fluctuation spectrum but also influences the nonlinear saturation mechanisms and ensuing transport.

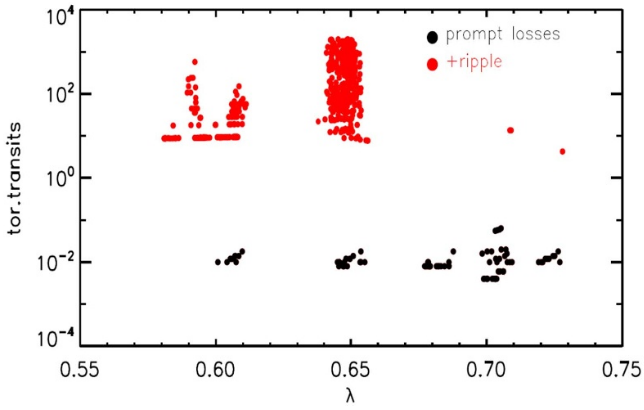

Figure 29. Loss times of ions with 510 keV energy as a function of pitch $\lambda = v_{\parallel}/v$. Run with $N_p = 106$ particles and toroidal turns $N_{tor} = 2000$. Red dots are losses occurring only in simulations with ripple, black dots also in those without ripple (prompt losses).

Prompt losses and ripple induced losses of EPs produced by negative NBI have been simulated with the Hamiltonian, guiding centre code ORBIT [122]. In the case of a beam at 510 keV and injection angle with respect to the FW of 40°, these losses were estimated to be, respectively, ~0.01% and ~0.07% [70, 71]. Numerical simulations with 10^6 fast ions [71] have shown that the vast majority of the losses are due to a ripple-resonant mechanism for particles with pitch (defined by $v_{\parallel}/v$ with $v_{\parallel}$ the parallel velocity of the particle with respect to the magnetic field and v the module of the velocity) $\lambda = 0.6$ and 0.65; such a behaviour is consistent with the theory of ripple-precession resonance (see figure 29). It should be noted that both the prompt and the resonant losses scale with the orbit width of the considered particles ($\Delta \sim q\ \rho_L$ for the far passing beam ions, and $\Delta \sim (2\ R/r)^{1/2}\ q\ \rho_L$ for the banana-trapped fast ions, with q the safety factor, ρ_L the Larmor gyroradius of the fast ion, R the major radius and r the minor radius). Thus, because of the safety factor dependence, both losses are reduced when plasma current is increased. These losses could result in hot spots on the FW. The maximum power load P_{max} in a hot spot is estimated to saturate at a value of $P_{max} = 63$ kW m^{-2} which is within the tolerance of PFC of the FW and negligible compared to the power flux of thermal particles on ICRH antennas, designed to withstand 2.5 MW m^{-2}. In addition, it is known that TAEs can interact with the ripple, which could in principle enhance fast ion losses in DTT experiments.

Super-Alfvénicity of the neutral beam will be necessary to mimic the EP physics of ITER. Roughly speaking, this would require that the ratio between the transit frequency of the EPs $\omega_{t,EP}$ and the Alfvén frequency ω_A, which scales as $\omega_{t,EP}/\omega_A \sim v_{th,EP}/v_A$, lies within the TAE and EAE (elliptical Alfvén eigenmodes) gaps (here $v_{th,EP}$ and v_A are, respectively, the thermal velocity of the EPs and the Alfvén velocity). The present choice of 510 keV NBI is marginally super-Alfvénic, and interesting operation for DTT from this point of view

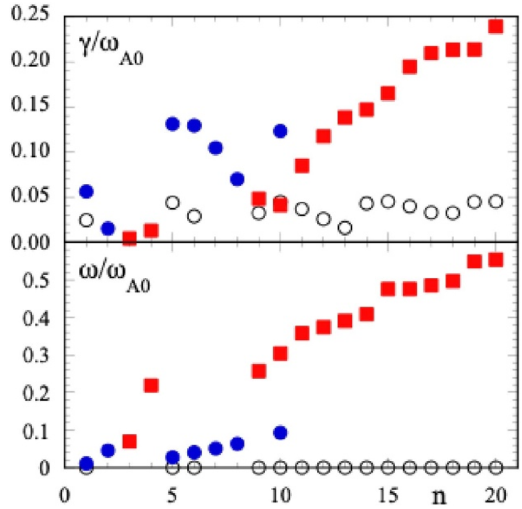

Figure 30. MARS and HYMAGYC results for a model full power DTT SN equilibrium: growth-rate (top panel) and frequency (bottom panel) vs. the toroidal node number *n*.

will require full exploitation of the machine performances (full plasma current and core plasma density, e.g. at fixed Greenwald fraction, and full magnetic field in order to maintain constant ρ_*, the dimensionless orbits).

Preliminary studies of linear stability of Alfvénic modes driven by a population of EPs have been carried out for the full power scenario using a *model* SN equilibrium: a Maxwellian distribution function has been assumed, with constant EP temperature (450 keV, somewhat lower than the nominal 510 keV), ITER-like EP density profile, major radius $R_0 = 2.09$ m and $B_0 = 6$ T. The study uses the code HYMAGYC (HYbrid MAgnetohydrodynamics GYrokinetic Code) [123], suitable to analyse EP-driven Alfvénic modes in general high-β axisymmetric equilibria, with perturbed electromagnetic fields fully accounted for. Several EP-driven modes have been found. In figure 30 the growth-rate and frequency (both normalized to the on-axis Alfvén frequency ω_{A0}) vs the toroidal mode number n, in the range $n = 1$–20, are shown. Infernal-like modes driven by EPs are shown using blue filled circles, and EP-driven Alfvénic modes are shown using red filled squares; results for purely ideal MHD modes are also given by black open circles. An internal kink mode ($n = 1$) and several infernal modes ($n \geqslant 5$), radially located within the $q = 1$ surface and in correspondence with the q-rational surfaces, are observed. The growth-rate for the EP-driven modes has its maximum for $n \geqslant 17$. In figure 31 the power spectra from two simulations considering, respectively, the toroidal mode number $n = 5$ and $n = 18$ are shown in the (s, ω) plane, where s is the normalized radial-like coordinate, and ω is the frequency. In the left frame, an infernal-like mode ($n = 5$) is shown: compared with ideal MHD results (see figure 30), the EPs contribution further enhances the growth-rate of the mode, while real frequency and radial location remain similar. In the right frame, an EP-driven mode (EPM) ($n = 18$) is clearly observed, with its real frequency located slightly below the toroidal gap and its radial location close to the position where the EP local drive is maximum ($s \approx 0.4$). The Shear Alfvén and magneto/acoustic continua, as calculated by the FALCON code [124] are superimposed: larger and darker symbols refer to Alfvénic oscillations, while smaller and lighter ones to ion sound waves.

Simulations with ORBIT of EP losses for the beam at 510 keV with ripple and with two TAE modes ($n = 10$ and $\omega = 245$ and 305 kHz) show a nonlinear interaction between the modes and the ripple: losses increase from 0.07% (without TAEs) to several percent (with TAEs), meaning that anyway the majority of injected fast ions remain confined in the plasma by the end of the simulation [125]. This increase of EP losses is also consistent with a ripple-resonant mechanism: the TAE waves determine a collisionless diffusion in the phase space, allowing for more precession resonances to be populated.

Regarding the power deposition, the simulations with 10^5 test particles in a worst-case scenario show that losses with TAE cover a much larger area of the machine below the mid-plane, even if the peak energy deposited in the 'hot spots' is still well below the power flux of thermal particles (2.5 MW m^{-2}) manageable by the front-end components of DTT [125].

DTT is expected to have a diverse population of energetic ions in a broad energy range, from hundred keV to a few MeV, a mix for which the diagnosis is experimentally challenging. For the first time, DTT will combine a mix of diagnostics based on both charge exchange and nuclear reactions. The present plan for the DTT EP diagnostic systems comprises a fast ion loss detector (FILD), a fast-ion $D\alpha$ (FIDA) system, a scintillator based neutral particle analyser (NPA), a time of flight neutron spectrometer (TOF) and gamma-ray spectrometers (GRS), implemented to accompany the evolution of the heating systems, as discussed in section 4.3.

5.4. Theoretical developments

The role of theory in the DTT conceptual design phase has been to identify machine parameters that could allow addressing general and fundamental physics issues for reactor-relevant fusion plasmas. Use of various forms of similarity scalings [118] has been of crucial importance for that objective. During the current preparatory stage, theory plays a crucial role in enabling predictions that exceed the limitations of existing models addressing fundamental physics issues that are already recognized as pertinent to reactor-grade burning plasmas. Specifically, it must delve into the phenomena of plasma self-organization in the context of substantial alpha particle heating and examine the interactions between thermal plasma and supra-thermal components. These considerations are vital for understanding the complex behaviours observed in ignited or sub-ignited thermonuclear plasmas. Once verified, these predictions can inform the conceptual design of experiments that will serve as a relevant testing ground for validation.

The power density profiles and characteristic wavelengths of collective modes in DTT are expected to strongly differ from those currently observed and will be shifted towards higher mode numbers (see section 5.3). Furthermore, the

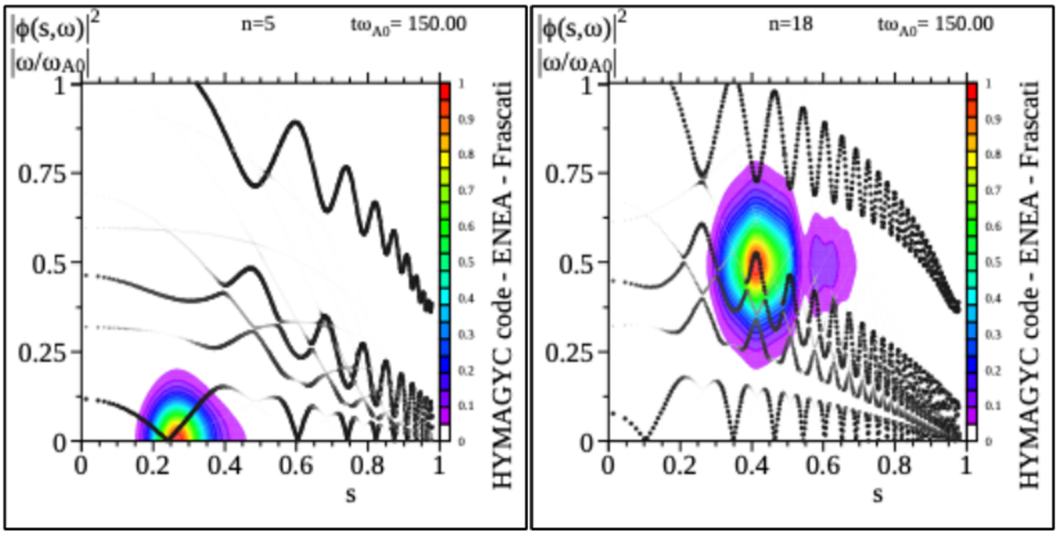

Figure 31. Frequency spectra of the electrostatic potential in the plane (s,ω) as obtained by two linear HYMAGYC simulations, with mode number $n = 5$ (left) and mode number $n = 18$ (right), respectively. Coloured structures refer to an infernal-like mode (left) and to an energetic particle driven mode (right). Dots refer to Shear Alfvén and magneto-acoustic continua, as calculated by the FALCON code; larger and darker symbols refer to Alfvénic oscillations, while smaller and lighter ones to ion sound waves.

dominant electron heating will introduce a different weighing of the electron-driven microturbulence. Another important novelty that will be a characteristic feature of DTT plasma operations is the presence of a non-perturbative EP population with characteristic energies larger than the critical energy, above which the collisional drag by thermal electrons on EP exceeds the pitch-angle scattering rate of thermal ions. In those conditions, both linear and nonlinear interaction of EPs with core plasma turbulence will be modified and predominantly affected by EP resonant and non-resonant diamagnetic response, rather than by the dilution effect due to mildly suprathermal ion contribution to the quasi-neutrality condition [121]. Determining how the power repartition between electrons and ions (ultimately expressed by the T_e/T_i ratio), depends on the heating mix, particularly as fast ions are introduced in the plasma, is a key area of investigation. In this context, DTT will provide a specific opportunity to compare electron heated plasmas without fast ions (when only the ECRH system is used) and with fast ions, with the additional possibility of varying their energy range and density. A simpler scenario is obtained when NBI at different power levels is added to EC heated plasmas while a more complex one is obtained when ICRH is used to generate MeV range ions. A large variety of heating schemes could be adopted, for example the more standard hydrogen and 3He minority heating, heating of the NBI deuterons at the second and third harmonic of the ion cyclotron resonance frequency or the three ions scenario [63, 126]. In all these cases, it will be necessary to characterize and understand the fast ion driven modes that are observed, the corresponding fast ion transport and the overall impact on turbulence. Understanding the mechanisms behind the impact of different energetic ion populations on turbulence must be aimed at finding what is the best mix of auxiliary heating systems to ensure that heating is effectively channelled from the electrons to the ions and, ultimately, the fusion neutron yield per MW of auxiliary heating power is maximized. Plasma operation scenarios will also reflect different plasma edge conditions and PWI at high density and low collisionality. These conditions must be addressed to improve our understanding of reactor-relevant plasmas. For all these reasons, predictive capabilities based on numerical simulations as well as fundamental theories for constructing relevant reduced models will play crucial roles and provide the necessary insights.

The complex nature of reactor-relevant plasmas requires particular attention to the accurate characterization of Zonal flows and more generally Zonal electromagnetic Fields [127, 128], which can be generated by various nonlinear processes, such as thermal plasma instabilities, EP-driven instabilities, and geodesic acoustic mode (GAM) interactions. The understanding and characterization of these zonal flows/fields is essential for predicting and controlling plasma performance due to their role in regulating plasma turbulent transport. This requires an analysis that accounts for multiple spatiotemporal scales in a self-consistent manner, considering realistic conditions such as equilibrium geometry, spatial non-uniformity, and kinetic effects [125]. Experimental studies and accompanying numerical simulations must be conducted in DTT to address these issues and provide insights into the complex behaviour of Zonal Flows and their impact on reactor relevant plasmas.

To this end, a global electromagnetic first principle-based approach is needed. In particular, the crucial role of EPs, due to their characteristic energies, requires the description of transport processes occurring on completely different spatiotemporal scales compared to background transport. To address this challenge, recently, the phase space zonal structures (PSZS) transport theory has been developed [129]. PSZS represent slowly evolving (on the transport time scale) structures in the phase space that are unaffected by

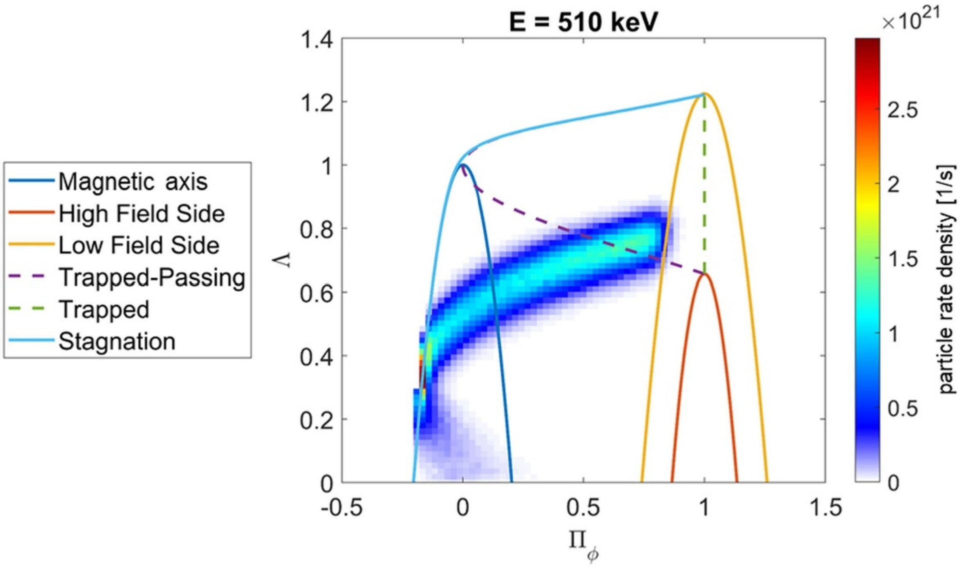

Figure 32. Distribution of newly born fast ions in DTT reference scenario at $E = 510$ keV in a space described by the normalized canonical angular momentum and the pitch angle.

collisionless dissipation, providing a suitable definition of plasma nonlinear equilibrium distribution functions [130]. PSZS must be calculated by adopting a two-step averaging procedure: first, an average along guiding centre equilibrium orbits is applied; second, a filter is used, on the axisymmetric particle response, to remove the fast spatiotemporal variations on the characteristic particle orbit scale-length and/or the hydrodynamic time scale. Consequently, PSZS depend solely on the equilibrium invariants of motion, such as the particle energy (per unit mass) $\mathcal{E} = v^2/2$, the magnetic moment $\mu = v_\perp^2/2B$, and the toroidal component of the canonical angular momentum P_ϕ. An equation for the evolution of PSZS has been derived (see equation (5) of [128]), which extends the concept of plasma transport processes to the phase space in the presence of collisions and sources, making it particularly relevant for weakly collisional plasmas with possible significant deviations from local thermodynamic equilibrium. Note that PSZS is not intended as an alternative to global gyrokinetic or hybrid guiding-centre/Monte-Carlo initial-value codes. Rather, PSZS provides a complementary reduced kinetic description of the slow, fluctuation-renormalized energetic-particle equilibrium that emerges from the nonlinear dynamics resolved by such codes. The specific physics retained by PSZS, which is usually not represented in conventional one-dimensional transport closures, is the meso-scale, non-Maxwellian phase-space structure generated by resonant wave-particle transport. They correspond to slowly evolving neighbouring equilibria, or phase-space corrugations, in constants-of-motion space. Their evolution includes the effect of fluctuation induced transport (resonant and non-resonant), sources, and collisions. Thus, PSZS keeps relevant information that is often neglected when global simulations are reduced to flux-surface-averaged diffusion coefficients or when transport models assume a prescribed background distribution.

The PSZS transport theory is particularly important for DTT since DTT plasmas will combine high density and low collisionality providing an ideal testbed for validating the predictions based on this novel theoretical framework. Distinctive features in DTT are the additional heating with both ICRH minority scheme as well as 510 keV NBI for the generation of EP populations significantly above the critical energy. As an illustrative example, figure 32 shows a distribution function for NBI newly born fast ions obtained for DTT reference scenario E [68] using the BBNBI code [131].

In the recently developed ATEP code [132], the PSZS governing equations are solved using linear gyrokinetic mode information to calculate phase space particle responses and corresponding fluxes. These are obtained, in turn, using the HAGIS code [133] assuming various perturbation amplitudes, allowing the implementation of the double averaging procedure already described. As an example, in figure 33 we show some plots of the orbit-average of $\dot{\delta p}_\phi$ caused by a single Toroidal Alfvén eigenmode as appearing in the PSZS equation in the quasi-linear limit.

It is therefore highly desirable for the scientific exploitation of DTT to have an automated workflow analysing the time-dependent stability of EP-driven modes in general tokamak geometry [134] based on the Integrated Modelling and Analysis System (IMAS) [135]. This automated workflow must leverage efficient computational methods and theory-based reduced models to deliver fast and reliable results. As an example, figure 34(*a*) illustrates the radial structure of the DTT continuous spectrum for toroidal mode number $n = 20$. The frequency normalized to the on-axis Alfvén frequency and the radial location at $\rho_{\mathrm{tor}} = 0.702$ of an $n = 20$ TAE mode is also indicated [136]. The corresponding normalized parallel mode structure of the magnetic stream function is shown in panel (b), while 2D and 3D mode structures are shown, respectively, in panels (c) and (d) assuming

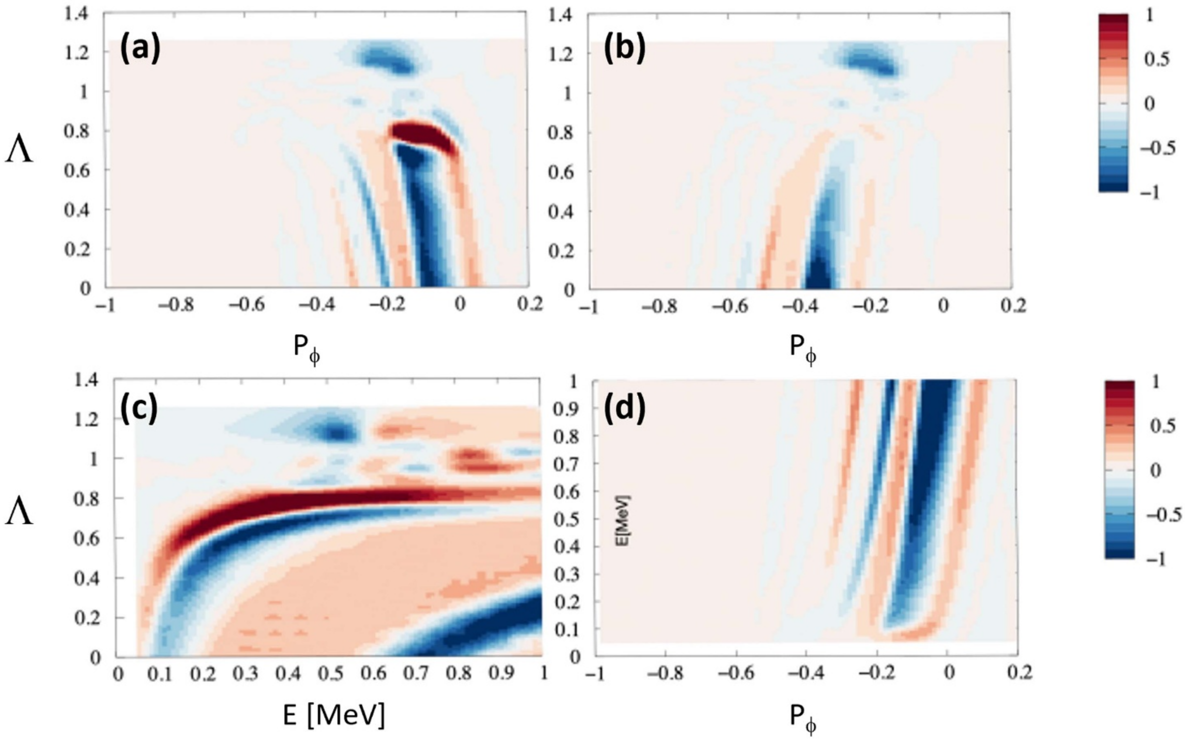

Figure 33. Orbit-averaged perturbation of the canonical toroidal momentum, $\dot{\delta} p_\phi$, produced by a single $n = 13$ TAE mode in an ITER pre-fusion scenario. Panels (a) and (b) show the dependence on P_ϕ and pitch parameter Λ at fixed energy $E = 0.5$ MeV, for co-passing/trapped and counter-passing/trapped particles, respectively. Panel (c) shows the structure in E-Λ space at fixed $P_\phi = -0.2$. Panel (d) shows the structure in P_ϕ -E space at fixed $\Lambda = 0.12$. The colour scale indicates the normalized orbit-averaged change in P_ϕ, with red and blue corresponding to opposite signs of radial phase-space transport. These coherent structures are signatures of resonant wave-particle interactions and indicate regions of enhanced radial transport in phase space.

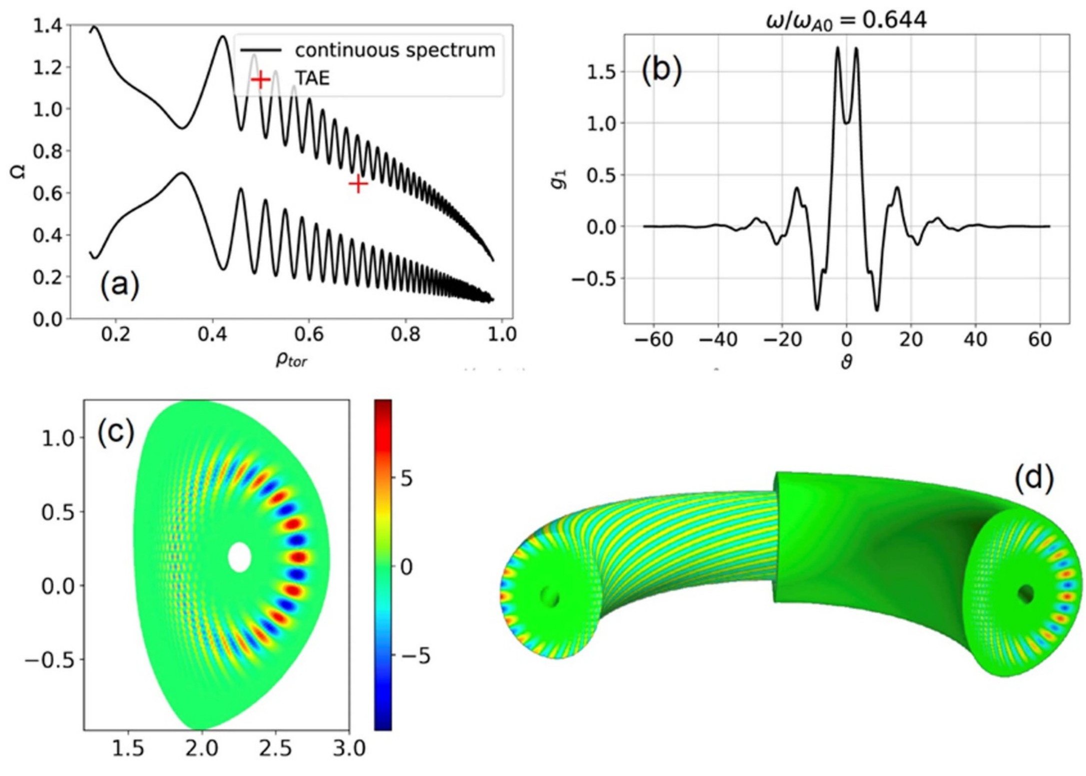

Figure 34. (*a*) Continuous spectrum ($n = 20$) and location of TAE in DTT; (*b*) normalized parallel mode structure of the magnetic stream function at $\rho_{\mathrm{tor}} = 0.702$; 2D (*d*) 3D mode structure ($n = 20$) obtained with an ad-hoc radial envelope.

Table 6. DTT programme high-level headlines. Expected relevance to ITER and/or reactors is indicated by a *.

Headline number	Headline contents	ITER	Reactor
Construction phase			
C.1	Integrated modelling for prediction of baseline and alternative scenarios, including assessment of MHD stability and Energetic Particles (EP) properties		
C.2	Modelling for support to design of first wall, divertor, fuelling & pumping, DTM (divertor test modules), heating & current drive (H&CD) systems		
C.3	Definition of necessary and suitable diagnostic systems		
C.4	Set up IMAS infrastructure and dedicated workflows	*	
	Phase 1		
1.1	ECRH and ICRH systems commissioning and optimization of basic functionalities	*	*
1.2	Commissioning and validation of fuelling & pumping systems and wall conditioning methods	*	*
1.3	Development of SN, NT and XD scenarios compatible with Phase 1 H&CD systems conditions	*	*
1.4	Development of half field/half current scenarios for initial high β_N studies		*
1.5	Optimization of ramp-up/ramp-down phases, in particular with respect to PFC conditions	*	*
1.6	Transport, MHD, EP initial studies, with validation of theory and modelling tools	*	*
1.7	Initial DTM testing activity	*	*
1.8	Extensive disruption and runaway electrons studies and mitigation, in support of ITER	*	
	Phase 2		
2.1	NBI commissioning and combined operation with ECRH and ICRH systems	*	*
2.2	Scenario optimization at higher power level and with NBI	*	*
2.3	Detached regimes optimization and control by impurity seeding in various scenarios	*	*
2.4	Experimental assessment of edge transport at high plasma current and comparison with λ_q scalings and theory	*	*
2.5	Transport, MHD, EP physics studies for assessment of high β_N, hybrid and advanced scenarios, including NBI heating and associated EP	*	*
2.6	Development of small/no ELMs scenarios and their control with NAS (non-axisymmetric) coils and pellets. Assessment of compatibility with high plasma performance.	*	*
2.7	Extensive DTM testing at high power, in particular for new FW and divertor materials	*	*
	Phase 3		
3.1	Extension and optimization of all scenarios at full heating power, in conditions of controlled core-edge integration	*	*
3.2	Wall erosion, W migration, D retention and removal studies and assessment in view of application to DEMO	*	*
3.3	Disruption prediction and mitigation studies, including SPI (shattered pellet injection), at full plasma performance	*	
3.4	Transport, MHD, EP physics studies for assessment of high β_N, hybrid and advanced scenarios in conditions of high power density, relevant for burning plasma physics		*
3.5	Validation of advanced theoretical frameworks and reduced transport models in the presence of EP at full plasma performance	*	*
3.6	Integrated component testing at maximum power fluxes, in view of DEMO		*

an ad-hoc radial envelope function. It is of utmost importance to emphasize the active development of these workflows, or similarly capable alternatives, for ensuring the accurate scientific exploitation of DTT. Such tools are crucial for validating theoretical results by means of a comparison with experimental data and synthetic diagnostics, thereby establishing a solid framework for a hierarchy of reduced transport models. This capability is especially timely given recent advances that allow selective experimental probing and reconstruction of 3D phase-space distribution functions enabling validation of phase space transport theories against experimental data.

Since the scaling of EP transport dependence on β_h/β (ratio of EP and thermal betas) is of crucial importance for future burning plasmas, the experimental variation of this ratio around projected values is of great theoretical interest. More specifically, the ratio of EP energies and thermal background temperatures has a strong influence on mode stability, saturation levels and EP transport. To this end, DTT as a W-machine will be able to apply similar strategies as other W-devices for reaching burning-plasma-relevant ratios: by allowing a controlled W influx, the thermal plasma β and thus background Landau damping can be reduced while keeping the NBI power and energy maximal. An additional novel element in these studies are the super-Alfvénic beam energies at DTT that enable mode destabilization via the primary resonance, i.e. $v = v_{\mathrm{Alfvén}}$; allowing, thus, another step closer to burning plasma conditions.

6. High-level headlines of the DTT research programme

The DTT project is in its construction phase, with a large fraction of the budget already committed in industrial contracts. In parallel, a dedicated programme of physics studies is being carried out, with significant contribution of international collaborators. In 2022, it was decided to build on these studies to produce the DTT Research Plan, involving the broadest possible community of European fusion institutes. The result of this activity is the first version of the DTT-RP [1], an extensive document of which the highlights have been presented in this overview paper. The complete document describes the objectives and research strategy of the DTT experiment and constitutes the basis for the construction of the DTT scientific programme and of subsequent device upgrades. The DTT Research Plan describes in detail the research headlines for each scientific and technical area, culminating in a set of high-level programmatic headlines. These are presented in table 6, classified by the project Phases (see figure 3) and connected to the device evolution summarized in table 2. As sketched in figure 3, Phase 1 and Phase 2 are expected to last 5 years each typically, leading to an exploitation of the device with full nominal parameters which could start approximately 10 years after the end of the construction phase.

Of course these headlines are more and more tentative as they are projected to the future exploitation phases, spanning a temporal horizon of ~30 years. The results obtained in the early research phases, as well as progress obtained in the framework of the international fusion programme and the needs of ITER will contribute to defining the subsequent programme of DTT. Moreover, the upgrades of the device itself will be impacted by technology options opened by the development of first-of-a-kind reactor projects. A relevant example is the possible implementation in DTT of a liquid metal divertor.

Acknowledgment

This paper is dedicated to the memory of Professor Francesco Romanelli, who always encouraged and supported the elaboration of the DTT Research Plan. The authors acknowledge the precious contributions of the DTT project team. In particular, the authors would like to thank S. Roccella and the DTT IVC-team for providing the models and the design of the in-vessel components shown in figures 9 and 10.

ORCID iDs

G. Giruzzi 0000-0001-9628-5968
C. Angioni 0000-0003-0270-9630
S. Brezinsek 0000-0002-7213-3326
M.V. Falessi 0000-0002-2105-226X
P. Mantica 0000-0001-5939-5244
E. Nardon 0000-0003-0427-2292
C. Sozzi 0000-0001-8951-0071
D. Terranova 0000-0001-9339-283X
D. Van Eester 0000-0002-4284-3992
P. Vincenzi 0000-0002-5156-4354
G. Vlad 0000-0003-1482-5436
P. Agostinetti 0000-0003-2103-7630
R. Albanese 0000-0003-4586-8068
G. Alberti 0000-0001-9835-5085
E. Alessi 0000-0002-8750-9867
L. Aucone 0000-0003-3949-678X
F. Auriemma 0000-0002-1043-1563
B. Baiocchi 0000-0002-1483-3113
L. Balbinot 0000-0002-7467-533X
T. Bolzonella 0000-0003-1128-964X
D. Bonfiglio 0000-0003-2638-317X
R. Bonifetto 0000-0002-3557-9177
M. Cavedon 0000-0002-0013-9753
J.W. Coenen 0000-0002-8579-908X
Y. Corre 0000-0002-6566-6116
A. Dal Molin 0000-0003-0471-1718
C. De Piccoli 0000-0002-5916-7361
R. Dumont 0000-0002-1030-138X
L. Figini 0000-0002-0034-4028
D. Fiorucci 0000-0002-5111-0336
L. Frassinetti 0000-0002-9546-4494
V. Fusco 0000-0003-1179-4363
A. Gallo 0000-0002-7472-7830
J. Garcia 0000-0003-0900-5564
J. Gaspar 0000-0003-0104-1616
M. Gobbin 0000-0001-5261-3683
J. Hillairet 0000-0002-1073-6383
C. Hopf 0000-0001-6824-7358
E. Joffrin 0009-0008-7527-0984
Y. Kominis 0000-0002-5992-7674
X. Litaudon 0000-0001-6973-9717
J. Lombardo 0009-0007-9349-0246
P. Maget 0000-0002-8746-8102
A. Mariani 0000-0003-0476-3825
J. Morales 0000-0002-3140-0504
R. Neu 0000-0002-6062-1955
L. Pigatto 0000-0002-0556-0440
F. Porcelli 0000-0002-3625-6417
D. Ricci 0000-0001-8794-4909
M. Richou 0000-0002-8447-868X

G. Spizzo 0000-0001-8586-2168
F. Subba 0000-0002-8170-4792

References

[1] Crisanti F. *et al* 2024 *Divertor Tokamak Test facility research plan, Version 1.0* (available at: www.pubblicazioni.enea.it/le-pubblicazioni-enea/edizioni-enea/anno-2024/divertor-tokamak-test-facility-research-plan-version-1-0.html)
[2] Romanelli F. *et al* 2024 *Nucl. Fusion* **64** 112015
[3] Romanelli F. *et al* 2025 The Divertor Tokamak Test project: progress towards the initial operation, preprint *IAEA Fusion Energy Conf.* (*Chengdu*)
[4] Reimerdes H. *et al* 2020 *Nucl. Fusion* **60** 066030
[5] Polli G.M. *et al* 2025 The Divertor Tokamak Test facility: machine design, construction and commissioning *IAEA Fusion Energy Conf.* (*Chengdu*)
[6] Albanese R. *et al* 2015 *Fusion Eng. Des.* **96–97** 664
[7] Siccinio M., Graves J.P., Kembleton R., Lux H., Maviglia F., Morris A.W., Morris J. and Zohm H. 2022 *Fusion Eng. Des.* **176** 113047
[8] Ambrosino R. *et al* 2021 *Fusion Eng. Des.* **167** 112330
[9] Ejima S., Callis R.W., Luxon J.L., Stambaugh R.D., Taylor T.S. and Wesley J.C. 1982 *Nucl. Fusion* **22** 1313
[10] Granucci G. *et al* 2015 *Nucl. Fusion* **55** 093025
[11] Di Grazia L.E. and Mattei M. 2022 *Fusion Eng. Des.* **176** 113027
[12] Farina D. 2007 *Fusion Sci. Technol.* **52** 154
[13] Romanelli M. 2014 *Plasma and Fus. Res.* **9** 3403023
[14] Pereverzev G. and Yushmanov P.N., 1991 ASTRA automated system of transport analysis in a Tokamak *Report of the Mak-Planck-Institut für Plasmaphysik, IPP 5/42*
[15] Fable E., Angioni C., Ivanov A.A., Lackner K., Maj O. , Medvedev S.Y., Pautasso G. and Pereverzev G.V. 2013 *Nucl. Fusion* **53** 033002
[16] Artaud J.F. *et al* 2018 *Nucl. Fusion* **58** 105001
[17] Staebler G.M., Belli E.A., Candy J., Kinsey J.E., Dudding H. and Patel B. 2021 *Nucl. Fusion* **61** 116007
[18] Houlberg W., Shaing K.C., Hirshman S.P. and Zarnstorff M.C. 1997 *Phys. Plasmas* **4** 3230
[19] Fajardo D., Angioni C., Maget P. and Manas P. 2022 *Plasma Phys. Control. Fusion* **64** 05501
[20] Saarelma S., Challis C.D., Garzotti L., Frassinetti L., Maggi C.F., Romanelli M. and Stokes C. 2018 *Plasma Phys. Control. Fusion* **60** 014042
[21] Luda T. *et al* 2023 *Plasma Phys. Control. Fusion* **65** 034001
[22] Eriksson L.G., Hellsten T. and Willen U. 1993 *Nucl. Fusion* **33** 1037
[23] Challis C.D., Cordey J.G., Hamnén H., Stubberfield P.M., Christiansen J.P., Lazzaro E., Muir D.G., Stork D. and Thompson E. 1989 *Nucl. Fusion* **29** 563
[24] Weiland M., Bilato R., Dux R., Geiger B., Lebschy A., Felici F., Fischer R., Rittich D. and van Zeeland M. 2018 *Nucl. Fusion* **58** 082032
[25] Baiocchi B., Aucone L., Casiraghi I., Figini L., Koechl F. and Mantica P. 2023 *Nucl. Fusion* **63** 106009
[26] Casiraghi I. *et al* 2023 *Plasma Phys. Control. Fusion* **65** 035017
[27] Crisanti F. *et al* 2024 *Nucl. Fusion* **64** 106040
[28] Mariani A. *et al* 2024 *Nucl. Fusion* **64** 046018
[29] Mariani A. *et al* 2024 *Nucl. Fusion* **64** 106024
[30] Bonanomi N. *et al* 2025 *Nucl. Fusion* **65** 016005
[31] Greenwald M. *et al* 1999 *Phys. Plasmas* **6** 1943
[32] Stober J., Maraschek M., Conway G.D., Gruber O., Herrmann A., Sips A.C.C., Treutterer W. and Zohm H. (ASDEX Upgrade Team) 2001 *Nucl. Fusion* **41** 1123
[33] Saibene G. *et al* 2005 *Nucl. Fusion* **45** 297
[34] Lunt T., Bernert M., Brida D., David P., Faitsch M., Pan O., Stieglitz D., Stroth U. and Redl A. 2023 *Phys. Rev. Lett.* **130** 145102
[35] Whyte D.G. *et al* 2010 *Nucl. Fusion* **50** 105005
[36] Chen X. *et al* 2017 *Nucl. Fusion* **57** 086008
[37] Lombardo J. *et al 2025 51st EPS Conf. on Plasma Physics* (*Vilnius 7–11 July 2025)* p 4.168
[38] Martin Y.R. *et al* 2008 *J. Phys: Conf. Ser.* **123** 012033
[39] ITER Physics Basis Editors *et al* 1999 *Nucl. Fusion* **39** 2175
[40] Verdoolaege G. *et al* 2021 *Nucl. Fusion* **61** 076006
[41] Pitts R.A. *et al* 2019 *Nucl. Mater. Energy* **20** 100696
[42] Maviglia F. *et al* 2021 *Nucl. Mater. Energy* **26** 100897
[43] Militello F. *et al* 2021 *Nucl. Mater. Energy* **26** 100908
[44] Roccella S. *et al* 2024 *IEEE Trans. Plasma Science* **52** 4167
[45] Furno Palumbo M., Roccella S., De Sano G., De Luca R., Iafrati M., Tatì A., Riccardi B., Paoletti D. and Polli G.M. 2026 *Fusion Eng. Des.* **222** 115435
[46] Eich T. *et al* 2013 *Nucl. Fusion* **53** 093031
[47] Chang C.S., Ku S., Hager R., Churchill R.M., Hughes J., Köchl F., Loarte A., Parail V. and Pitts R.A. 2021 *Phys. Plasmas* **28** 022501
[48] Innocente P., Ambrosino R., Brezinsek S., Calabrò G., Castaldo A., Crisanti F., Dose G., Neu R. and Roccella S. 2022 *Nucl. Mater. Energy* **33** 101276
[49] Balbinot L., Rubino G., Casiraghi I., Calabrò G. and Innocente P. 2025 *Nucl. Mater. Energy* **42** 101835
[50] Bufferand H. *et al* 2015 *Nucl. Fusion* **55** 053025
[51] Reiter D., Baelmans M. and Börner P. 2005 *Fusion Sci. Technol.* **47** 172
[52] Romazanov J. *et al* 2019 *Nucl. Mater. Energy* **18** 331
[53] Kirschner A. *et al* 2019 *Nucl. Mater. Energy* **18** 239
[54] Bernert M. *et al* 2020 *Nucl. Fusion* **61** 024001
[55] Eich T., Manz P., Goldston R.J., Hennequin P., David P., Faitsch M., Kurzan B., Sieglin B. and Wolfrum E. 2020 *Nucl. Fusion* **60** 056016
[56] Fanale F., Baiocchi B., Bruschi A., Busi D., Bussolan A., Figini L., Garavaglia S., Granucci G. and Romano A. 2023 *Fusion Eng. Des.* **192** 113797
[57] Ceccuzzi S. *et al* 2025 *Fusion Eng. Des.* **213** 114849
[58] Salvia C., Bettini P., Cardinali A., Ceccuzzi S., Greco S., Van Eester D. and Zanon F. 2025 *Fusion Eng. Des.* **215** 114916
[59] Ravera G.L., Ceccuzzi S., Granucci G., Cardinali A., Napoli F., Piras S., Ponti C. and Schettini G. 2023 *Fusion Eng. Des.* **191** 113754
[60] Ceccuzzi S. *et al* 2023 *AIP Conf. Proc.* **2984** 030015
[61] Cioffi A. *et al*, 2026 *EPJ Web Conf.* vol **346** p 03006
[62] Cardinali A. *et al* 2025 *Plasma Phys. Control. Fusion* **67** 085018
[63] Kazakov Y. *et al* 2021 *Phys. Plasmas* **28** 020501
[64] Brambilla M. 1999 *Plasma Phys. Control. Fusion* **41** 134
[65] Van Eester D. and Koch R. 1998 *Plasma Phys. Contr. Fusion* **40** 1949
[66] Agostinetti P. *et al* 2024 *IEEE Trans. Plasma Sci.* **52** 3802
[67] Vincenzi P. *et al* 2023 *Fusion Eng. Des.* **189** 113436
[68] De Piccoli C. *et al* 2024 *Front. Phys.* **12** 1492095
[69] Hirvijoki E., Asunta O., Koskela T., Kurki-Suonio T., Miettunen J., Sipilä S., Snicker A. and Äkäslompolo S. 2014 *Comput. Phys. Commun.* **185** 1310
[70] Spizzo G. *et al* 2021 *Nucl. Fusion* **61** 116016
[71] Gobbin M. and Spizzo G. 2023 *Plasma Phys. Control. Fusion* **65** 075013
[72] Mazzitelli G., Apicella M.L., Ciattaglia S., Colangeli A., Maddaluno G., Marocco D., Martone R. and Villari R. 2017 *Fus. Eng. Design* **122** 375
[73] Utili M. *et al* 2025 *Fusion Eng. Des.* **221** 115347
[74] Balbinot L. *et al*, 2025 Defining operational scenarios for DTT in metallic environment: a modeling study of

core-edge dynamics and plasma-wall interaction *IAEA Fusion Energy Conf.* (*Chengdu*)
[75] Villari R. *et al* 2020 *Fus. Eng. Design* **155** 111551
[76] Palomba S. *et al* 2025 *Fusion Eng. Des.* **219** 115269
[77] Albanese R. *et al* 2017 *Fusion Eng. Des.*. **122** 365
[78] Lacquaniti M., Sias G., Fanni A., Pironti A., Giorgetti F., Calabrò G., Aymerich E. and Baruzzo M. 2023 *Fusion Eng. Des.* **192** 113775
[79] Belpane A. *et al* 2025 *Fusion Eng. Des.* **219** 115271
[80] Nielsen P., Gowers C., Salzmann H., Giudicotti L. and Pasqualotto R. 2019 *JINST* **14** C11018
[81] Marocco D., Gandolfo G., Panza F., Anagnostopoulou V., Centioli C., Pompili F. and Pontesilli M. 2026 *Fusion Eng. Des.* **222** 115538
[82] Anagnostopoulou V., Gandolfo G., Panza F., Colangeli A., Flammini D., Angelone M., Pillon M., Gelfusa M. and Marocco D. 2026 *Fusion Eng. Des.* **222** 115537
[83] Causa F. *et al* 2019 *Rev. Sci. Instrum.* **90** 073501
[84] Giudicotti L., Fassina A., Pasqualotto R. and Franz P. 2020 *JINST* **15** C01042
[85] Fiorucci D. *et al* 2025 *JINST* **20** C06061
[86] Mandl W., Wolf R.C., Hellermann M.G.V. and Summers H.P. 1993 *Plasma Phys. Control. Fusion* **35** 1373
[87] Offeddu N. *et al* 2022 *Rev. Sci. Instrum.* **93** 123504
[88] Peluso E. *et al* 2025 *Fusion Eng. Des.* **215** 114947
[89] D'Agostino V. *et al* 2025 *Fusion Eng. Des.* **215** 114981
[90] Moseev D. *et al* 2018 *Rev. Mod. Plasma Phys.* **2** 7
[91] Coda S., Iantchenko A., Brunner S., Toussaint M. and Tanaka K. 2021 *Nucl. Fusion* **61** 106022
[92] White A.E. *et al* 2008 *Rev. Sci. Instrum.* **79** 103505
[93] Bagnato F., Giudicotti L., Fassina A., D'isa F.A., Palomba S., Gabellieri L. and Pasqualotto R. 2025 *JINST* **20** C10012
[94] Fontana M. *et al* 2023 *Phys. Plasmas* **30** 122503
[95] Ruffini F. *et al* 2025 *JINST* **20** C05030
[96] Silva F.D., Santos J., Silva A., Ferreira J., Heuraux S., Ribeiro T., De Masi G., Cavazzana R., Marchiori G. and Tudisco O. 2025 *JINST* **20** C09004
[97] Mazon D. *et al* 2025 *Nucl. Fusion* **65** 113001
[98] Fusco V. *et al*, 2022 *47th EPS Conf. on Plasma Physics P2a.125*, (available at: http://ocs.ciemat.es/EPS2022PAP/pdf/P2a.125.pdf)
[99] Lütjens H., Bondeson A. and Sauter O. 1996 *Comput. Phys. Commun.* **97** 219
[100] Bondeson A., Vlad G. and Lütjens H. 1992 *Phys. Fluids* **B4** 1889
[101] Porcelli F., Boucher D. and Rosenbluth M.N. 1996 *Plasma Phys. Control. Fusion* **38** 2163
[102] Basiuk V., Huynh P., Merle A., Nowak S. and Sauter O. 2017 *Plasma Phys. Control. Fusion* **59** 125012
[103] Granucci G. *et al* 2024 *Nucl. Fusion* **64** 126036
[104] Casiraghi I. *et al* 2021 *Nucl. Fusion* **61** 116068
[105] Pigatto L., Bolzonella T., Bonotto M., Fusco V., Liu Y.Q., Marchiori G., Villone F. and Vlad G. 2024 *Nucl. Fusion* **64** 016023
[106] Albanese R., Bolzonella T., Chiariello A.G., Cucchiaro A., Iaiunese A., Lampasi A., Martone R., Piron L., Pizzuto A. and Zumbolo P. 2023 *Fusion Eng. Des.* **189** 113437
[107] Piron L. *et al* 2024 *Nucl. Fusion* **64** 066029
[108] Hender T. *et al* 2007 *Nucl. Fusion* **47** S28
[109] Sozzi C. *et al* 2021 Termination of discharges in high performance scenarios in JET *IAEA Fusion Energy Conf., virtuale edition*
[110] Esposito B. *et al* 2011 *Plasma Phys. Control. Fusion* **53** 124035
[111] Nardon E. *et al*, 2023 *Modelling of runaway electron dynamics in tokamak disruptions*, *IAEA Fusion Energy Conf.* (*London*)
[112] De Vries P. *et al* 2012 *Plasma Phys. Control. Fusion* **54** 124032
[113] Hoelzl M. *et al* 2021 *Nucl. Fusion* **61** 065001
[114] Emanuelli E., Vannini F., Hoelzl M., Schwarz N., Nardon E., Bandaru V., Bonfiglio D., Kryzhanovskyy A., Ramogida G. and Subba F. 2026 *Fusion Eng. Des.* **223** 115588
[115] Paz-soldan C. *et al* 2021 *Nucl. Fusion* **61** 116058
[116] Wang T., Qiu Z., Zonca F., Briguglio S., Fogaccia G., Vlad G. and Wang X. 2018 *Phys. Plasmas* **25** 062509
[117] Wang T., Wang X., Briguglio S., Qiu Z., Vlad G. and Zonca F. 2019 *Phys. Plasmas* **26** 012504
[118] Pizzuto A. *et al* 2010 *Nucl. Fusion* **50** 095005
[119] Wei G., Zonca F., Valerio Falessi M. and Qiu Z. 2025 *Nucl. Fusion* **65** 106035
[120] Zonca F., Chen L., Briguglio S., Fogaccia G., Milovanov A.V., Qiu Z., Vlad G. and Wang X. 2015 *Plasma Phys. Control. Fusion* **57** 014024
[121] Chen L. and ZONCA F. 2016 *Rev. Mod. Phys.* **88** 015008
[122] White R.B. and Chance M.S. 1984 *Phys. Fluids* **27** 2455
[123] Vlad G. *et al* 2025 *Rev. Mod. Plasma Phys.* **9** 27
[124] Falessi M.V., Carlevaro N., Fusco V., Giovannozzi E., Lauber P., Vlad G. and Zonca F. 2020 *J. Plasma Phys.* **86** 845860501
[125] Gobbin M. *et al* 2026 *Plasma Phys. Control. Fusion* **68** 055006
[126] Nocente M. *et al* 2020 *Nucl. Fusion* **60** 124006
[127] Diamond P.H., Itoh S.-I., Itoh K. and Hahm T.S. 2005 *Plasma Phys. Control. Fusion* **47** R35
[128] Falessi M.V., Chen L., Qiu Z. and Zonca F. 2023 *New J. Phys.* **25** 123035
[129] Falessi M.V. and Zonca F. 2019 *Phys. Plasmas* **26** 022305
[130] Zonca F., Chen L., Briguglio S., Fogaccia G., Vlad G. and Wang X. 2015 *New J. Phys.* **17** 013052
[131] Asunta O., Govenius J., Budny R., Gorelenkova M., Tardini G., Kurki-Suonio T., Salmi A. and Sipilä S. 2015 *Comput. Phys. Commun.* **188** 33
[132] Lauber P.H., Falessi M., Meng G., Hayward-schneider T., Popa V.-A., Zonca F. and Schneider M. 2024 *Nucl. Fusion* **64** 096010
[133] Pinches S.D. 1998 *Comput. Phys. Commun.* **111** 133
[134] Popa V.A. *et al* 2023 *Nucl. Fusion* **63** 126008
[135] Imbeaux F. *et al* 2015 *Nucl. Fusion* **55** 123006
[136] Wei G., Falessi M.V., Wang T., Zonca F. and Qiu Z. 2024 *Phys. Plasmas* **31** 072505